FISH TALES: LOSS OF STAG2 PROMOTES MIGRATION OF EWING SARCOMA

by

Melissa Richardson

Submitted in partial fulfilment of the requirements
for the degree of Master of Science

at

Dalhousie University
Halifax, Nova Scotia
June 2018

DEDICATION

To all my family and friends who have shown continuous support throughout this journey, encouraging me to follow my dreams and inspirations. In memory of the departed who motivated me to enter this field. Thank you everyone, you are a true blessing to have/had in my life.

TABLE OF CONTENTS

List of Tables

List of Figures

Abstract

Ewing sarcoma (EwS) is a bone and soft tissue cancer affecting children and adolescents. The most unfavorable prognostic factor of EwS is the presence of metastasis, however this process is still poorly understood. Therefore, we developed a zebrafish xenotransplantation model to better visualize the metastatic behaviour of EwS migration *in vivo.* STAG2, a cohesin complex subunit mutated in 88% of metastatic EwS cases, appears to promote EwS cell motility. The impact of *STAG2* knockout on EwS migration and other mechanisms involved with STAG2 loss and cell migration were evaluated by the knockout of *STAG2* in EwS cell lines (A673 and TC71) using CRISPR/Cas9 technology. EwS cell lines were fluorescently labeled prior to xenotransplantation into the larval hindbrain ventricle. *STAG2* knockout was determined to promote cell migration in both A673 and TC71 cell lines. *STAG2* knockout had a greater effect on EwS cell migration with EWS-FLI1^{low} expression and moreover, reduced the expression of EWS-FLI1. Therefore, STAG2 loss may contribute to EwS metastasis through regulation of EWS-FLI1 and represent a new biomarker in this disease.

List of Abbreviations Used

µl	Microlitres
ACT-D	Actinomycin
CMTMR	Cell Tracker Orange dye
CPM	Cyclophosphamide
DMSO	Dimethyl sulfoxide
DOX	Doxorubicin
Dpf	Days post fertilization
Dpi	Days post injection
ECM	Extracellular matrix
eGFP	Enhanced green fluorescent protein
EMT	Epithelial-to-mesenchymal transition
ETO	Etoposide
ETS	Erythroblast transformation sequence
EwS	Ewing sarcoma
FBS	Fetal bovine serum
IFO	Ifosfamide
Min	Minutes
ml	Millilitres
MMPs	Matrix metalloproteinases
PBS	Phosphate buffered saline
sgRNA	Single guide RNA
STAG2	Stromal antigen 2
VCR	Vincristine

Acknowledgements

First and foremost, I would like to thank my supervisor, Dr. Jason Berman for his endless support, guidance, and for giving me this opportunity, which has helped me grow as both a person and scientist. Secondly, I would like to thank all members of the Berman laboratory for their support, advice, training and friendship. Being part of the Bermanites was an adventure both in and outside the laboratory. Additionally, I would like to express my appreciation to Vinothkumar Rajan for his mentorship, insights and time taken to assist me in troubleshooting experiments. I would also like to thank Mandy Iniguez for her insights towards this project, and the organization and supply of the cell lines used in this study.

I would like to thank members of my committee including Dr. Graham Dellaire, Dr. Kimberly Stegmaier, Dr. Angelica Oviedo, and Dr. Conrad Fernandez for their advice and guidance throughout this process. An additional thank-you to Dr. Oviedo who dedicated time to help organize and analyze the histology samples with me. I am grateful to Dr. Christopher McMaster for taking on the challenge of being my external examiner. Lastly, I would like to thank my family and close friends who offered me love, care and support throughout this process, especially when needed most.

Thank you all!

Chapter 1: Introduction

1.1 Ewing Sarcoma

Ewing sarcoma (EwS) is an aggressive cancer of bone and soft tissue predominately found in children and adolescents between 10-15 years old. While this disease is considered rare, EwS is the second most common bone cancer in children, accounting for 2.9% of all childhood cancers (Crompton et al. 2014 and Chaturvedi et al. 2014). EwS belongs to the "EwS family of tumours", consisting of similar bone cancers, including Askin tumours and peripheral primitive neuroectodermal tumours, that are characterized by an EWS-ETS chromosomal translocation (Chaturvedi et al. 2014).

In addition to the characteristic fusion gene present in EwS, recurrent mutations have been identified in known tumour suppressors; however, the frequency of these mutations is low. In fact, EwS has one of the lowest densities of somatic mutations and structural variations in comparison to other cancers (Chaturvedi et al. 2014 and Crompton et al. 2014). By employing whole genome sequencing, it has been estimated that on average, there are only 361 somatic mutations in non-repetitive regions and six mutations in protein coding regions per EwS tumour (Brohl et al. 2014). Despite the low density of somatic mutations, the three most recurrently mutated tumour suppressor genes in EwS have been described, including *STAG2, CDKN2A and TP53* (Chaturvedi et al. 2014; Crompton et al. 2014; Brohl et al. 2014).

Despite recent advancements in treatment that have increased 5-year overall survival of localized EwS to approximately 70%, the efficacy of these treatments drops

dramatically when the disease metastases, resulting in a poor prognosis of only 15-30% 5-year overall survival (Howlader et al. 2013 and Brohl et al. 2014). Many researchers have now directed their focus towards understanding and identifying key factors involved with promoting metastasis of EwS in hopes to produce new targeted anti-metastatic treatments, and ultimately improve the overall survival of this disease.

1.1.1 EwS Cell Origin

EwS was first described by an American pathologist, James Ewing, in 1921 as a "round cell sarcoma of unknown origin and nature" (Ewing 1921). While Ewing was unable to confidently classify the origin, it was hypothesized to be endothelial. Since then, numerous theories have come forth regarding its histogenesis, including hematopoietic (Kadin and Bensch 1971), fibroblastic (Dickman 1982), neural crest (Cavazzana 1988), and mesenchymal progenitor/stem cells (Riggi 2005). As of late, the latter two are the leading candidates.

The neural crest is a temporary group of cells that arise from the formation of the ectoderm cell layer and later migrate to give rise to numerous diverse cell lineages such as melanocytes, smooth muscle and bone (Staege 2004). It has been identified that EwS expresses similar cell surface antigens as the neuroectodermal lineage (Lipinski 1986) and genes of neural tissues (Staege et al. 2004). In addition, it has been shown that both EwS and peripheral primitive neuroectodermal tumours harbour the same t(11;22)(q24; q12) translocation, a key hallmark of EwS initiation and progression (Staege et al. 2004).

Mesenchymal stem cells are multipotent stromal cells that differentiate into various cell types including osteoblasts, chondrocytes and myocytes. Like the neural crest, mesenchymal stem cells share similarities in relation to the EWS-FLI translocation. For example, upon the introduction of EWS-FLI expression in mesenchymal stem cells xenografted into mice, tumours that formed had a small round cell morphology and the EwS biomarker, CD99. Unlike other human cell types into which EWS-FLI1 expression was induced, mesenchymal stem cells were able to retain the ability to spread and grow (Riggi et al. 2008).

While both theories provide strong evidence, the neural crest and mesenchymal stem cell origin may in fact not be mutually exclusive, but actually be an extension of each other. For example, neural crest stem cells have been shown to contain some mesenchymal lineage plasticity, and likewise, neural derived mesenchymal stem cells have been identified in the bone marrow of developing mice (Lee et al. 2007). Therefore, another recognized hypothesis is that EwS origin could instead derive from neural derived mesenchymal stem cells or neural crest stem cells harbouring mesenchymal potential (Toomey et al. 2010). Nonetheless, further studies are needed to confirm the origin of EwS.

1.1.2 The EWS-FLI1 Chromosomal Translocation

Chromosomal translocations are formed through the mechanical breakage and recombination of two chromosome segments that may result in the fusion of genes otherwise separated. EwS is commonly characterized by the presence of an EWS-ETS

translocation located within the nucleus, known to be a key factor involved with the initiation and progression of this disease (Brohl et al. 2014). Specifically, the majority of EwS cases harbour a chromosomal translocation between the *EWS* gene on chromosome 22 (exon 7) and the *FLI1* gene, a member of the ETS (erythroblast transformation sequence) family of transcription factors, on chromosome 11 (exon 6) (Toomey et al. 2010). This translocation, t(11;22)(q24; q12), has been identified in approximately 85-90% of EwS cases (Howlader et al. 2013 and Brohl et al. 2014). The pathogenic ability of EWS-FLI1 was demonstrated by Franzetti et al who transformed NIH3T3 (fibroblast) cells into tumours upon the induction of EWS-FLI1 expression within xenografted mice (Franzetti et al. 2017).

The amino-terminal EWS portion of the fusion gene is an RNA binding domain of uncertain function but believed to play an important role in transcriptional regulation, oncogene transformation, and the binding of EWS-FLI1 to target genes (Guillon et al 2009). The carboxyl-terminal FLI1 portion of the translocation serves as a DNA binding domain involved with various processes such as hematopoiesis, cell growth and differentiation in humans (Burgert et al. 1990). EwS cells that lack the specific EWS-FLI1 translocation are commonly found harbouring other similar fusion genes involving the *EWSR1* gene paired with either *ERG, ETV1, ETV4 or FEV*, all of which are believed to mimic the same functionality as the EWS-FLI1 chromosomal translocation (Toomey et al. 2010 and Sankar et al. 2011).

The EWS-FLI1 translocation plays an important role in the pathogenesis of EwS by acting as a massive regulator, modulating the expression of target genes and

promoting oncogenesis (Chaturvedi et al. 2014). While little is still understood about this fusion protein, it has been demonstrated through various studies to repress more genes than it activates. In fact, one study alone found 222 downregulated target genes of EWS-FLI1 (> 1.8-fold decrease) that were categorized in three main classes, including those encoding focal adhesion proteins, modulators of the extracellular matrix (ECM) interactions, and regulators of the actin cytoskeleton. All three of these downregulated groups are consistent with cellular phenotypes observed in EwS, such as the regulatory ability of EWS-FLI1 on EwS proliferation and migration, both crucial fundamental components of malignant cancers (Chaturvedi et al. 2014; Brohl et al. 2014; Crompton et al. 2014). As proliferation is a key part of invasion, where the uncontrolled growth of cancer cells can invade the basement membrane into surrounding tissue, different gene expression and microenvironmental ques are required for the migration of EwS cells after invasion. For example, it has been demonstrated that EWS-FLI1 is a suppressor of integrins α1, α4, and β1, and the intercellular adhesion molecule 1 (ICAM1), all cell-matrix interaction proteins, whereas EWS-FLI1 upregulates plakophilin and occludin, which are essential for cell-cell adhesion (Franzetti et al. 2017).

Posttranslational modifications have been identified to play a key role in the regulation of EWS-FLI1 transcriptional activity, including acetylation, phosphorylation, glycosylation, and ubiquitination. For example, the regulation of EWS-FLI1 activity has been demonstrated to be largely due to ubiquitin-mediated processes, where the attachment of ubiquitin triggers a variety of outcomes such as degradation and signalling, depending on the ubiquitin acceptor site and chain link. In addition, it has

been shown that EWS-FLI1 can be deported out of the nucleus for degradation, suggesting tight maintenance of EWS-FLI1 to balance the rapid cytosolic degradation (Gierisch et al. 2016).

Interestingly, a study conducted by Franzetti et al discovered that EWS-FLI1 expression levels may also contribute as a major source of phenotypic cell-to-cell heterogeneity in EwS, enabling individual cells to switch between proliferation and migration (Franzetti et al. 2017). This study further clarified that the capability of EwS cells to switch from proliferation to migration was due to their capability to alternate between EWS-FLI1^{high} levels, shown to promote initiation and proliferation, and EWS-FLI1^{low} levels, which promotes metastasis. This was demonstrated by the doxycycline inducible shRNA knockdown of *EWS-FLI1* in EwS cell lines that decreased cell proliferation and formed a strong tendency for cells to migrate within zebrafish larvae (Franzetti et al. 2017). These findings suggest that the EWS-FLI1 translocation is not only involved with the initiation, progression and proliferation, but also paradoxically, the suppression of cell migration.

1.1.3 Clinical Presentation and Diagnosis of EwS

EwS can present in almost any bone or soft tissue, but most commonly is found in the pelvis, axial skeleton and femur as a solid mass of increasing size (Hakan et al. 2010). Typically, in long tubular limb bones, the lesion is situated in the diaphysis, or midsection of the long bone, rather than the metaphysis, which is the growth plate on either side of the diaphysis and site of the more common osteosarcoma (Heare, Hensley

and Orfano 2009). When the disease metastases, common sites include the lungs, bone, bone marrow, and rarely the lymph nodes, liver and central nervous system (Horowitz et al 1992). As previously mentioned, EwS is predominately found within bone that commonly have soft tissue components, although less than 10% of EwS cases are found isolated to the soft tissue without bone involvement (Nesbit 1990 and Hakan et al 2010).

Through gross inspection of the neoplasm, EwS usually presents as a whitish-gray soft mass that arises in the marrow spaces and is frequently accompanied with necrotic and hemorrhagic areas in and around the tumour (Iwamoto 2007 and Hakan et al. 2010). Due to hemorrhage and thus the onset of inflammation, a misleading diagnosis of infection may occur (Iwamoto 2007).

Symptoms of EwS can be highly variable, and the lack thereof can lead to a delayed diagnosis. Symptoms that arise largely depend on the site of the lesion, however pain is universally the most common symptom, occurring in approximately 90% of EwS cases (Hakan et al. 2010). In addition, fever has been recognized in approximately one fifth of cases, but similarly to hemorrhages, can lead to a misdiagnosis of osteomyelitis, or infection in the bone. Other symptoms include stiffness, pleural effusion (in the context of lung lesions), weight loss, and sometimes a pathologic fracture (Ozaki et al. 2015).

As previously mentioned, the diagnosis of EwS, especially in the early stages can be difficult. Often, without progressing pain, patients do not seek medical attention

until the presentation of a suspicious mass (Iwamoto, Y. 2007). Therefore, delays in diagnosis are most common with tumors located in the central axis, the body core, since tumours need to be extremely large before symptoms occur. Currently, the most common diagnostic imaging techniques includes magnetic resonance imaging (MRI), computed tomography (CT), plain radiography, and biopsies for histological analysis of the tissue in question (Iwamoto, Y. 2007 and Hakan et al. 2010). Using the plain radiograph, EwS may appear as an ill-defined porous lesion accompanied by periosteal reaction, or "onion skin", which appears as new bone formation in response to injury (Horowitz et al. 1992 and Iwamoto, Y. 2007).

Biopsied tissues can be analyzed through various techniques, the most basic being the histological observation of a homogeneous population of small round cells with high nuclear cytoplasmic ratios and increased mitotic activity. In addition, biopsied tissues are commonly analyzed for specific pathologic biomarkers such as CD99 (**Figure1.1.3**). CD99 is a cell surface glycoprotein, encoded by the *MIC2* gene, reported in approximately 90% of EwS cases and used by pathologists as a diagnostic biomarker of EwS (Ambros et al. 1992). Important to note, however, CD99 can also be expressed in other cell types, including leukocytes; therefore, to verify the presence of EwS, further characteristics including lack of neural markers (S-100 protein, leu-7 and PgP9.5), the presence of periodic acid-schiff staining (polysaccharides), and the absence of reticulin and leukocyte markers like CD45 (also called LCA), a common antigen on leukocytes, can be used to help differentiate EwS from other cancers, such as lymphomas and peripheral neuroectodermal tumours (Ambros et al. 1992 and Hakan et al. 2010).

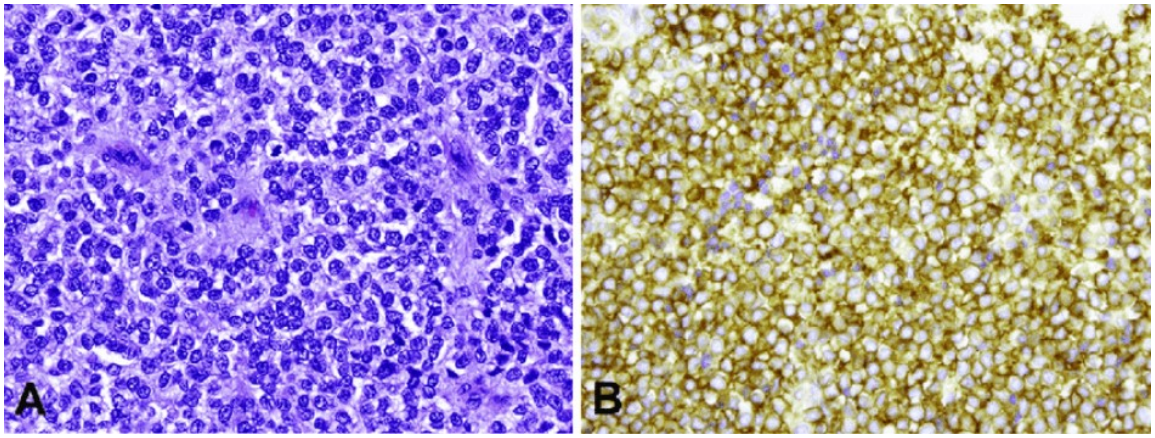

Figure 1.1.3. Microscopic images showing small round cell neoplasms (H&E staining) and strongly positive immunohistochemical staining of CD99 (A) Hematoxylin and eosin staining demonstrates the characteristic EwS morphology including small round cells with a high nuclear to cytoplasmic ratio. (B) Immunohistochemical (brown) staining of CD99 is strongly evident in the membranes surrounding EwS cells. (Figure modified from Choi et al. 2014 with permission (Appendix B)

1.1.4 Treatment and Prognosis of EwS

The most unfavorable prognostic factor in EwS is the presence of distant metastasis and failure of chemotherapy response. In fact, prior to the development of chemotherapies, the 5-year overall survival rate of localized EwS was less than 10% (Horowitz et al. 1992). Due to modern advances in multidisciplinary treatment regimens, including chemotherapy, surgery, radiotherapy and through clinical trials, the 5-year overall survival of patients with localized EwS has risen to 70% (Crompton et al. 2014).

Up until 1960, radiotherapy was the standard treatment until chemotherapy was implemented into treatment protocols (Cripe 2011). Currently, chemotherapy is now the standard treatment for EwS, and consists of various combinations of six drugs including doxorubicin (DOX – antitumor antibiotic), cyclophosphamide (CPM- alkylating agent), vincristine (VCR – vinca alkaloid), actinomycin-D (ACT-D – antitumor antibiotic), ifosfamide (IFO – alkylating agent) and etoposide (ETO – vinca alkaloid) (Burgert et al. 1990 and Ozaki 2015). Upon the establishment of the six drugs as chemotherapies in 1980, overall survival began to dramatically increase (Horowitz et al. 1992).

Following the implementation of chemotherapy, groups such as the Intergroup EwS study, investigated co-treatments on 331 patients displaying localized EwS with VAC and DOX (VACD) regimens, which improved the 5-year overall survival rate. In this study, different combinations of chemotherapies were compared, including VAC regimen only (VCR, ACT-D and CPM) (24% 5-year overall survival), VAC and lung

irradiation (44% 5-year overall survival), and lastly, VACD (60% 5-year overall survival) (Nesbit et al. 1990). Further studies investigated various combinations of drugs in hopes of increased survival. At present, the North American standard chemotherapy is VDC + IE regimens (IFO + ETO) every 2 weeks, as the study conducted by Womer et al showed this regimen was tolerable from the side effect point of view and more efficacious than every 3-week therapy (Womer et al. 2012; Grier et al. 2003; Nesbit et al. 2010). Typically, between 14-17 cycles of chemotherapy are administered with alternating drug regimens and surgery. In addition, EwS is sensitive to radiotherapy, therefore this modality is incorporated between intervals of chemotherapy for local control in dosages of 36-60 Gray (Cripe 2010).

While chemotherapy can be an effective treatment in many cases of EwS, it is also associated with harmful side effects. Side effects of chemotherapy depend on the individual and dosage, however commonly include fatigue, risk of infection, nausea, vomiting, diarrhea, and hair loss (Lau et al. 2005 and Kolb et al. 2013). Long term effects may include cardiac abnormalities (myocardial ischemia or severe arrhythmias from doxorubicin), secondary malignancies (particularly from etoposide), and infertility (from cyclophosphamide and ifosfamide) (Fleischer et al. 2011).

The introduction of new multimodality treatments and techniques have improved the survival of EwS patients; however, these treatments dramatically lose efficacy when the disease metastasizes. Approximately 25% of EwS patients exhibit metastasis at diagnosis, and those with localized EwS typically have micrometastasis in the absence of systemic chemotherapy (Horowitz et al. 1992 and Kolb et al. 2013). Even

in cases of localized primary tumours involving chemotherapy and surgery and/or radiotherapy, patients may still experience metastatic relapse after local control (Wang and Schulz et al. 2006). These results have led to investigating additional potential chemotherapy options and alternative treatments to address the inadequate treatment of metastatic EwS (Lau et al. 2005; Baruchel et al. 2012; Kolb et al. 2013).

1.2 Metastasis

Metastasis is one of the most important aspects of cancer progression and a primary cause of cancer morbidity and mortality, estimated to be responsible for approximately 90% of cancer deaths (Chambers et al. 2002); this observation has remained consistent for over 50 years (Faguet et al. 2008). Throughout the development of cancer, there is a potential risk of cancer cells leaving the primary tumour site to migrate to distant parts of the body. This migration allows for the colonization of cancer to form new tumours that have the capability for secondary metastasis, further increasing tumour burden (Faguet et al 2008 and Seyfried et al. 2013). Despite the serious consequences resulting from tumour metastasis, the exact mechanisms and processes involved with metastatic capabilities are still poorly understood. The difficulty in experimental analysis of metastasis is likely due to the fact it is a “hidden process”, meaning it is dynamic and occurs within the body at different sites, and thus is inheritably difficult to directly observe within typical models without having to sacrifice to observe the internal sites (Seyfriend et al. 2013).

1.2.1 Metastatic Cascade

Metastasis is a multi-event complex process that involves cancer cell detachment from the primary tumour, intravasation into the circulation/lymphatic system, evasion of immune system defense mechanisms, extravasation into distant capillary beds, invasion into surrounding tissues, and ultimately the formation and proliferation of a new secondary tumour (Chambers et al. 2002 and Seyfried et al. 2013) (**Figure 1.2.1**). There are six recognized traits that cells require for malignant growth, including self-sufficiency from external growth signals, insensitivity to negative growth signals, resistance to apoptosis, limitless replicative potential, sustained angiogenesis and lastly the ability to invade distant tissues (Pantel and Brakenhoff 2004).

To metastasize, cancer cells must first detach from the primary tumour and intravasate into the circulation or lymphatic system. Detachment from the tumour mass is commonly associated with the reduction or loss of intracellular adhesion molecules and therefore an increased mobility and penetration through the surrounding stroma (Krakhmal et al. 2015). Cancer cells can migrate either as individual cells or collectively. Within many malignant human tumours, cells migrate and form groups or nests to achieve collective invasion; this collective behaviour is similarly seen in groups of migrating animals to increase protection and probability of survival. Analogously, this behaviour has also been observed in the development of multicellular organisms, such as in the neural crest and neuroblasts during embryonic development (Wang et al. 2016). It has been shown that the more poorly differentiated the cancer, the less likely they are to migrate as a collective group and instead as individual cells. Interestingly,

however, Wang et al also observed that even poorly differentiated cancer cells form loosely attached small nests or intertwined cords as they invade stroma. In addition, while intercellular adhesion appears to be coordinated, cancers cells can be heterogenous, including cells that can be leaders and those that can be followers (Wang et al. 2016 and Liu et al. 2017).

The “leader” and “follower” phenomenon in collective migration is similar to “tumour budding” or clusters of malignant cells commonly located in close proximity ahead of the invasive front of the tumour. These “budding” cells are associated with tumour detachment and a reduced level of the cell-cell adhesion molecule, E-cadherin, a key hallmark of epithelial-mesenchymal transition (EMT). Complete EMT is characterized by the complete transition of epithelial cells to mesenchymal, which will be further discussed in the following section (Grigore et al. 2016). Notably, during the process of EMT, the epithelial originated cells can exhibit both epithelial and mesenchymal characteristics, retaining a hybrid of EMT commonly called partial EMT. Furthermore, partial EMT has been identified to enhance invasion, generate circulating tumour cells or cancer stem cells, and drug resistance (Saitoh 2018). The exact mechanisms underlying a leading cell has not yet been identified.

Upon reaching the vasculature, cancer cells must cross the endothelial barrier to enter circulation (Chiang et al. 2016). Many factors contribute towards successful metastasis of cancer cells, including the microenvironment, proteases, signaling molecules and environmental conditions at the tumour associated vasculature (Chiang et al. 2016 and Petra et al. 2017).

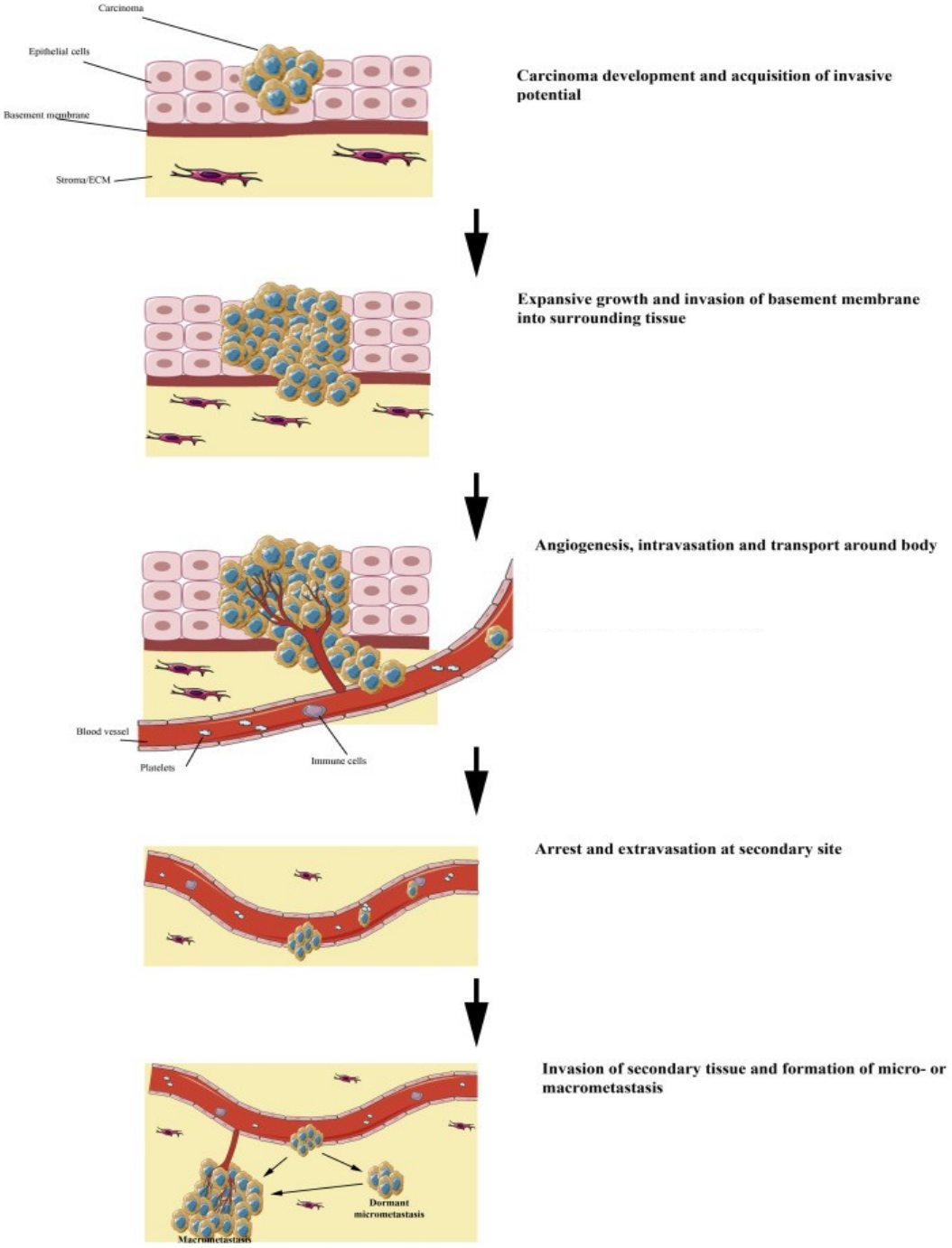

Figure 1.2.1. Illustration of key steps in the metastatic cascade. Following oncogenic transformation of cells, primary tumour cells detach and seek vasculature to obtain oxygen and nutrients for growth and expansion, followed by intravasation into the circulation or lymphatic system. Through exploitation of the vasculature for cell migration, metastatic cancer cells can arrest and extravasate at a distant secondary site to invade and proliferate into a new secondary tumour. (Figure adapted from Jiang et al. 2015 with permission)

1.2.2 Key Factors that Promote Metastasis

It is apparent that the vast majority of tumours cells within a primary tumour, even those of already disseminated tumours, are unable to complete distant metastasis either due to death or dormancy. This dormancy phenomenon is likely the reason why within the clinical setting, cancer patients can be cancer free and later experience relapse (Chiang et al. 2016). Determining key factors that differentiate the successful metastatic or dormant cancer cells from the rest is a main focus of cancer research in the area of metastasis.

One of the basic principles for cancer development is the interplay between oncogenes and tumour suppressors and is thus recognized as a key factor behind the initiation and progression of cancer. Tumour suppressor genes are commonly characterized by their ability to inhibit cell proliferation and tumour development, and therefore loss of function mutations in tumour suppressors are common within cancers to promote replication and metastasis (Albini and Pfeffer 2006). The *TP53* gene is one of the most renowned tumour suppressors, known for its role in the tight regulation of many cellular pathways including cell growth, cell cycle progression, DNA integrity and apoptosis, and thus is frequently mutated in most human cancers (Li et al. 2010).

Interestingly, while approximately 50% of all human malignancies have dysfunctional p53, only 10% of EwS cases have been identified to carry dysfunctional p53, and in fact, *TP53* can paradoxically be found overexpressed. In addition, both the knockout of the *STAG2* gene or silencing of the *EWS-FLI1* fusion gene have been

observed to result in the overexpression of p53 (Albini and Pfeffer 2006; Li et al. 2010). Specifically, EWS-FLI1 has been demonstrated to silence *TP53* through either the Notch signaling pathway or the formation of a protein complex involving EWS-FLI1 and p53 (Van der Ent et al. 2014). Important to note, however, it is still unclear if the interaction between EWS-FLI1 and p53 occurs directly or if it mediated by an oncogenic binding partner. While high expression of p53 has also been identified in other cancers such as intestinal tumour cancers, this phenomenon is still poorly understood as it has been accepted that p53 is a tumour suppressor without enough evidence to suggest otherwise (Albini and Pfeffer 2006; Brohl et al. 2014; Crompton et al. 2014).

In general, a series of cellular events are required to complete cancer metastasis, however in addition, the microenvironment within invasive sites differ from the initial primary tumour microenvironment, triggering multiple stresses at both genetic and epigenetic levels. Numerous studies have emerged focusing on different factors and characteristics of cancer and its microenvironment. The microenvironment has been shown to play a large role in the spread and colonization of different cancer types. This idea was first proposed in 1889 by Stephen Paget who related cancer cells to “seeds” that are dependent upon the “soil” or microenvironment of the organ or tissue. Interestingly, this idea was challenged by James Ewing in 1920, who suggested that there was a circulatory pattern between primary tumours and the specific secondary organ, and that these mechanical factors influenced the tissue that a cancer can access rather than the cancer “homing” to it. Since then, it has been concluded that both hypotheses are correct and not mutually exclusive (Chambers et al. 2002); different

vascular routes affect the metastatic spread, however, the proliferation and colonization of a secondary tumour in a specific site may also depend on the molecular regulation that may or may not stimulate the growth of specific cancer cells**.**

As previously mentioned, EMT is a key factor involved with tumour cells entering circulation and seeding metastasis, allowing cells to adopt a migratory and invasive behavior (Liu et al. 2017). A variety of other mechanisms and molecules have now been identified in the physiological and pathology of EMT, including the modification of cell-substrate adhesion complexes, reorganization of cell-cell complexes, and the expression of multiple proteases including matrix metalloproteinases (MMPs). MMPs can play an important role in cell invasion through the degradation of virtually any component of the ECM and participate in substrate binding (Gilles et al. 2005). In addition, another key factor involved with metastasis and EMT is anoikis resistance. Tumour resistance to anoikis or programmed cell death mediated by the lack of adhesion to the ECM, is driven by (epi)genetic alternations or signal responses from the tumour microenvironment leading to the inactivation of apoptosis. A common hallmark of EMT is the reduction of E-cadherin expression or function, which additionally confers anoikis resistance (Wang et al. 2017).

Despite progression made in gene-expression profiling, the biology underlying patterns of metastasis remain unclear. Research has employed the use of mice xenografts to model metastasis by studying the end-point of metastasis for the identification of molecular alternations in cancer cells that may contribute to metastasis. In addition, direct analysis of EwS samples can provide exploratory measures

for gene-expression profiling, which was used by Crompton et al to identity STAG2 as a newly recognized tumour suppressor that when lost, promotes EwS metastasis (Crompton et al. 2014).

1.3 The *STAG2* Gene and Cohesin Complex

The stromal antigen 2 gene (*STAG2*), located on the X chromosome (Xp25), encodes for the STAG2 protein, one of the core subunits that make up the cohesin complex. Cohesin complexes are composed of a heterodimer that holds together a SMC1 (SMC1A or SMC1B) and SMC3 protein, attached by the hinge domain and RAD21, along with a STAG protein (**Figure 1.3.1**).

Prior to prophase, the cohesin complex is scattered along the chromosome arms, forming a loop around the sister chromatids and maintaining their adhesion throughout most of the cell cycle. During prophase, the cohesin complexes are phosphorylated by polo-like kinase 1 (PLK1), a serine/threonine-protein kinase, and dissociated from the chromatin, aside from the centromeres where the cohesin complex remains. During anaphase, the double-strand-break repair protein (RAD21), a subunit of the cohesin complex, is cleaved leading to dissociation of the cohesin complex from the centromeres and complete segregation of the sister chromatids (Petra et al. 2017). Key functions of the cohesin complex include the organization and arrangement of the sister chromatids during cell division, DNA repair, and importantly in the context of this project, the regulation of gene transcription in both proliferating and non-proliferating cells (Peters et al. 2008).

While mutations in other protein components within the cohesin complex have been associated with aneuploidy, an abnormal number of chromosomes in a cell, this mechanism is not believed to be the case for STAG2 loss in many cancers. Studies investigating this phenomenon confirmed that the majority of cancer cells carrying these *STAG2* mutations, such as EwS and bladder cancer were euploid. Therefore, it is instead hypothesized that STAG2 loss promotes cancer through altering different cohesin functions like transcription regulation (Galeev et al 2016).

Two proteins, WAPL and PDS5, have been identified to directly interact with the cohesin complex, specifically with STAG2 and RAD21. In fact, not only have these proteins been found to regulate STAG2 and RAD21, but their association with the cohesin complex is dependent on the presence of RAD21 and STAG2 (**Figure 1.3.1**). (Peters et al. 2008 and Solomon et al. 2011).

Interactions and key functions of the cohesin complex and STAG2 are still poorly understood, however studies have started investigating implications of STAG2 and the lack thereof, specifically in relation to cancers. A recent study conducted by Crompton et al determined that 88% of EwS patient samples with a complete loss of STAG2 were metastatic (7/8 samples), compared to 27% of metastatic samples that still carried the functional *STAG2* gene (14/51 samples). It was therefore suggested that STAG2 loss is associated with the metastasis of EwS (Crompton et al. 2014).

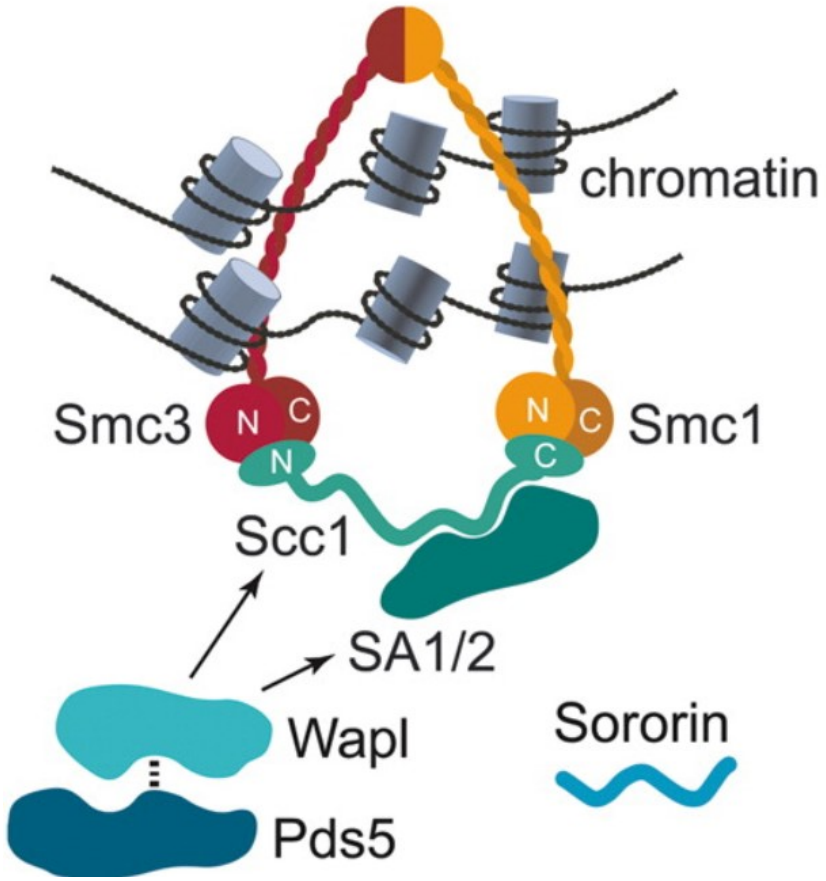

Figure 1.3.1 Illustration of the cohesin complex. The cohesin complex is composed of a heterodimer between SMC1 (SMC1A or SMC1B) and SMC3 proteins, attached by the hinge domain and RAD21 (SCC1), along with the STAG1/2 protein (SA1/2). PDS5 and WAPL are two regulatory proteins associated with STAG1/2 and RAD21 that may play a role with protein-protein interactions. (Figure reproduced from Peters et al. 2008 with permission)

1.3.1 Mutation Induced Loss of STAG2

Numerous studies have identified STAG2 as the most mutated subunit within the cohesin complex associated with multiple cancer types. In fact, recent genome studies have identified *STAG2* as recurrently mutated in the cohesin complex in approximately 7.3% of all human cancers (Peters et al. 2008). Specifically, *STAG2* mutations have been observed in approximately 15-22% of EwS cases (Thota et al. 2014; Daniloski and Smith 2017), and in addition, has been found in 6% of acute myeloid leukemia (AML) (Kon et al 2013), 26% of bladder cancers (Walter et al. 2012), as well as other cancer types.

Most *STAG2* mutations are of deleterious nature, resulting in the loss of function, therefore it is strongly suggested to represent a new tumour suppressor (Daniloski and Smith 2017; Petra et al. 2017). The *STAG2* gene consists of 33 coding exons, however, the majority (83%) of these mutations are located on the coding region and splice sites of exons 9,11,12 and 20 (Solomon et al. 2011). The majority of *STAG2* variants include nonsense, frameshift, splice site and structural variants, and 5' deletions that result in the absence of protein expression (Crompton et al. 2014).

In addition to determining a significant correlation between STAG2 loss and metastasis, the study conducted by Crompton et al carried-out gene set enrichment analysis (GSEA) of 11 EwS samples with loss of STAG2. A metastatic signature is a group of genes in a cell with a unique characterization of gene expression due to the altered or unaltered biological processes of cancer. It was determined that 2/11 samples harboured enriched metastatic signatures including LIAO and BIDUS (upregulated genes

in samples with intrahepatic metastatic hepatocellular carcinoma and genes regulated by endometrial tumours from patients with lymph node metastasis, respectively) in comparison to samples with STAG2 expression (Crompton et al. 2014).

Interestingly, there have been cases documented in which STAG2 was expressed at diagnosis, but lost at the time of relapse, suggesting the acquisition of *STAG2* mutations during the initial treatments or a sub-clonal expansion containing loss of function mutations at the time of relapse (Tirode et al. 2014; Daniloski and Smith 2017).

Throughout various studies, two important genes have emerged in relation to STAG2. Firstly, it has been shown that mutations of *TP53* often co-occur with *STAG2* mutations in patient samples, and both are associated with poor survival (Crompton et al. 2014; Solomon et al. 2011; Brohl et al. 2014). Secondly, by GSEA of RNA sequenced EwS samples, Crompton et al reported that STAG2 loss resulted in a decreased expression of enriched genes otherwise upregulated by EWS-FLI1 activity, likely due to a decrease in EWS-FLI1 chromatin binding in the absence of STAG2 expression (**Figure 1.3.2**). This suggests that STAG2 loss may affect the EWS-FLI1 binding to a subset of chromatin binding locations (Crompton et al. 2014).

Despite these observations, the implications of STAG2 loss and its role in increased metastasis is still poorly understood. Further studies are needed for confirmation in more animal models, some of which may allow for a better observation of migration, such as the transparent zebrafish larvae model.

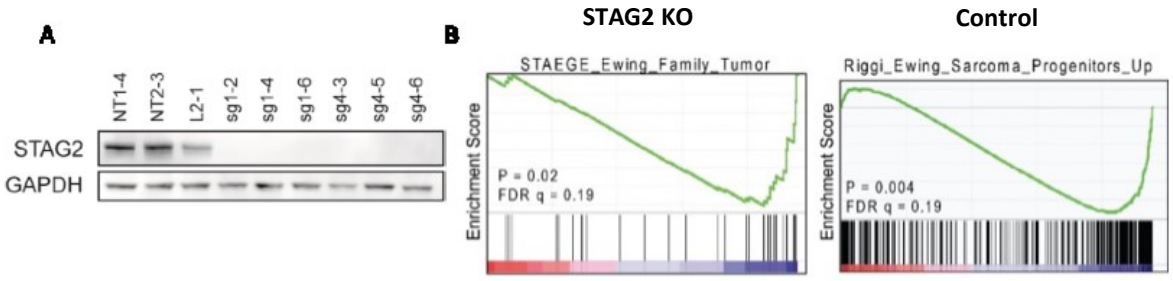

C

ChipSeq Mark	# Peaks	Depleted	Induced
FLI1	2,498	762	19

Figure 1.3.2. STAG2 loss results in a decreased expression of genes upregulated by EWS-FLI1 activity due to a decrease in EWS-FLI1 chromatin binding. A673 EwS cell line clones were engineered with CRISPR/Cas9 technology with different single guide RNAs that result in loss of function frameshift mutations of *STAG2*. (A) Western blot analysis was used for complete *STAG2* knockout confirmation. (B) Two GSEA plots of running enrichment scores for clones confirmed for *STAG2* knockout were selected for transcriptome sequencing (RNAseq). *STAG2* knockout (left) and controls (right) were used to determine the enriched gene score changes of EWS-FLI1 signatures induced by STAG2 loss. (C) CHIP-seq was performed in two controls and two *STAG2* knockout clones to identify changes in the EWS-FLI1 chromatin binding locations. (Figure modified from Crompton et al. 2016 (Appendix B))

1.4 Zebrafish as a Cancer Model

Zebrafish (*Danio rerio*) are small tropical fish located in the fresh water rivers of northern India and Pakistan (White et al. 2008). Both zebrafish adults and larvae are being employed as models to study various human diseases, such as cancer. As early as the 1930s, zebrafish were used as a development and embryological model, and first brought attention to the transparent nature of the larvae allowing for *in vivo* visualization of cell-biological events (Laale 1977). Despite the 300 million years between our last common ancestors, cancer is still much the same between humans and zebrafish. In fact, cancer is commonly seen within fish in the wild, which has been used to investigate the exposure of water-borne carcinogens. It is recognized that teleosts, can display a wide variety of benign and malignant tumours within various organs, much like humans (Hawkins et al 1985 and Spitsbergen et al. 2000).

In the 1980s, the development of genetic zebrafish techniques such as cloning, mutagenesis and transgenesis became available and further expanded the application of zebrafish as a human disease model. Since then, thousands of mutants have been developed, leading to the establishment of zebrafish as a mainstream model. Through the use of mutant and transgenic zebrafish, we can directly address the role of various genes in tumorigenesis and examine metastasis of cancer cells in various microenvironments more similar to that of humans, such as the expression of various growth factors and cytokines known to play an essential role in tumorigenesis (Stoletov and Klemke 2008).

One such example, in relation to this project, is the creation of a transgenic zebrafish line with heat-shock promoter controlled EWS-FLI1 expression that results in the formation of tumours strongly resembling human EwS. Unfortunately, the incidence of tumour formation within these EWS-FLI1 expressing transgenic fish was observed to be relatively low and resulted in abnormalities in development such as stunted growth (Leacock et al 2012).

In addition to genetic screening, small molecule compounds can be directly absorbed by zebrafish within the water, affirming the zebrafish as a prime model for mass drug screening within a multi-cellular organism (Peterson et al 2000 and Kari et al. 2007). Studies have employed zebrafish as a drug screening tool in the search of new EwS treatments. A study conducted by van der Ent et al. discovered that through the combinational treatment of Yk-4-279 and Nutlin 3, an inhibitor of mdm2 (negative regulator of p53), the transcriptional activity of EWS-FLI1 can be blocked while stabilizing p53.

In addition, this study confirmed that the co-treatment of these two drugs inhibited proliferation and migration *in vivo* in zebrafish xenotransplanted with EwS cells (van der Ent et al. 2014). The establishment of zebrafish as a xenograft model has further enhanced experimental capabilities for cancer researchers.

1.4.1 Zebrafish Xenotransplantation

The attention of zebrafish in the field of research has been further fueled by their establishment as a xenograft model, providing an increased understanding and

visualization of human cancer cells engrafted into transparent zebrafish. Xenotransplantation is the process by which species-specific cells or tissue are transplanted into another species to utilize as a biological tool to study the behaviour, response, progression, and metastasis of human cancer cells (van der Ent et al. 2014 and Peterson et al. 2000).

The utilization of zebrafish for xenotransplantation provides many beneficial attributes in cancer research. In comparison to mice, zebrafish require minimum care and thus are more cost effective to maintain in a laboratory setting (Goessing et al. 2007 and Sterri et al. 2003). In addition to being easily maintained, zebrafish reproduce in large quantities, where a pair of zebrafish can produce hundreds of offspring weekly that develop rapidly. In fact, zebrafish larvae can be used for xenotransplantation as early as two days post fertilization and can remain self-sufficient for up to seven days, using the yolk sac as their source of nutrition.

Zebrafish share a high degree of genetic conservation to humans, sharing approximately 70% of our protein-coding genes, and 84% of genes known to be associated with human disease (Howe 2013). In addition, one of the major advantages of zebrafish xenotransplantation is the immature immune system of larvae, which lack an adaptive immune response for up to 4-6 weeks post fertilization. This offers an advantage in comparison to mice models, where immunosuppression is not a necessary variable (Trede et al. 2004). Lastly, another important aspect of zebrafish for xenotransplantation of cancer cells is the transparency of larvae, which allows for

repeated *in vivo* imaging of xenografted cancer cells, and the direct visualization of the progression and spread of human cancer cells without having to sacrifice their host.

As previously mentioned, multiple mutant zebrafish lines have been developed throughout the years to advance our ability to investigate cancer progression and metastasis. One such example includes the development of the roy$^{-/-}$; nacre$^{-/-}$ (*casper*), a zebrafish double mutant model that lacks melanocytes and iridophores resulting in larvae and adults being predominately transparent (**Figure 1.4.1A**). Due to lack of pigmentation, there is a dramatic reduction in light absorption and reflection, enabling the use of fluorescent microscopic imaging of *in vivo* processes (Delov et al. 2014 and White et al. 2008). An additional zebrafish model that enhances fluorescent microscopic visualization is the transgenic *Tg(fli1a: eGFP)* zebrafish larvae *caspers* (**Figure 1.4.1B)**. This transgenic fish expresses enhanced green fluorescence protein (eGFP) in endothelial cells under the control of the *fli1a* promoter, enabling clear visualization of the vasculature and any defects that may arise (Delov et al. 2014).

Zebrafish provide multiple sites that can be utilized for xenotransplantation to investigate different cancer behaviour characteristics such as metastasis, proliferation and angiogenesis. Published sites include the yolk sac, hindbrain ventricle, duct of Cuvier (circulation), and the caudal vein (Corkery et al. 2011 and Veinotte et al. 2014). Different sites can be more advantageous than others based upon the behaviour being studied and the cancer cell type. For example, to study the metastasis of solid tumours, such as Ewing sarcoma, the initial injection site should be injected into a closed cavity to study both the invasion out of the initial site and migration to the rest of the larva, whereas

hematopoietic cancers, such as AML, are better suited to be directly injected into circulation.

Importantly, in context of this project, the use and publication of the zebrafish model has previously been employed to investigate EwS metastasis in Dr. Jason Berman's laboratory with collaborators. In this study, *casper* mutants were used as the xenotransplantation model to investigate the role of Y-box binding protein 1 (YB-1) in the metastasis of EwS. Through the transplantation of fluorescently labeled TC32 EwS cell lines harbouring knockdown of the *YB-1* gene, significantly reduced migration was observed, and aided in the establishment of YB-1 as a critical regulator of hypoxia-inducible factor 1α (HIFI1α) expression in EwS (El-Naggar et al. 2015).

This study highlighted the relevance of using zebrafish as a cancer model to observe and discover mechanisms of EwS metastasis. Using both *casper* and transgenic *Tg(fli1a:eGFP) casper* larvae, the metastatic capability of EwS can be directly imaged and recorded, granting a deeper understanding and visualization of processes such as metastasis that otherwise would be a "hidden process".

A

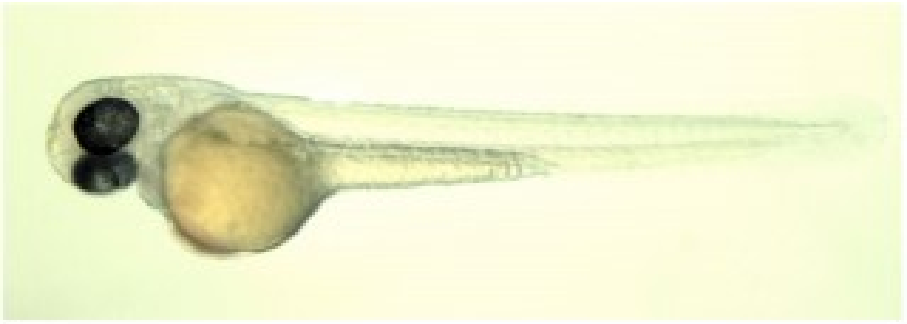

B

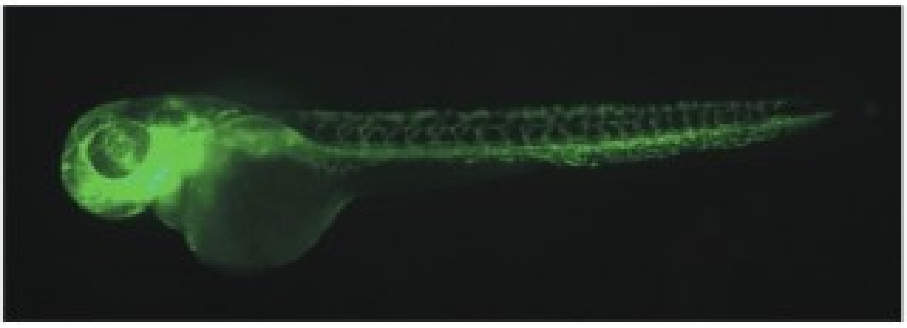

Figure 1.4.1. Select mutant zebrafish lines. (A) a 2-days post fertilization (dpf) transparent *casper* mutant zebrafish larva and (B) a 2dpf transgenic, *Tg(fli1a:eGFP) casper* zebrafish larva, with GFP labeled vasculature under the *fli1a* promoter gene. This project includes both zebrafish lines, however the majority of experimentation was completed using *casper* larvae. (Figure modified from panel developed by Andrew Coombs and Angela Young of the Berman Laboratory)

1.5 Rationale

Given the difficulties of direct observation of cancer cell migration in mice models, new animal models such as transparent zebrafish can be additionally used to study metastasis; a vital understanding that can help discover and develop alternative methods of therapeutics to improve the poor survival of this disease. This is especially true for patients with metastatic EwS, having a 5-year overall survival rate of only 15-30% despite recent advances in treatment. In addition, a large portion of patients that are initially diagnosed with localized EwS will experience relapse and share similar fates to that of metastatic EwS. Moreover, through the use of zebrafish larvae as a transplantation model, we can directly observe the effects of STAG2 loss in EwS and observe patterns of migration to expand our knowledge of its metastasis.

I hypothesize that EwS cell lines will be successfully xenografted into the zebrafish larvae and exhibit similar metastatic behaviour to that observed in human patients. I also hypothesize that knocking out the *STAG2* gene will promote the migration of EwS cell lines, and alter various gene transcript levels, such as *EWS-FLI1*.

In summary, prior to this project, EwS cells have been successfully xenotransplanted into zebrafish larvae and displayed metastatic behaviour (El-Nagger et al. 2015). In addition, STAG2 loss has been shown to promote an increased metastatic capability, and alter transcriptional regulation of various genes, such as *EWS-FLI1* (Crompton et al. 2014). In the context of these previous findings, the goal of this study is to use the zebrafish larvae xenotransplantation model to study EwS migration and

investigate the role of STAG2 loss in this process. In addition, the goal of this study is to investigate potential mechanisms underlying STAG2 loss and cell migration, including EWS-FLI1 expression, anoikis resistance, and downstream genes altered by STAG2 loss.

Chapter 2: Methodology

2.1 Zebrafish Husbandry and Care

Zebrafish (*Danio rerio*) were raised and maintained according to standard protocol (Hans et al. 2007 and White et al. 2008). Zebrafish *Tg(nacre$^{-/-}$; roy$^{-/-}$)*, commonly called *caspers*, genetically modified zebrafish demonstrating a complete lack of melanocytes and iridophores, were used for all *in vivo* experiments. For the twelve-hour time lapse study, *casper* larvae expressing eGFP under a *fli1a* promoter, *Tg(fli1a:eGFP),* were used to exploit their fluorescent vasculature. Adult fish were maintained in a recirculating commercial housing system at 28.5˚C under a 14:10 light: dark condition schedule. The optimal temperature for zebrafish growth occurs at 28°C, however, to accommodate the injected cancer cell lines, zebrafish larvae employed for xenotransplantation experiments were incubated at 35°C to allow for normal growth and development of both zebrafish and injected cell lines (Lee et al. 2005; Haldi et al. 2006). All zebrafish larvae were maintained in E3 embryo medium (5 mM NaCl, 0.17 mM KCl, 0.33 mM $CaCl_2$, 0.33 mM $MgSO_4$) in 10 cm petri dishes. Larvae were cleaned and provided with new media daily. Larvae were euthanized by tricaine overdose (1mg/ml) at seven days post fertilization (dpf), followed by 6.15% bleach solution to ensure complete mortality prior to disposal. Use of zebrafish in this study was approved by the Dalhousie University Committee of Animal Care (protocol # 17-005).

2.2 Cell Lines and Cell Culture

EwS cell lines were provided by Dr. Kim Stegmaier's lab (Dana-Farber Cancer Institute, Boston United States). STAG2 protein expression was knocked out in two human EwS cell lines (A673 and TC71) using CRISPR/cas9 technology with different single guide RNAs (sgRNAs) including TC71 (sg1-6, sg4-15 and sg4-18) and A673 (sg4-6 and sg1-2). Non-targeting (NT) cell lines including NT2-3 (A673), NT2-5 and NT1-6 (TC71) served as controls (**Table 2.2**).

Human EwS cell lines were treated with 1 µg/ml of puromycin (Gibco A11138-03) for the duration of three days to select for cells with successful knockout of *STAG2*. EwS cell lines were grown to no more than 80% surface confluency and trypsinized with 0.25% trypsin ethylenediaminetetraacetic acid (EDTA) (Gibco). TC71 cell lines were cultured in Roswell Park Memorial Institute medium (RPMI) 1640 (Gibco) and supplemented with 10% fetal bovine serum (FBS) (Wisent). A673 cell lines were cultured in 1X Dulbecco's Modified Eagle Medium (DMEM) (Gibco) with 10% FBS and 1% 100mM sodium pyruvate (Gibco).

Table 2.2. CRISPR target guides used to create A673 and TC71 *STAG2* knockouts and NT controls. The first number following sg/NT represents the sgRNA used and the second number refers to the clone number used for expansion and experimentation. For example, cell lines called sg4-15 represents the guide sgSTAG2-4 and the clone number 15, which was selected for expansion and expression. (Figure adapted with permission from Crompton et al. 2014)

Designation	Target Sequence
sgNT-1	GTAGCGAACGTGTCCGGCGT
sgNT-2	GACCGGAACGATCTCGCGTA
sgSTAG2-1	ATTTCGACATACAAGCACCC
sgSTAG2-2	AATTCATTGGCGTGTTAGTA
sgSTAG2-4	TGGAGATTATCCACTTACCA

2.3 Labeling Cell lines

EwS cell lines (~5 million cells) were transferred into 15 ml Falcon™ conical centrifuge tubes post trypsinization. Cells were centrifuged for five minutes at 450xg and supernatant was removed. Cells were re-suspended in 10 ml of 1X Phosphate Buffered Saline (PBS) (Gibco) with the addition of 30 µl of Cell Tracker Orange (50 ul in 1ml DMSO) (CMTMR) dye (Orange excitation/emission spectra of 541/565 nm maxima) (Invitrogen) and incubated at 37°C for 20 minutes. To remove excess dye, cell lines were washed three additional times, twice with 10 ml of 1X PBS and once with medium before resuspension in approximately 80 µl of flow buffer (1X PBS with 2% FBS and 1mM EDTA solution).

2.4 Xenotransplantation

At 2dpf, *casper* zebrafish larvae were re-located to 35°C for approximately one hour prior to xenotransplantation. Larvae were anesthetized with a 5% Tricaine (ethyl 3-aminobenzoate methane sulfonate salt, MS -222, Sigma –Aldrich) solution prior to injections. Larvae were arrayed on a six-lane indentation agarose plate made with 60 ml embryo water and 1.2 g agarose (Fisher Scientific) to hold anesthetized zebrafish in place. Capillary injection needles were pulled using a micropipette puller (Sutter Instrument Co. Model: P-97) and were backloaded with 10 µl of fluorescently labeled EwS cell lines. Approximately 50-100 EwS cells (TC71 or A673) were manually injected into the yolk sac or hindbrain ventricle of each larvae using a PLI-100A Pico-injector microinjection system (Harvard, Apparatus, Holliston MA).

Following injections, zebrafish were kept at 35°C for the remainder of experiments. Approximately four hours post injection, zebrafish were screened for the presence of fluorescent cells. Larvae with hindbrain ventricle xenotransplanted EwS cell lines were screened to ensure no cells were present outside the initial injection site. Larvae with yolk sac xenotransplanted EwS cell lines were screened for a uniform solid bolus and the absence of local or distal migration. This screening process was used to ensure cellular migration was not due to injection error. Positively screened larvae were collected for further experiments, while negatives were sacrificed and discarded.

2.5 Live Cell Microscopy and Cell Migration Assay

Fluorescently labeled A673 or TC71 cell lines were injected into the hindbrain ventricle (**Figure 2.5.1A**) or yolk sac (**Figure 2.5.1B**) of 2dpf larvae and monitored for migration over five consecutive days post injection (dpi). An inverted Axio Observer Z1 microscope equipped with a Colibri LED light source (Carl Zeiss, Westlar, Germany), an Axiocam Rev 3.0 CCD camera, and Axiovision Rel 4.0 software (Carl Zeiss Microimaging Inc.) were used to observe the migration of fluorescent EwS cell lines within the transparent zebrafish larvae model. Microscope LED excitation/emissions include BFP: 405 nm, GFP:488 nm, and red fluorescence: 555 nm.

Each day post injection, hindbrain ventricle xenotransplanted larvae were scored for the presence or absence of migrated EwS cells in specific locations, including the dorsal surface, yolk sac and tail **(Figure 2.5.2)**. Regarding yolk sac xenotransplantation site larvae, only local dissemination within the yolk sac and presence of migrated EwS

cells to the tail were scored. Three replicates (n=50-70 zebrafish larvae) were completed for each cell line. To validate the absence of passive spread of EwS cells from the hindbrain ventricle, fluorescent microspheres sized at approximately 10 microns (123 CounteBeads Invitrogen Thermo Scientific) were injected into the hindbrain ventricle and monitored for migration for five consecutive days. Following the completion of the migration assays, one sgRNA *STAG2* knockout and control was selected for each cell line for further experimentations. Selected cell lines included TC71 sg4-15, TC71 NT2-5, A673 sg4-6, and A673 NT2-3.

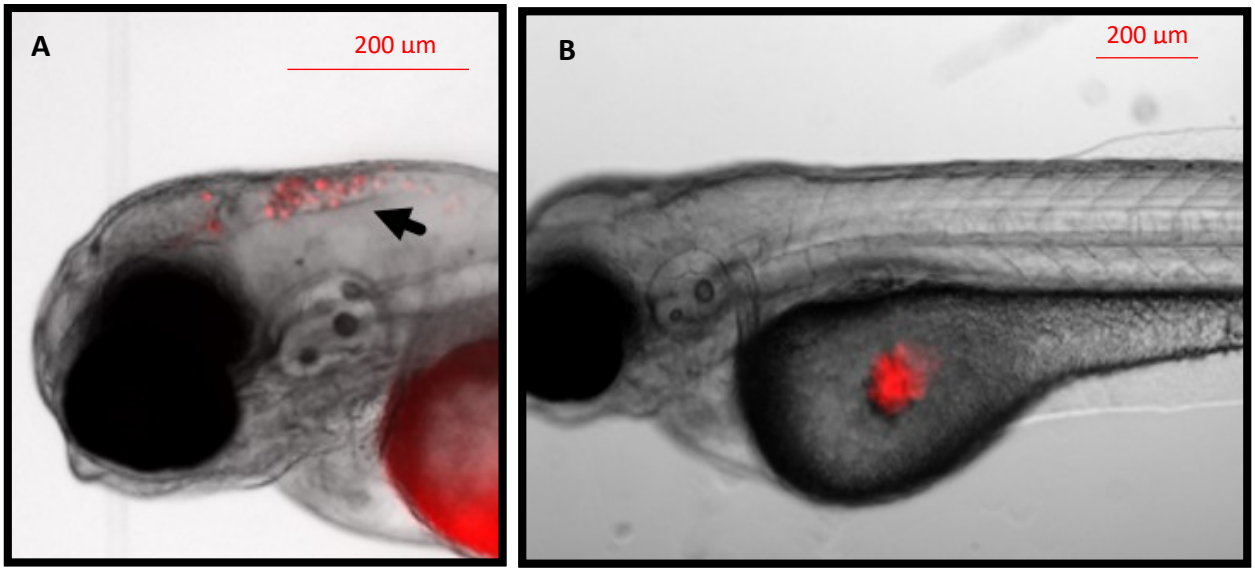

Figure 2.5.1. Visualization of hindbrain ventricle and yolk sac injection sites. Approximately 50-100 fluorescently labeled EwS cells were injected into the hindbrain ventricle (A) or yolk sac (B) of 2dpf zebrafish larvae. (A) Injection needle tip was positioned perpendicular to the otolith of the 2dpf zebrafish larvae and inserted directly into the hindbrain ventricle for xenotransplantation. (B) Needle was inserted directly into the yolk sac to inject a uniform bolus of cells located in the center of the yolk sac.

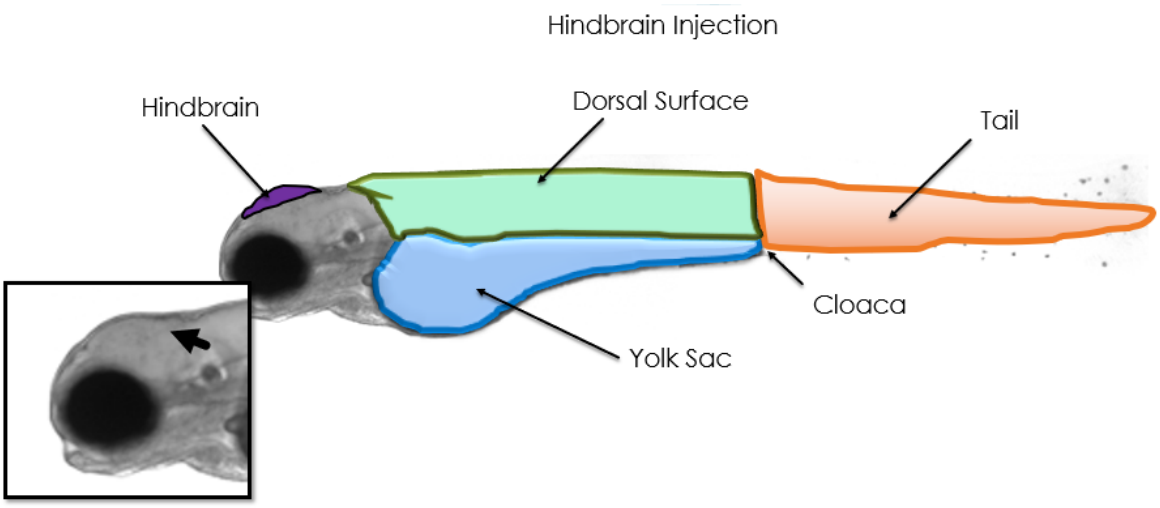

Figure 2.5.2. Illustration of the areas of interest for migration assays. The hindbrain ventricle was the site for EwS cell line injection. Areas of interest included the dorsal surface, yolk sac and tail (posterior to cloaca). Each area of interest was scored for the absence or presence of migrated A673 or TC71 cell lines.

2.6 Cell Proliferation and Viability Quantification

To determine the proliferation rate of EwS cells within the hindbrain ventricle, 15-20 xenotransplantation larvae were selected 1dpi (baseline), 3 and 5dpi (endpoint) (Corkery et al. 2011). Larvae were sacrificed by tricaine overdose and resuspended with 1 ml of 1X PBS in a 1.5 ml Eppendorf tube followed by the addition of 54 µl collagenase (Sigma-Aldrich, Oakville, ON, Canada) at 100 mg/ml. Samples were heated to 37˚C for approximately 30 minutes to dissociate the larvae into a single cell suspension. In addition, physical force was exerted by pipetting samples up and down ten times at five to ten-minute intervals until samples were visibly dissociated. Following dissociation, the addition of 200 µl FBS was added to slow the enzymatic reaction of collagenase, preventing further breakdown. Samples were centrifuged at 450xg for five minutes and washed with 1 ml of 30% FBS/PBS solution. Samples were centrifuged again and resuspended in FBS/PBS at a final volume equivalent to 10 µl/ larvae.

Ten boli of 10 µl were dropped onto a Superfrost microscope slide (Fisher Scientific) and left for 15 minutes to allow for suspended cells to settle to the surface of slide. Each bolus was imaged using the fluorescent Axio Observer Z1 microscope at 5x objective under the 541/565 nm maxima fluorescence channel within a six-tile grid. Cell quantification was calculated using the ImageJ™ program (NIH, Bethesda, MD, USA), where the average number of cells per larvae was determined (Corkery et al. 2011).

2.7 Histology of Injected Zebrafish

TC71 sg4-15 and A673 sg4-6 cell lines were separately injected into the hindbrain ventricle of zebrafish larvae and screened for the presence of migrated cells 3dpi. Three larvae of each cell line containing migrated cells were selected, sacrificed, and placed into 10% formalin prior to sending to the IWK Histology Lab. Larvae were cross sectioned and stained with both H&E and human CD99, a marker only expressed in human EwS cells.

2.8 Time Lapse Imaging

Two dpf *caspers* and transgenic *Tg(fli1a: eGFP) casper* larvae were xenotransplanted with fluorescently labeled TC71 sg4-15 (*STAG2* knockout) cells and screened for one larvae to be used for twelve-hour time lapse imaging. Prior to imaging, the selected larva was anesthetized in 2% tricaine water and transferred into 0.7% Ultrapure™ low melting point agarose at 35˚C to hold the larvae placed in a glass bottom microscopic plate with a 1.5 mm coverslip, positioned in a lateral orientation. After the agarose solidified, Methylene-blue free E3 medium with 2% Tricaine was added.

Twelve-hour time lapse imaging was done using the Axio Observer Z1 microscope (Zeiss) to capture emission at 541/565 nm maxima (CMTMR) and brightfield (white light) or 492/517 nm maxima ((eGFP) fluorescence (*Tg(fli1a:eGFP) casper* larvae) of the desired larva every five minutes. The 541/565 nm emission channel granted visualization of xenotransplanted TC71 cells; brightfield captured the zebrafish under

white light, and the GFP channel visualized the eGFP fluorescent vasculature of the *Tg(fli1a:eGFP) casper* larvae. This method was used to identify specific routes of migration used by xenotransplanted EwS cells out of the hindbrain ventricle throughout the larva.

2.9 Flow Cytometry – Live Cell Annexin V Staining Anoikis Assay

Approximately $1x10^5$ cells of each cell line (TC71 4-15, TC71 2-5, A673 4-6, and A673 2-3) were seeded into separate wells of 12-well plates (VWR), one coated with PolyHEMA to prevent cellular adherence, and one uncoated that served as control. Two extra wells containing either A673 or TC71 cell lines were treated with 0.05% of Camptothecin stock solution (20 mM diluted in DMSO) (Cayeman Chemical company) four hours prior to flow cytometry measurements to serve as apoptotic controls.

After two days incubation, cells were collected first by harvesting the media to account for floating dead cells and then 0.5 ml of Accutase followed by termination of reaction using complete culture media. Samples were centrifuged at 450xg for five minutes and supernatant was discarded. Samples were washed twice with phosphate buffered saline (PBS) (Gibco) and resuspended in 1X binding buffer (BD Pharmingen PE Annexin V Apoptosis Detection Kit) at the concentration of approximately $1x10^6$ cells/ml. Next, 100 µl of each sample was transferred to a 5-ml culture tube followed by the addition of 5 µl of PE Annexin V (BD Pharmingen PE Annexin V Apoptosis Detection Kit) and incubation for 15 minutes in a dark room. Lastly, an additional 400 µl of 1X binding buffer was added to each sample before 4 µl of 7AAD viability staining solution

(Invitrogen eBioscience™) was added. Compensation was performed using unstained, Annexin V staining only, and 7AAD only controls, and Camptothecin treated cells labelled with both 7AAD and Annexin V staining served as positive staining controls. Samples were read with a BD Fortessa flow cytometer with a green laser (532 nm), a band pass filter 575/25 (PE), and a band pass filter 660/40 (7AAD).

2.10 AlamarBlue® Cell Viability Assay

Approximately 5000 cells were seeded into each well of a 96 well plate (Corning™). Following a 24-hour incubation, AlamarBlue™ (Thermo Fisher Scientific) was added accounting 10% of the media volume and left to incubate for a three-hour period. The plates were read in a Tecan MzooPro plate reader at the excitation wavelength of 540- 570 nm. Viable cancer cells metabolize/reduce resazurin, found in the AlamarBlue™ dye, to resorufin, which emits fluorescence at 590 nm, therefore the amount of fluorescence is proportional to the number of viable cells.

2. 11 Western Blot Analysis

2.11.1 Preparation of Samples

Cells were harvested after the addition of 1 ml trypsin and the neutralization of whole cell media. Cells were washed twice with 10 ml of 1X PBS and centrifugated at 450xg. Cells were resuspended in a 1.5 ml Eppendorf with 50 µl of lysis buffer (2 mM of sodium orthovanadate, 10 mM NaF, 20 mM sodium beta-glycerolphosphate, and 1 mM PMSF in RIPA (Sigma)) and 1X protease inhibitor (Complete Mini Roche), then chilled on ice for 30 minutes to allow for complete cell lysis. Cells were centrifuged at maximum

rotation (~16,000xg) for 10 minutes at 4˚C to remove cellular debris. Protein concentration was determined by BCA using the microBCA protein assay kit (Pierce, Thermo Scientific).

2.11.2 Western Blotting

Briefly, protein were reduced by boiling in Lamelli buffer containing 2-Mecaptoethanol. Proteins were separated by molecular weight using a 12 well mini-protean TGX precast gels (BioRad). Protein were transferred to PVDF membrane (0.45 pore size; Immun-Blot®) and the transfer was performed at 90v for an hour using a Criterion™ blotter transfer apparatus (BioRad). Total protein was estimated by soaking the PVDF membrane in 0.1% Naphthol Blue Black stain (0.1% Naphthol, 10% MeOH and 2% CH_3COOH diluted in H_2O) for 20 minutes, followed by multiple rinses with water. Lastly, imaging was done with a ChemiDoc™ Touch Imaging System (BioRad).

Prior to adding secondary antibodies, each membrane was washed three times, 5 minutes each, with 1X TBST at room temperature. Secondary antibody solution (5% filtered milk powder (Carnation fat-free instant skim milk powder) diluted in 1X TBST, and anti-mouse (1:2500, Cell Signaling) or rabbit antibody (1:2500, Cell Signaling)) were added to the designated membrane and left on a shaker for one hour at room temperature. Triplicate washes were done with 1X TBST for five minutes. The western blot was developed using Enhanced Chemiluminescence (Super Signal® West Dura Extended Duration Substrate (Thermo Scientific)) and imaged using BioRad ChemiDoc™ Imaging Touch System. Western blot bands were quantified using ImageLab ™ software.

2.12 RNA Isolation for Targeted Transcriptome Analysis

Each cell line, including TC71 sg4-15 (*STAG2* knockout), NT2-5 (control), A673 sg4-6 (*STAG2* knockout) and NT2-3 (control), were fluorescently labeled and xenotransplanted into the hindbrain ventricle of 2dpf larvae. At 3 dpi, larvae were screened for migration and sacrificed. Immediately following euthanasia, the head of each larvae was dissected from its body (**Figure 2.12.1**). The head, containing the non-migrated EwS cells, and the body, containing the migrated EwS cells, were transferred into separate Eppendorf tubes containing 0.5 ml of TRIzol™ Reagent (Ambion®). Approximately one hundred injected larvae of each cell line were collected over two consecutive weeks. In addition to the head and tail samples, un-injected samples of each cell line were harvested with TRIzol™ for targeted transcriptome analysis. Following suspension in TRIzol™, all samples were homogenized using the powerGen125 (Fisher Scientific).

RNA was extracted using TRIzol™ with Phasemaker™ tubes (Thermo Scientific) and resuspended in nuclease free water. RNA was also isolated from freshly cultured cell lines and harvested. The RNA quantity and quality were validated using the Nanodrop^{c} prior to shipping to University of Washington, St.Louis for a targeted RNAseq using QIAseq Targeted RNA panel specific for Human Cancer Transcriptome (Qiagen, RHS-003Z). This can provide transcriptome data for 395 commonly mutated genes in cancer.

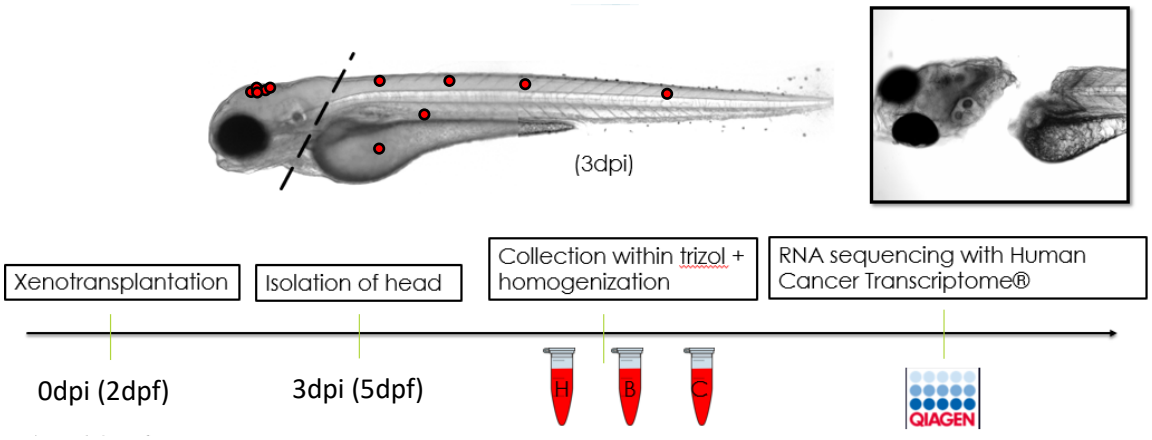

Figure 2.12.1. Collection of migrated and non-migrated EwS cell lines for targeted transcriptome analysis. Each of the EwS cell lines (TC71 sg4-15, TC71 NT2-5, A673 sg4-6, and A673 NT2-3) were injected separately into 2dpf *caspers* and screened at 3dpi to select larvae with the presence of migrated EwS cells. "H" represents head, "B" represents body, and "C" represents cell lines only. Following sacrifice of selected larvae, the head was separated from the body through a diagonal incision starting at the pericardium in tangent to the yolk sac to prevent hindbrain ventricle disturbance.

2.13 Statistical Analysis

Unpaired two tailed t-tests were used to analyze differences in intensities for the western blots, AlamarBlue® cell viability assays and flow cytometry. Proliferation assays were analyzed using a two-way Anova comparison with post Bonferroni. Lastly, migration assays were analyzed using comparison of proportions N-1 Chi-squared test as recommended by Campbell (2007) and Richardson (2011).

Chapter 3: Results

3.1 The Hindbrain Ventricle of Zebrafish Larvae is an Optimal Site to Inject EwS Cells to Evaluate Migration

Historically, the yolk sac of zebrafish larvae has been thought to be the ideal initial site for evaluating cell migration mainly because the yolk sac offers a physiologically isolated cavity where a large quantity of cells can be xenografted and migratory changes can be clearly outlined (El-Nagger et al. 2015; White et al. 2008; Corkery et al. 2011). Upon EwS cell line injection, there was almost no significant difference in migration observed between *STAG2* knockout cells and control cells for both the A673 and TC71 cell lines (**Figure 3.1.1**). While there was a large percentage of larvae with migration within the yolk sac, very little larvae displayed the presence of EwS cells in the tail for both control and *STAG2* knockout cell lines. In fact, the only difference observed was at 4dpi for the A673 cell line, where the control cells (NT2-3) had significantly increased local dissemination within the yolk sac. No significant difference in distal migration to the tail between *STAG2* knockout cells and control cells was observed for both TC71 and A673 cell lines (**Figure 3.1.2**). The lack of significant difference between *STAG2* knockout and control cells called into question the yolk sac as the optimal injection site for migration evaluation. As an alternative strategy, the hindbrain ventricle was explored as an injection site to evaluate EwS cell migration (Haldi et al. 2006).

There was a significantly higher rate of larval mortality when EwS cell lines were injected into the yolk sac compared to the hindbrain ventricle. No significant difference was observed between the mortality rate of STAG2 knockout or control Ewing sarcoma cell line injected larvae. At 3dpi, the mortality of larvae injected with either control or *STAG2* knockout A673 or TC71 cell lines into the yolk sac was approximately 54-57%, but only 9-11% when injected into the hindbrain ventricle (**Figure 3.1.3**). At 5dpi, the mortality rate of larvae injected with either control or *STAG2* knockout A673 or TC71 cell lines into the yolk sac was approximately 95% compared to 23-39% when injected into the hindbrain ventricle (**Figure 3.1.3**). The same larval mortality pattern was observed for all additional EwS sgRNA *STAG2* knockout cell lines that were injected into the hindbrain ventricle. Based on these data, the hindbrain ventricle was chosen as the initial injection site to conduct EwS migration assays in the zebrafish larvae in all subsequent experiments.

The hindbrain ventricle is not as biologically inert as the yolk sac, so there arises a question if the cells could migrate outside of the hindbrain due to physiological reasons. To verify the absence of passive spread of EwS cells out of the hindbrain ventricle, fluorescent microspheres were injected into the hindbrain ventricle of 2dpf zebrafish and monitored for five consecutive dpi. No spread of microspheres was observed to the dorsal surface, yolk sac or tail. The only movement of microspheres was at 4dpi and 5dpi to the thymus (approximately 30% of larvae), found below the otolith (**Figure 3.1.4**).

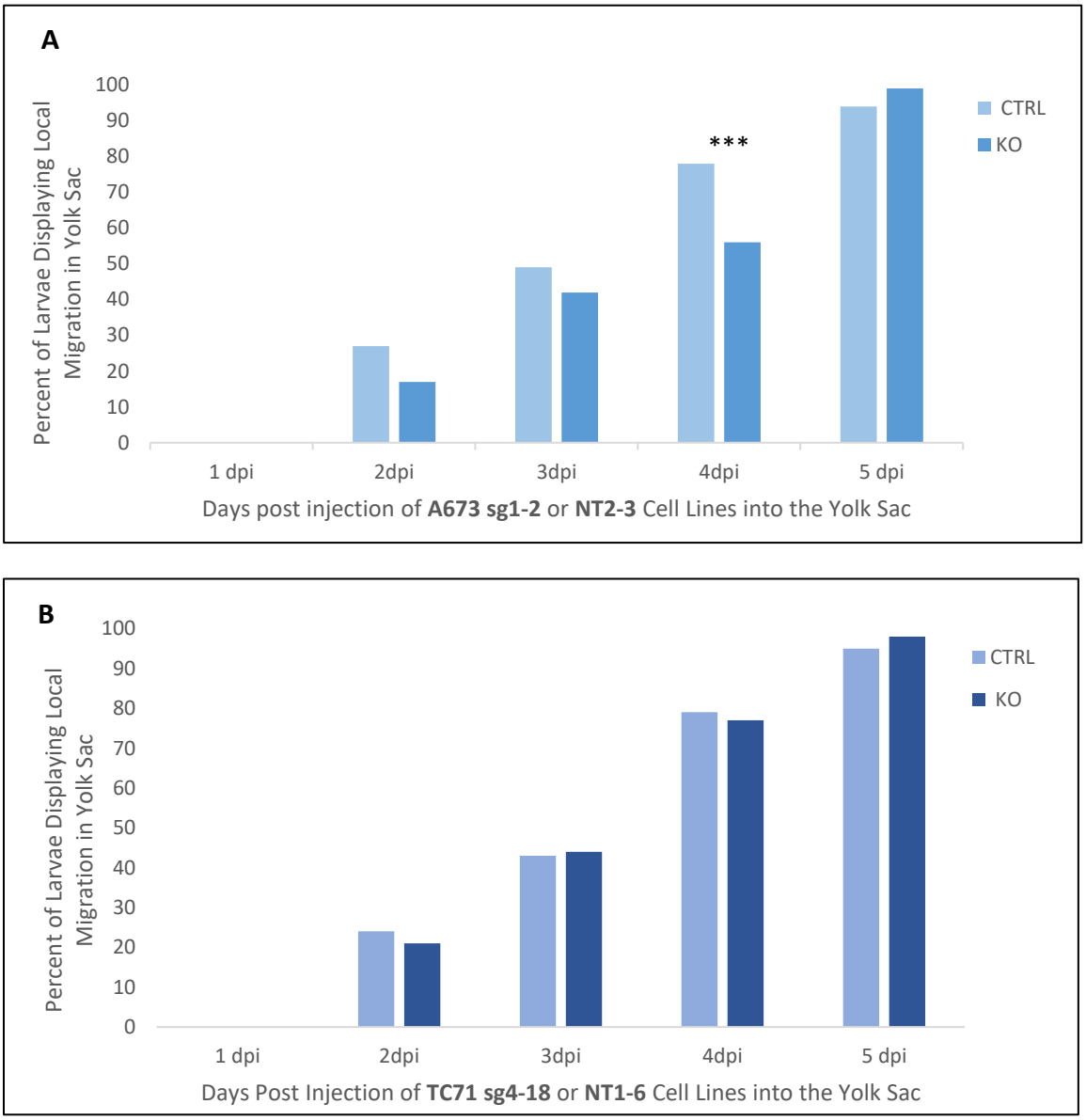

Figure 3.1.1. *STAG2* Knockout in A673 and TC71 cell lines does not promote local migration when injected into the yolk sac. Zebrafish larvae were monitored for the presence of local migration within the yolk sac for five consecutive days post injection. Either (A) A673 sg1-2 (*STAG2* knockout)/NT2-3 (control) or (B) TC71 sg4-18/NT1-6 cell lines were injected into the yolk sac of 2dpf larvae. Three replicates were completed for each cell line (n=50-70 larvae each). *** $p<0.001$.

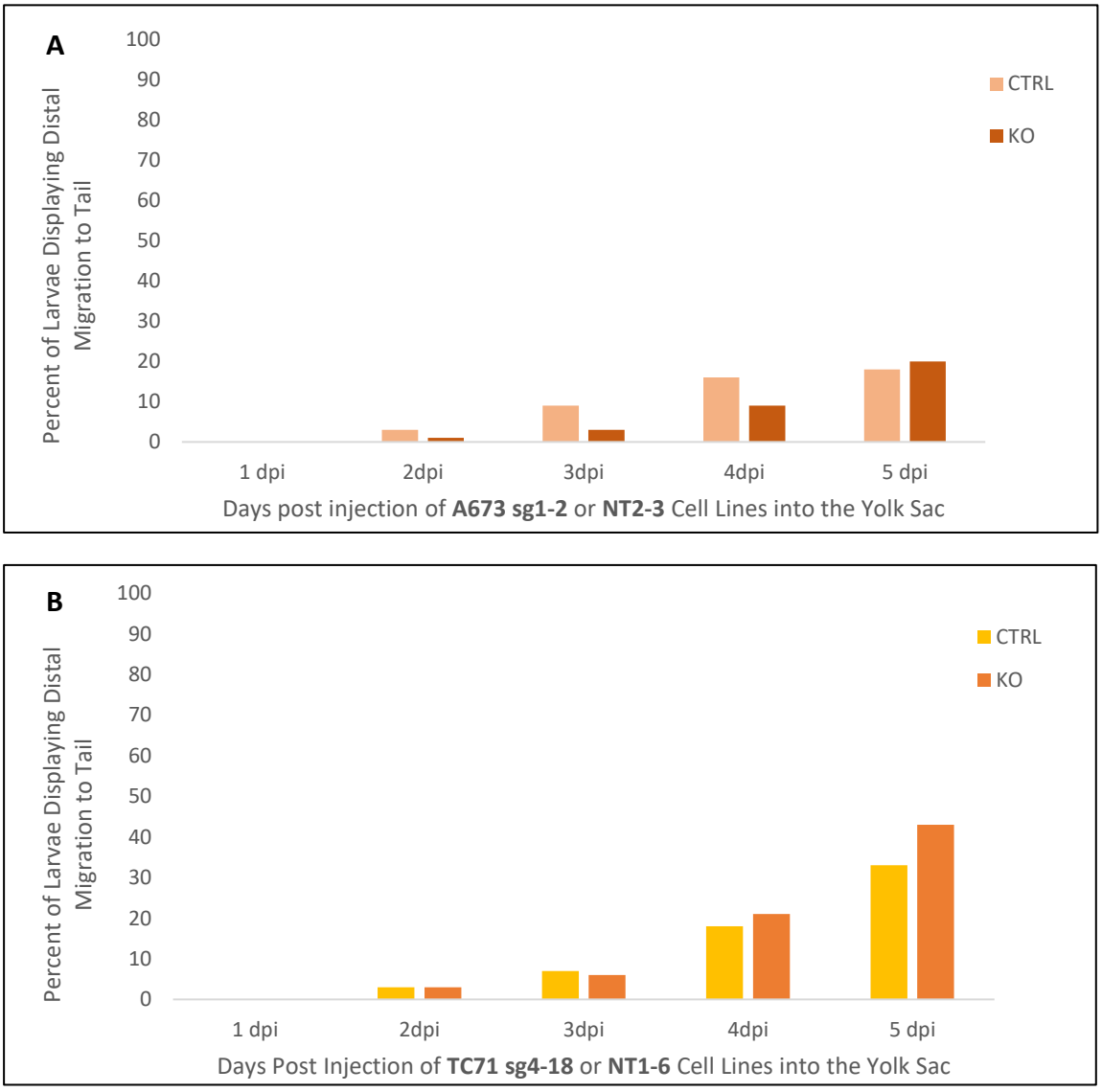

Figure 3.1.2. STAG2 knockout in A673 and TC71 cell lines does not promote distal migration to the tail when injected into the yolk sac. Zebrafish larvae were monitored for the presence of distal migration to the tail for five consecutive days post injection. Either (A) A673 sg1-2 (*STAG2* knockout)/NT2-3 (control) or (B) TC71 sg4-18/NT1-6 cell lines were injected into the yolk sac of 2dpf larvae. Three replicates were completed for each cell line (n=50-70 larvae each).

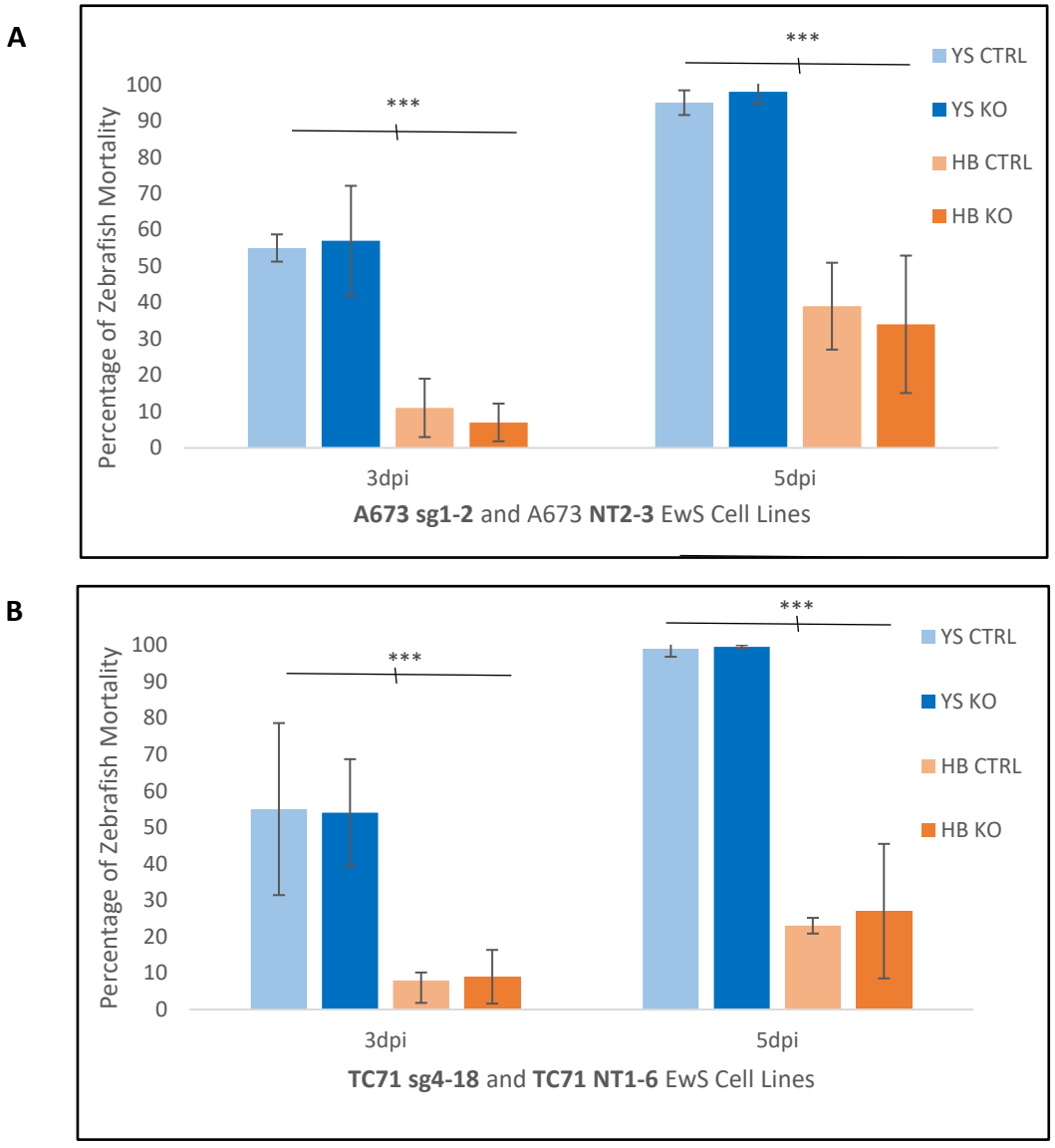

Figure 3.1.3. Larvae with A673 or TC71 EwS cell lines injected into the yolk sac had significantly higher larval mortality compared to larvae with EwS cells injected into the hindbrain ventricle. The mortality rate of injected with A673 or TC71 cell lines were monitored during the migration assays. (A) the injection of A673 sg4-6 (*STAG2* knockout) or NT2-3 (control) cell lines into the yolk sac (YS) or hindbrain ventricle (HB) of 2dpf larvae. (B) the injection of TC71 sg4-15 (*STAG2* knockout) or NT2-5 (control) cell lines into the yolk sac or hindbrain ventricle of 2dpf larvae. Three replicates were completed for each cell line (n=50-70). *** $p<0.0001$.

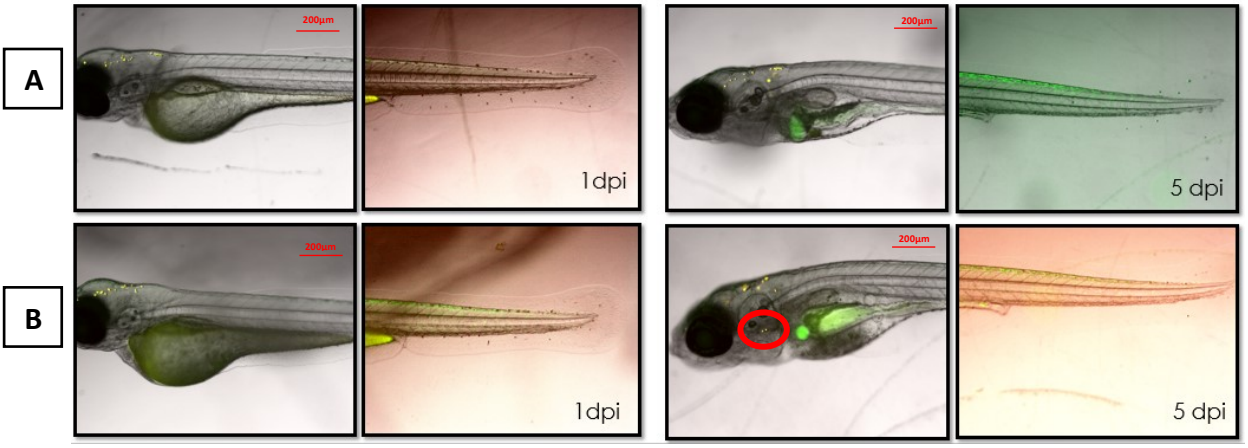

Figure 3.1.4. Microsphere Injections into the hindbrain ventricle confirmed the absence of passive spread of EwS cell lines from the hindbrain ventricle. Fluorescent microspheres (green fluorescent spheres ~10 microns) were injected into the hindbrain ventricle of 2dpf zebrafish and monitored for migration into the dorsal surface, yolk sac and tail. (A) and (B) are two separate larvae, however the (B) larva displayed passive spread of microspheres to the thymus. Two replicates were completed (n=10-20 larvae). The red circle indicates the location of the thymus.

3.2 *STAG2* Knockout in A673 and TC71 EwS Cell Lines Promote Cell Migration

A xenotransplantation platform was employed to determine the percentage of zebrafish larvae that displayed the presence of migrated EwS cell lines. Cells were initially injected into the hindbrain ventricle and monitored for migration to three specific locations: the dorsal surface, yolk sac, and tail each day from1-5dpi (**Figure 2.5.2**). Two different sets of single-guide RNAs (sg1-2 and sg4-6) were separately used to knockout *STAG2* in the A673 cell line, and a non-targeting sgRNA (NT2-3) targeting a cryptic sequence served as the control. Three replicates were performed for each cell line (n=50-70 zebrafish larvae per replicate). A673 sg4-6 (**Figure 3.2.1A**) and sg1-2 (**Figure 3.2.1B)** cell lines (*STAG2* knockout) showed significantly increased migration to the dorsal surface (40-50% of larvae population) in comparison to the control (20-30% of larvae population) at 2dpi (p= 0.0312 and 0.01, respectively) and 3dpi (p= 0.0372 (sg1-2)). *STAG2* knockout in A673 cell lines did not promote an increased number of larvae displaying migrated EwS cells to the yolk sac (**Figure 3.2.2A+B**) or tail (**Figure 3.2.3A+B**). Overall migration, which included the combination of dorsal surface, yolk sac and tail migration, was collectively increased for *STAG2* knockout A673 cell lines sg1-2 (60-80% of larvae population) in comparison to the control (40-50% of larvae population), specifically at 2dpi (p= 0.0315) and 3dpi (p= 0.0037) for A673 sg1-2 (**Figure 3.2.4A+B**).

In addition, three different sets of single-guide RNAs (sg1-6, 4-15, and 4-18) were separately used to knockout *STAG2* in the TC71 cell line, and non-targeting sgRNAs (NT1-6 and NT2-5) served as controls (n= 50-70 zebrafish larvae for each replicate of the

three completed). *STAG2* knockout in TC71 cell lines resulted in significantly increased cell migration to the dorsal surface (40-50% of larvae population) in comparison to controls (25-35% of larvae population), at 2dpi ($p<0.01$ (sg1-6) and <0.05 (sg4-15)), 3dpi ($p= 0.0329$ (sg4-15)), and 5dpi ($p= 0.0496$ (sg1-6) and 0.002 (Sg4-15)) (**Figure 3.2.1 C-E**). Unlike in A673 cells, *STAG2* knockout in TC71 cell lines did result in a significant increase in the number of larvae displaying migration to the yolk sac (up to 60-70% of larvae population; (3-5dpi) $p< 0.01$) (**Figure 3.2.2 C-E**) and tail (20-50% of larvae population; (2-4dpi) $p<0.01$)(**Figure 3.2.3 C-E**) compared to controls (up to 30-60% and 10-25%, respectively). *STAG2* knockout in TC71 cell lines resulted in a significantly increased overall migration, specifically from 2dpi ($p<0.05$) to 5 dpi ($p<0.01$) (**Figure 3.2.4 C-E**).

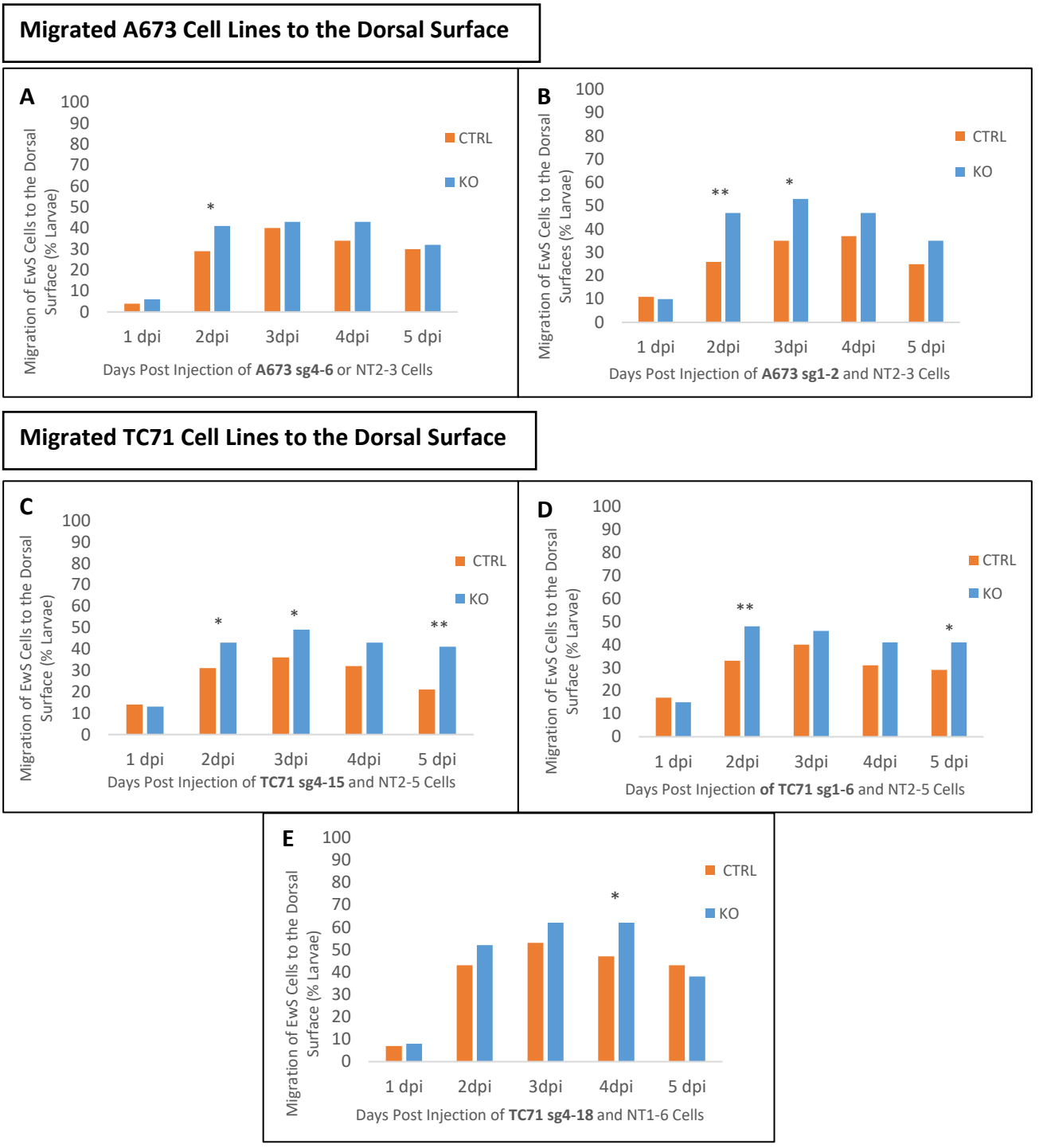

Figure 3.2.1. *STAG2* knockout (KO) in A673 and TC71 cell lines significantly increased cell migration to the dorsal surface. Zebrafish larvae were monitored for five consecutive dpi for the presence of migration of (A) A673 sg4-6 and NT2-3 cells, (B) A673 sg1-2 and NT2-3 cells, (C) TC71 sg4-15 and NT2-5 cells, (D) TC71 sg1-6 and NT2-5, and (E) TC71 sg4-18 and NT1-6, to the dorsal surface. Three replicates were completed for each cell line (n=50-70 larvae each). *p<0.05 and ** p<0.01.

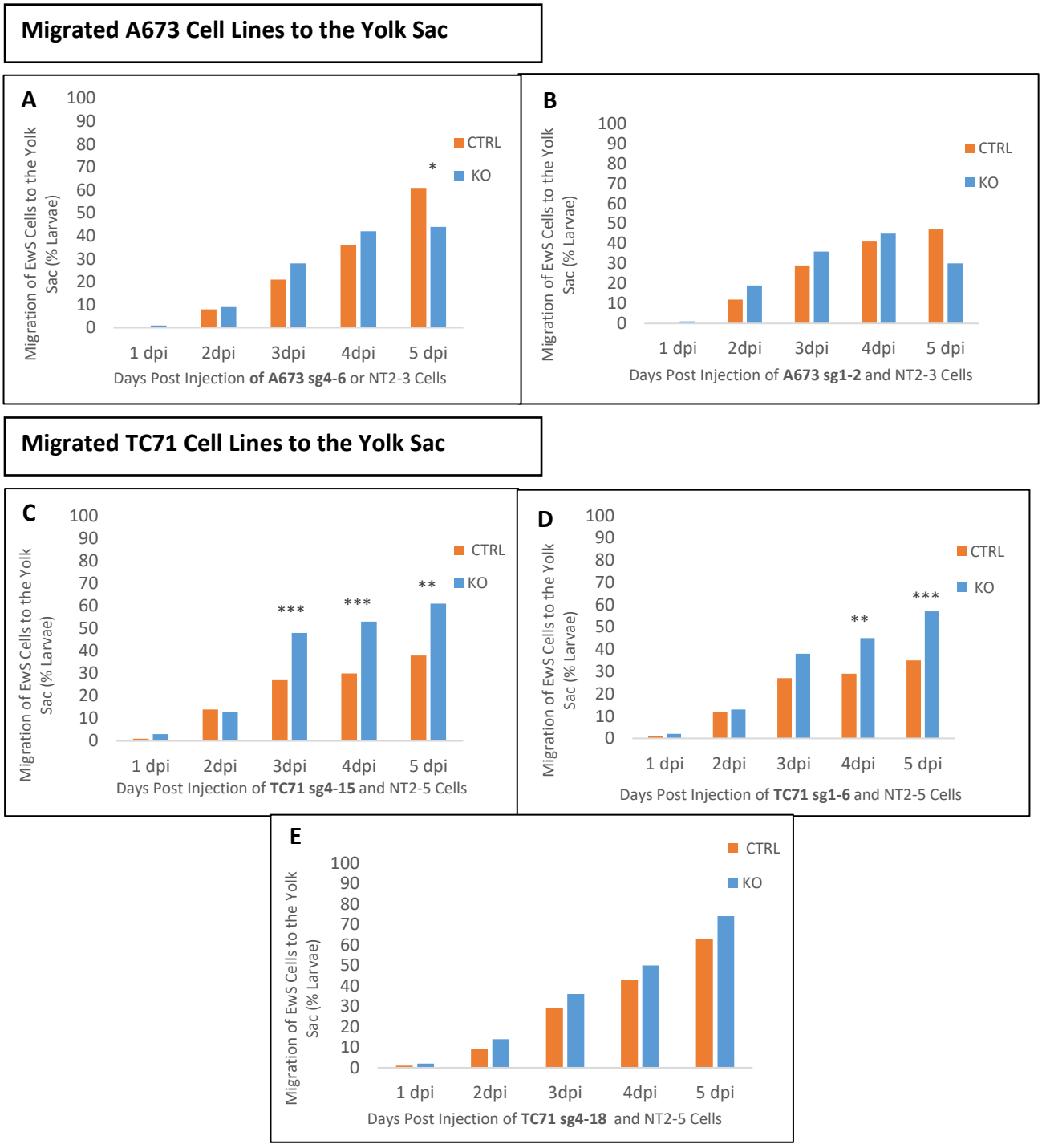

Figure 3.2.2. STAG2 knockout (KO) in TC71 cell lines significantly increased cell migration to the yolk sac. Zebrafish larvae were monitored for five consecutive dpi for the presence of migration of (A) A673 sg4-6 and NT2-3 cells, (B) A673 sg1-2 and NT2-3 cells, (C) TC71 sg4-15 and NT2-5 cells, (D) TC71 sg1-6 and NT2-5, and (E) TC71 sg4-18 and NT1-6, to the yolk sac. Three replicates were completed for each cell line (n=50-70 larvae each).* $p<0.05$, ** $p<0.01$ and *** $p<0.001$.

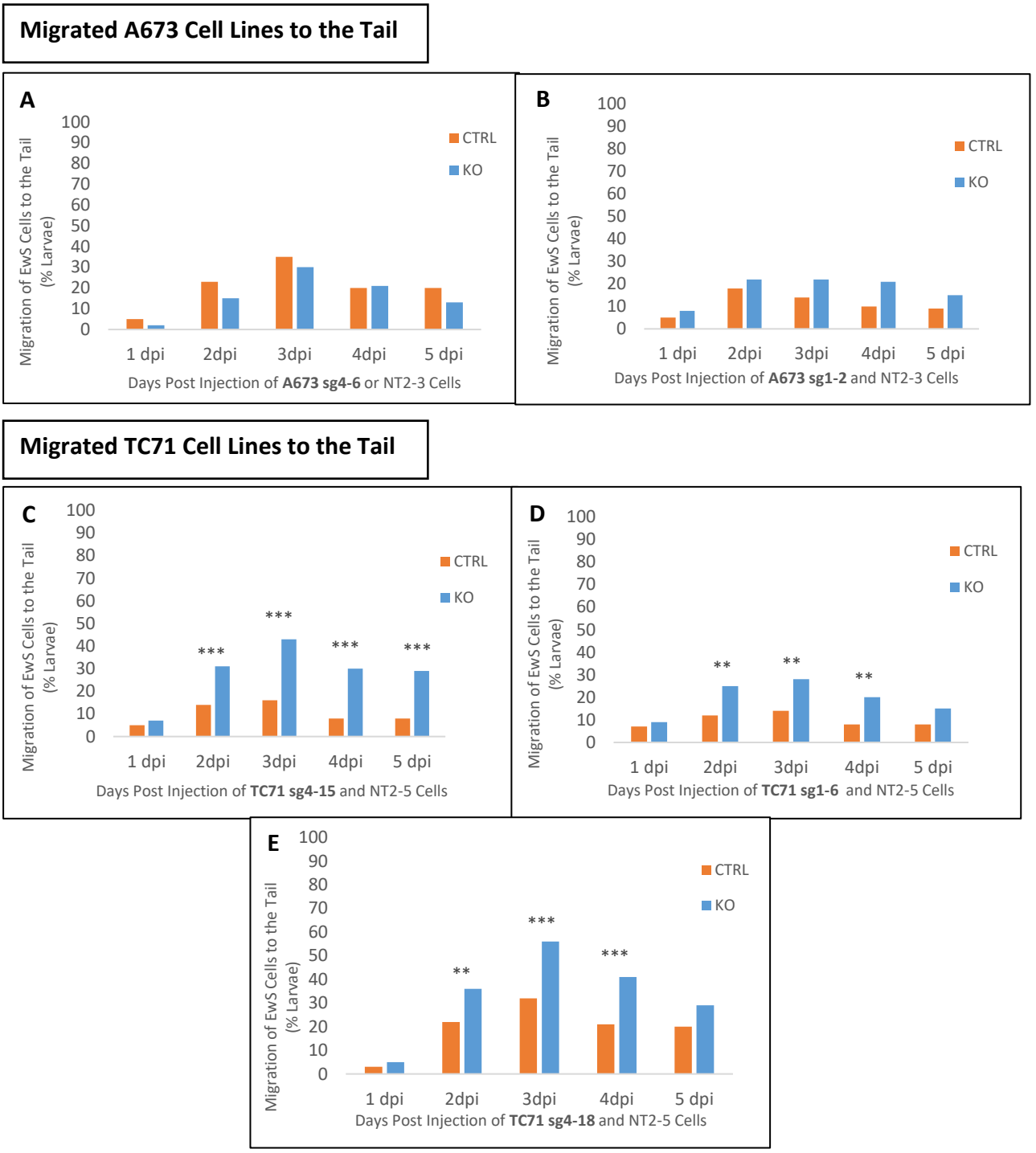

Figure 3.2.3. *STAG2* knockout (KO) in TC71 cell lines significantly increased cell migration to the tail. Zebrafish larvae were monitored for five consecutive dpi for the presence of migration of (A) A673 sg4-6 and NT2-3 cells, (B) A673 sg1-2 and NT2-3 cells, (C) TC71 sg4-15 and NT2-5 cells, (D) TC71 sg1-6 and NT2-5, and (E) TC71 sg4-18 and NT1-6, to the tail. Three replicates were completed for each cell line (n=50-70 larvae each).* $p<0.05$, ** $p<0.01$ and *** $p<0.001$.

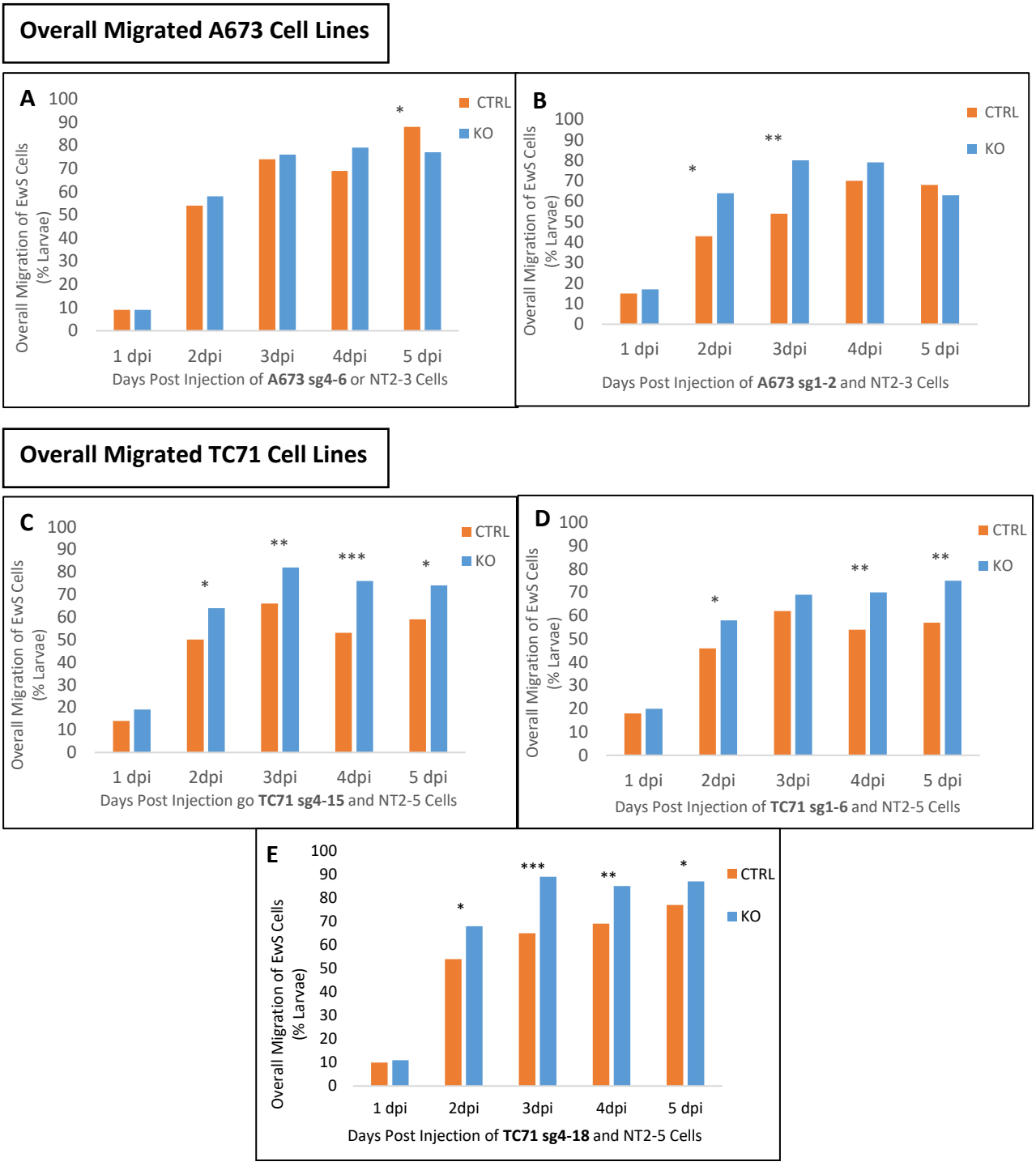

Figure 3.2.4. STAG2 knockout (KO) in A673 and TC71 cell lines significantly increased <u>overall migration</u>. Zebrafish larvae were monitored for five consecutive dpi for the presence of migration of (A) A673 sg4-6 and NT2-3 cells, (B) A673 sg1-2 and NT2-3 cells, (C) TC71 sg4-15 and NT2-5 cells, (D) TC71 sg1-6 and NT2-5, and (E) TC71 sg4-18 and NT1-6 outside the hindbrain ventricle. Three replicates were completed for each cell line (n=50-70 larvae each).* * $p<0.05$, ** $p<0.01$ and *** $p<0.001$

3.3 Cell Proliferation of EwS Cell Lines is Limited within the Zebrafish Hindbrain Ventricle

An *ex vivo* cell proliferation assay was employed to investigate the ability of TC71 and A673 cell to proliferate in the hindbrain ventricle of zebrafish larvae. Following the quantification of fluorescent EwS cell lines, no significant difference in proliferation between 1, 3 and 5dpi was observed in both control and *STAG2* knockout A673 and TC71 cell lines (**Figure 3.3.1**). At 3dpi, A673 cell lines had no significant change in relation to baseline (A673: fold change of 0.94 (*STAG2* knockout) and 0.99 (control), and TC71: 1.16 (*STAG2* knockout) and 1.05 (control)). At 5dpi, A673 cell lines had an insignificant increase in fold change of 1.2 (*STAG2* knockout) and 1.13 (control), and TC71 also remained consistent with the fold change at 3dpi resulting in a fold change of 1.16 (*STAG2* knockout) and 1.18 (control) in relation to the baseline.

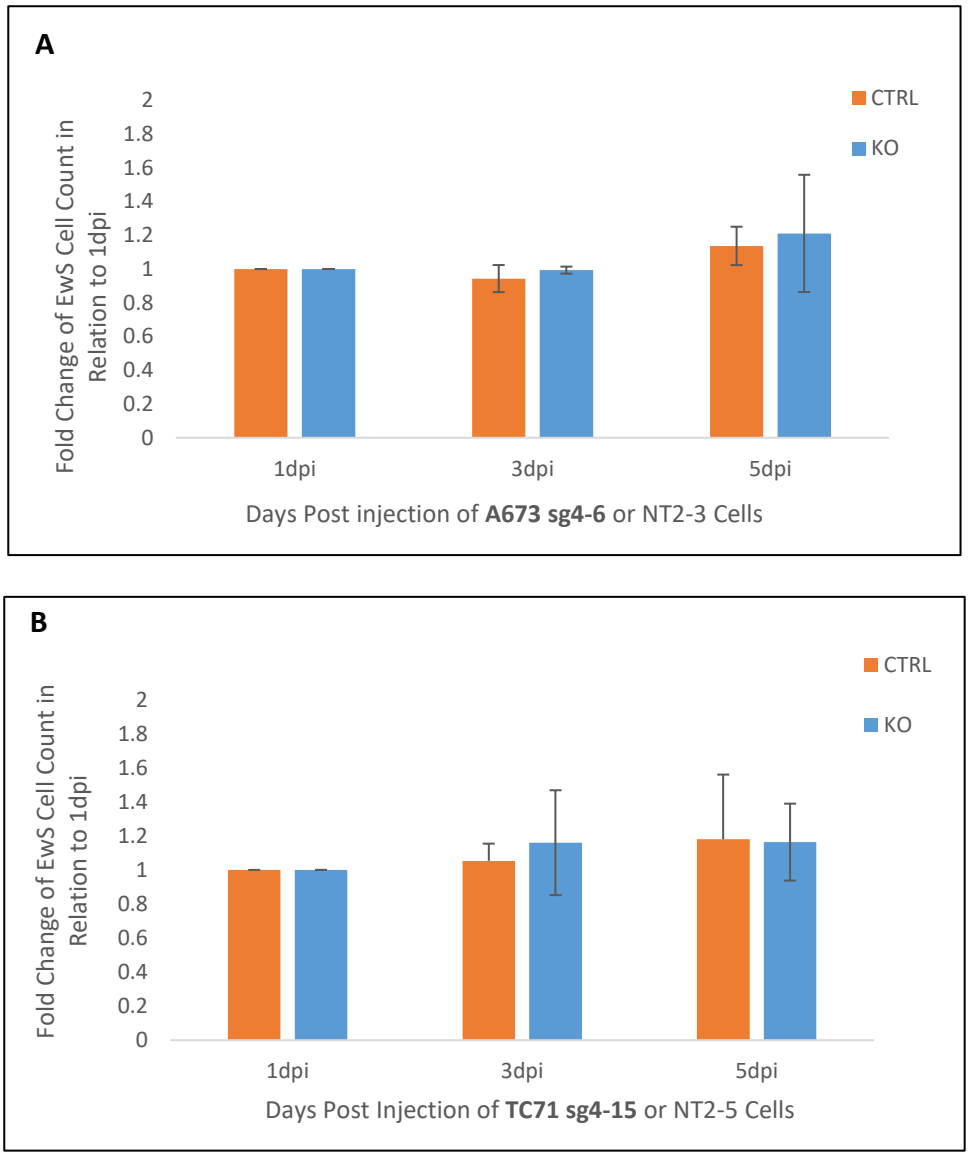

Figure 3.3.1. The proliferation of TC71 and A673 cell lines is limited within the hindbrain ventricle of zebrafish larvae. Larvae injected with (A) A673 sg4-6 and NT2-3 or (B)TC71 sg4-15 and NT2-5 cell lines into the hindbrain ventricle, were selected at 1, 3 and 5 dpi for EwS cell quantification. Three replicates were completed for each cell line (n=15-20 larvae).

3.4 EwS Cell Lines Migrate out of the Hindbrain Ventricle via Vasculature such as the Posterior Cerebral Vein (PCeV) and Ultimately Migrate towards the Yolk Sac

Following the establishment of the hindbrain as an ideal site to inject EwS cells, and the determination that EwS cells can migrate to the three specified areas of zebrafish larvae, there arose the question of the route EwS escape from the hindbrain. EwS cell migration out of the hindbrain ventricle was studied through the analysis of 12-hour time lapse videos. The movement of a single cell leaving the hindbrain ventricle towards the otolith in a 3dpi *casper* larvae was captured using live imaging. In addition to migrating out of the hindbrain ventricle, this cell was observed to return to the hindbrain ventricle and leave once again with multiple EwS cells following behind (**Figure 3.4.1 A**). Additionally, 12-hour time lapse imaging demonstrated the collection of EwS cells to/within the anterior of the yolk sac (**Figure 3.4.1B**). Furthermore, by employing the *Tg(fli1a: eGFP) casper* larvae with fluorescent vasculature, it was determined that the EwS cells (*STAG2* knockout; TC71 sg4-15) were able to migrate out of the hindbrain ventricle through the posterior cerebral vein (PCeV) (**Figure 3.4.1C**).

To further confirm the location of migrated EwS cells out of the hindbrain ventricle, zebrafish larvae, injected with either A673 or TC71 cell lines, were sent for histology. Through the analysis of the stained slides, in addition to an EwS tumour within the hindbrain displaying mitotic cells (**Figure 3.4.2**), suspicious cancer cells were present along the thin lining of the yolk sac and within the lymphatic vessel, however we were unable to confirm by immunohistochemical staining for technical reasons including availability of anti-CD99 antibody within the time frame of this study (**Figure 3.4.3**).

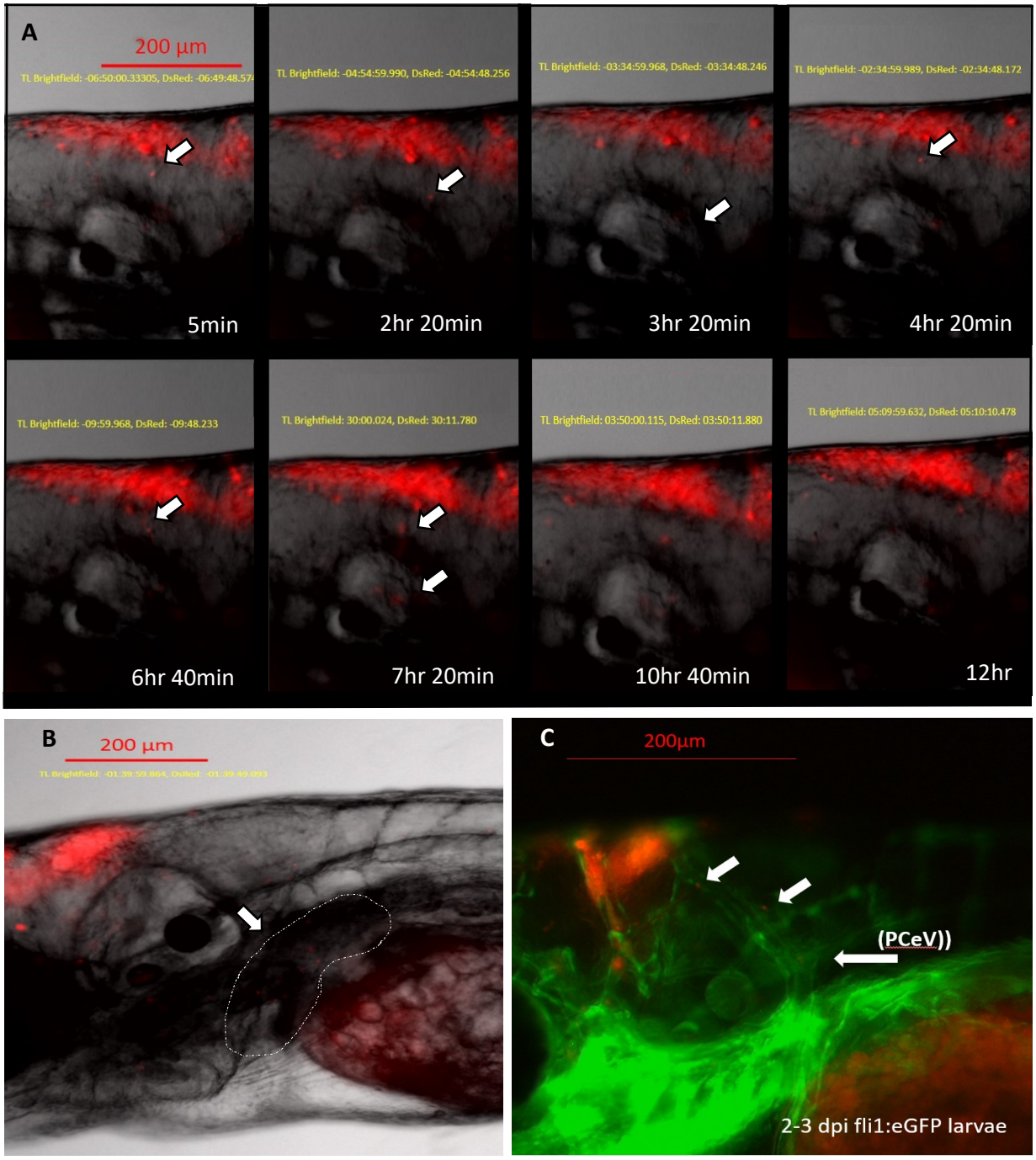

Figure 3.4.1. EwS cell lines migrate out of the hindbrain ventricle via vasculature such as the posterior cerebral vein (PCeV). 12-hour time lapse imaging of (A and B) 2-3dpi casper and (C) *Tg(fli1a: eGFP) casper* larvae with fluorescent vasculature (green) injected with TC71 4-15 *STAG2* Knockout cells (red) into hindbrain ventricle to investigate route taken by migrating cells. (A) Leader cell identified by white arrow, seen from 5min to 6hr 40min images. At 4hr 20 min, the leader cell returned to hindbrain and by 6hr 40min guided EwS cells out of hindbrain. (B) Collection of EwS anteriorly to/within the yolk sac. (C) EwS cells were observed traveling out the hindbrain via the PCeV

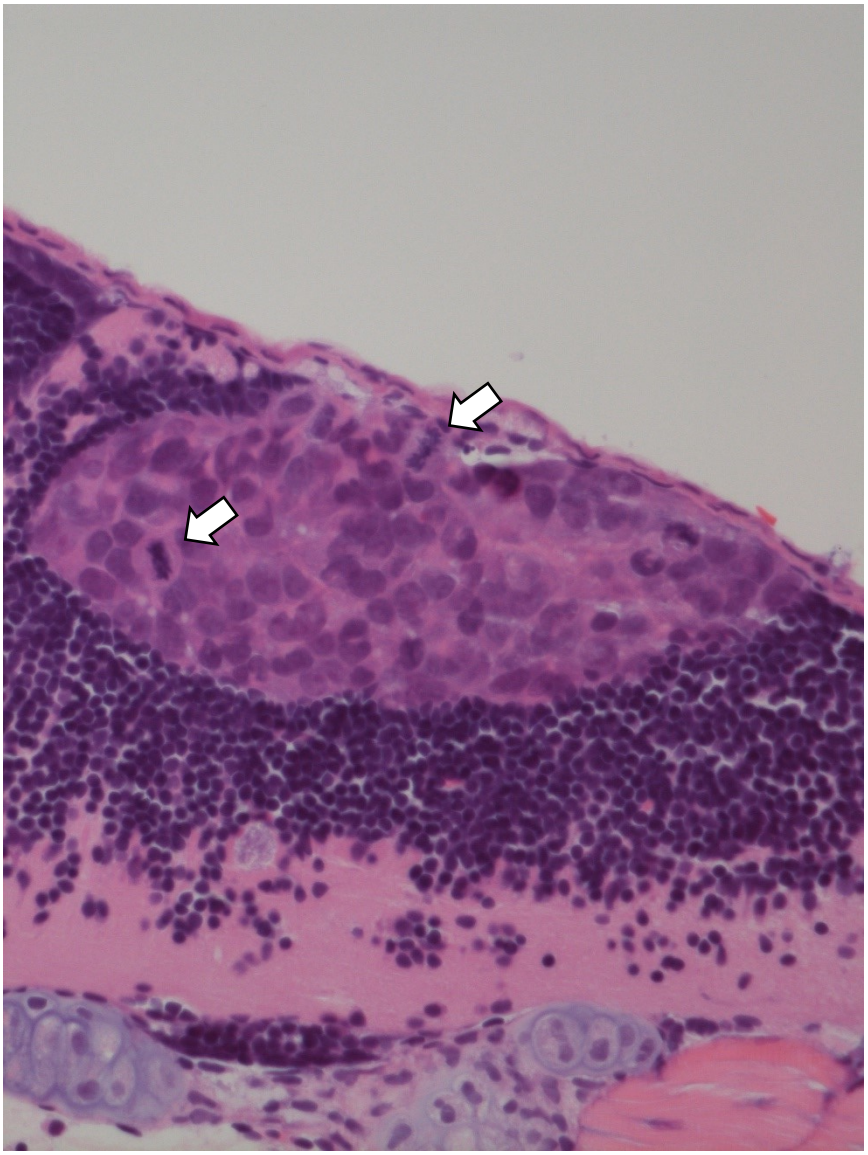

Figure 3.4.2. **EwS tumour within the hindbrain displaying mitotic cells observed by H&E staining.** H&E staining of 3dpi casper with a TC71 sg4-15 (*STAG2* knockout) tumour within the hindbrain. Mitotic cells are pointed to by the white arrow. Ewing sarcoma cells are identified by a high nuclear to cytoplasmic ratio. EwS tumour cells were confirmed through immunohistochemical staining.

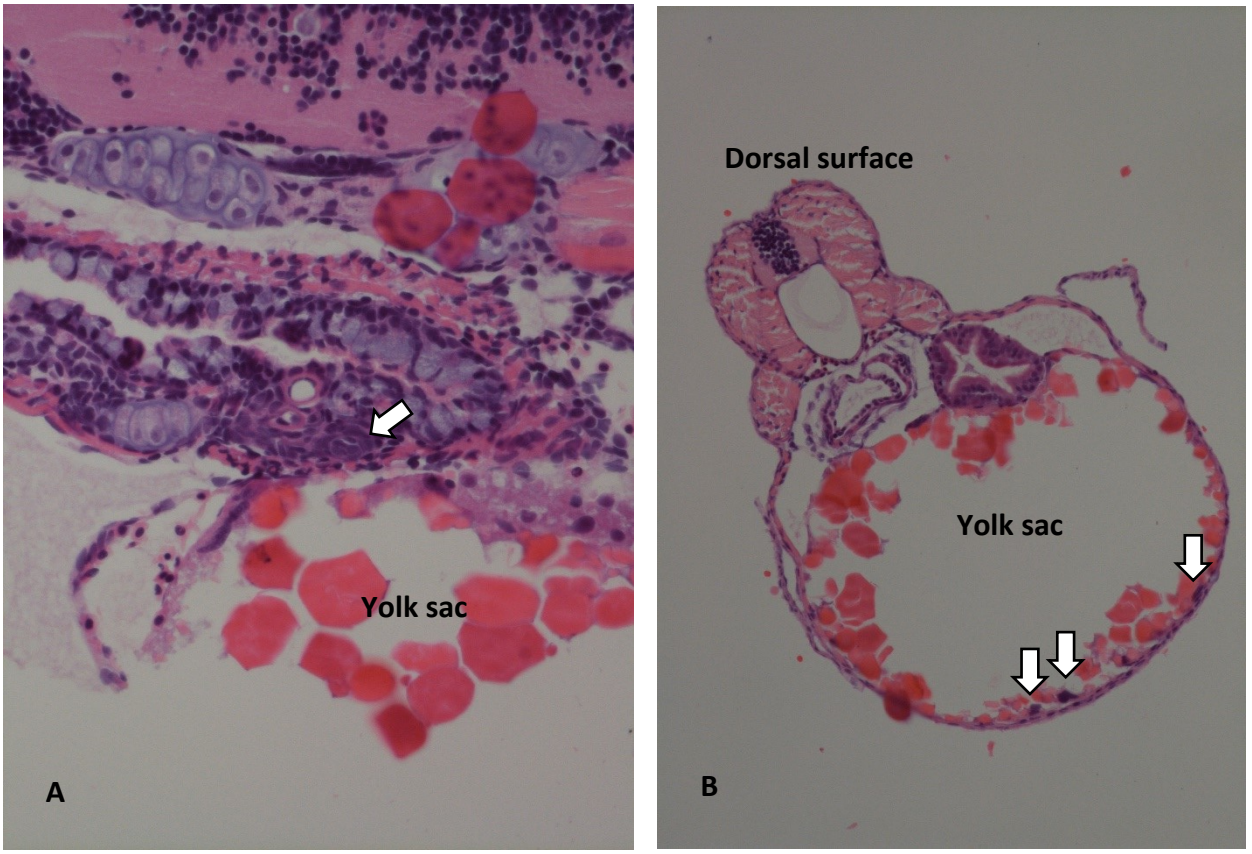

Figure 3.4.3. Suspicious EwS tumour present by pathologic observation. (A) below the hindbrain and otolith, white arrow points to a lymphatic vessel surrounding blood vessels with a suspicious presence of EwS cells (TC71 sg4-15). A portion of the yolk sac is found beneath. (B) Suspicious EwS cells (TC71 sg4-15) appear adherent to the lining of the yolk sac (white arrows). We were unable to confirm EwS identity by immunohistochemical staining due to technical reasons.

3.5 *STAG2* Knockout Reduces the Expression of the EWS-FLI1 Translocation

Western blots were used to explore the expression levels of EWS-FLI1 in both *STAG2* knockout and control A673 and TC71 cell lines. Unaltered A673 (NT2-3) and TC71 (NT2-5) cells were used as the reference point for their corresponding *STAG2* knockout cell line, having a value of 1.0. *STAG2* knockout in the TC71 cell line resulted in a 42% down-regulation in EWS-FLI1 expression ($p<0.0001$) (**Figure 3.5.1**). *STAG2* knockout in the A673 cell line resulted in a 14% reduction in expression of EWS-FLI1, which was not significant ($p= 0.2913$) (**Figure 3.5.1**). Three replicates were completed for each cell line. A second band sized at approximately 150 KDa was also observed, however its identity is unknown at this time.

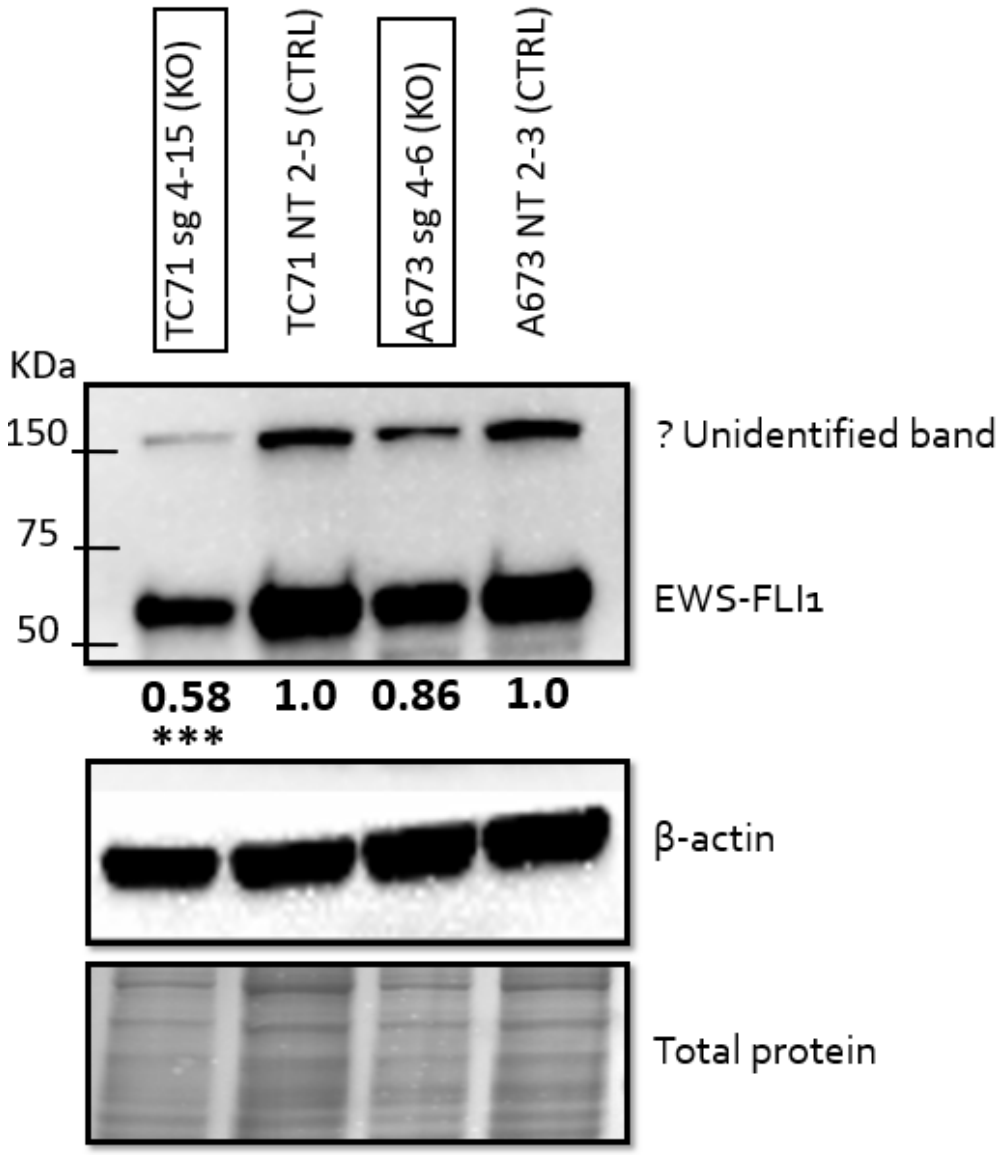

Figure 3.5.1 STAG2 loss reduces the expression of EWS-FLI1. Western blots were employed to determine the levels of EWS-FLI1 expression in TC71 and A673 cell lines with *STAG2* knockout (KO) or NT controls (CTRL). Western blot controls included both β-actin and total protein. Three replicates were completed for each cell line. ***p<0.001

3.6 *STAG2* Knockout does not Play a Significant Role in the Anoikis Resistance of A673 and TC71 Cell Lines

Prior to these experimentations, the attempt to co-inject *STAG2* knockout and control EwS cell lines together was carried out through the lenti-virus fluorescent transduction of TC71 and A673 cell lines to separately label control (red) and *STAG2* knockout (green) cell lines different colours. Although this experiment was not continued due to variables such as difficulty in visualizing control cells, it was observed that control cells were dulling in fluorescence within the acellular anoikis environment of the yolk sac. Therefore, experiments were conducted to determine if *STAG2* knockout promoted anoikis resistance.

Two assays were used to investigate the effect of STAG2 loss on anoikis resistance in EwS cell lines including an alamarBlue® cell viability assay and flow cytometry. Using the alamarBlue® cell viability assay, a 50% (A673) and 20% (TC71) reduction in viable cells was observed for both *STAG2* knockout and control cell lines when suspended in PolyHEMA coated wells compared to the uncoated well controls (**Figure 3.6.1**). Three replicates were completed for each cell line.

Flow cytometry was chosen to perform a more sensitive assay, where a modest trend was observed with *STAG2* knockout TC71 cell lines showing a decreased staining of annexin V, a cellular protein that detects phosphatidylserine, a marker of early apoptosis, located on the cytoplasmic surface of the plasma membrane. However, no significant difference was observed between the *STAG2* knockout and control cells across two replicates (**Figure 3.6.2**).

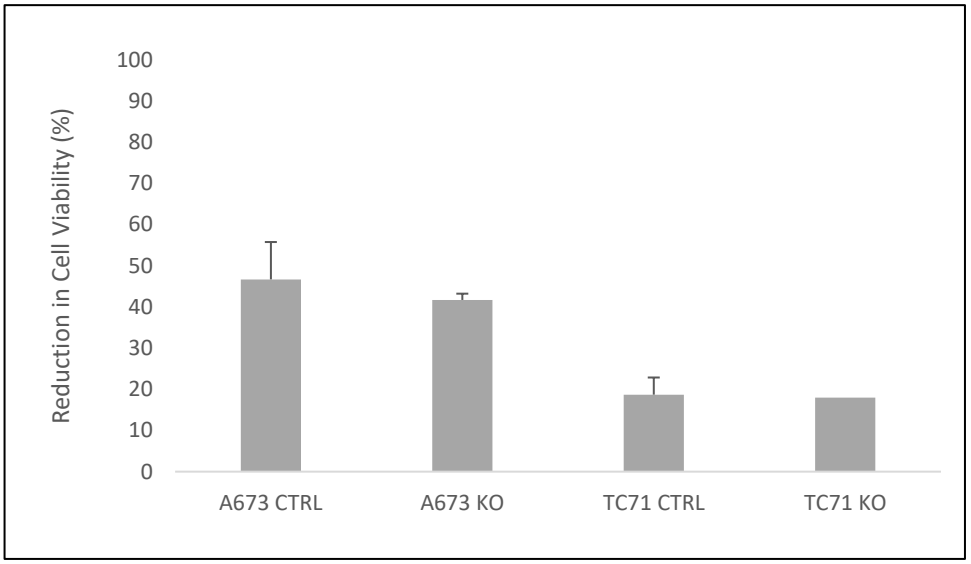

Figure 3.6.1. *STAG2* knockout does not promote cell viability when grown suspended on polyHEMA coated plates. The cell viability of A673 sg4-6 (*STAG2* knockout) and NT2-3 (control) and TC71 sg4-15(*STAG2* knockout) and NT2-5 (control)) cell lines cultured in coated (polyHEMA) wells were compared to controls cultured in non-coated wells post 24 hours of incubation for the alamarBlue® cell viability assay.

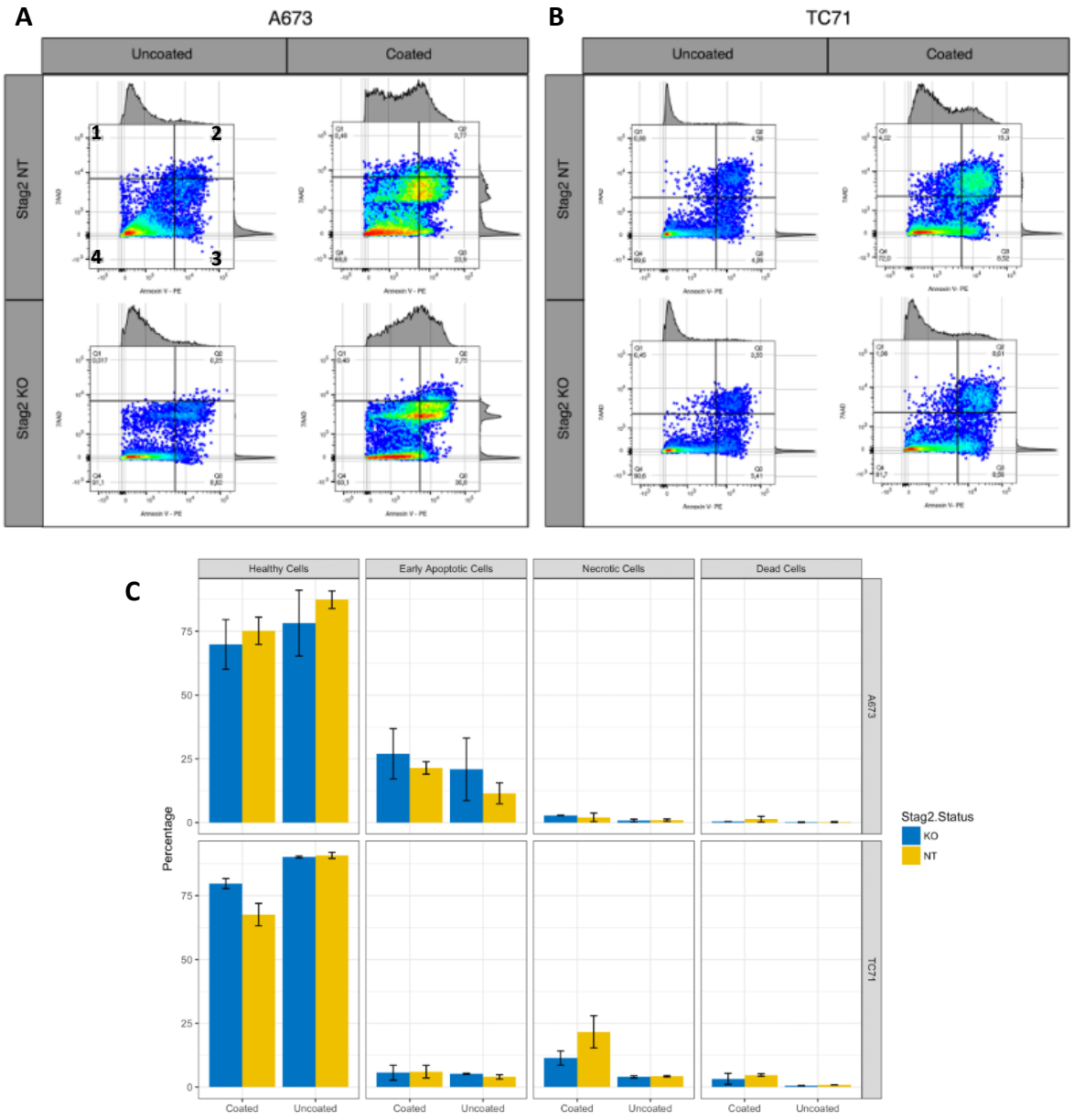

Figure 3.6.2. *STAG2* knockout does not promote anoikis resistance in A673 and TC71 cell lines. Flow cytometry with annexin V staining was used to investigate the population of cells undergoing apoptosis when cultured in polyHEMA coated, non-adherent plates, and control uncoated plates. (A) A673 knockout and control cells and (B) TC71 *STAG2* knockout and control cells. First and second quadrants represent individual cells undergoing apoptosis, with annexin V staining, third represents completely dead cells, and the last represents healthy cells. (C) is a bar graph representation of the four quadrants.

Chapter 4: Discussion

Zebrafish have emerged as a new mainstream model for genetic analysis, drug screening, and an *in vivo* model for xenotransplantation of cancer cells (Laale et al. 1977; White et al. 2008; Delov et al. 2014; Corkery et al. 2011; El-Nagger et al. 2015). The establishment of zebrafish as a xenotransplantation model provides enhanced opportunities to analyze the migration, a small yet important step in metastasis of human cancer cells within a transparent model, allowing for repeated visualization without sacrificing the recipient larvae. This xenotransplantation model was employed to study the migration of EwS in the context of *STAG2* loss, a recurrently mutated gene of the cohesin complex in 88% of metastatic EwS samples (Crompton et al. 2014). The goals of this project were to utilize the zebrafish as an *in vivo* xenotransplantation model to determine if STAG2 loss promotes cell migration of EwS cell lines, and to investigate additional factors involved with STAG2 loss and cell migration, including EWS-FLI1 expression, anoikis resistance and downstream factors of STAG2 loss.

4.1 The Zebrafish Xenotransplantation Model can be used to Study EwS

The employment of zebrafish as a xenotransplantation model to study EwS has previously been undertaken in Dr. Berman's laboratory, which demonstrated the role of the YB-1 protein in EwS metastasis (El-Nagger et al. 2015). This study used TC32 EwS cell lines, which are identified to have endogenous absence of the STAG2 protein, therefore we employed two additional EwS cell lines, A673 and TC71 that carry wild-type *STAG2* (Crompton et al. 2014 and Brohl et al. 2014). The presence of STAG2 enabled the

utilization of experimentally designed *STAG2* knockout cell lines to compare the effects of STAG2 loss on cell migration.

EwS cell lines, A673 and TC71, were successfully labeled with a CMTMR dye and distinguished as bright fluorescent cancer cells throughout the entire body of the transparent larvae. Although previous studies that investigated EwS employed the yolk sac as the primary injection site, unsatisfactory results and viability was observed in this study when the A673 and TC71 cell lines were xenotransplanted into the yolk sac. Therefore, the first objective of this study was to determine the optimal site to inject EwS cell lines in the context of cell migration assays.

4.1.1 The Zebrafish Hindbrain Ventricle Performs better than the Yolk Sac as a Xenograft Site for Migration Assays of EwS

In previous studies, the yolk sac was employed as the primary site for xenograftment of cancer cells such as EwS and leukemia cells (El-Nagger et al. 2015 and Corkery et al. 2011). Following this previous study, the yolk sac was initially selected as the site to xenograft A673 or TC71 cell lines for the investigation of EwS migration. As described in this previous study, local migration and distal migration to the tail were scored for the presence of migrated EwS cell lines (El-Nagger et al. 2015). The migration of EwS cells was classified as the presence of >6 cells within the tail for distal migration, however, fewer than six cells for both the cell lines in this study were observed within the tail. Therefore, there was no minimum cell count for the tail to be classified positive for migrated EwS cells in this study. Surprisingly, when the yolk sac was employed as the

initial injection site, similar capability to migrate and high larval viability found in the previous study was not observed with the A673 and TC71 cell lines.

Another important variable observed in yolk sac injections was the high mortality of larvae. As shown in **Figure 3.1.3**, approximately 54-57% of larvae injected with A673 or TC71 cell lines died by 3dpi and 95% by 5dpi compared to only 9-11% (3dpi) and 23-39% (5dpi) when EwS cell lines were injected into the hindbrain ventricle. The massive larval mortality, along with the low migratory capability of A673 and TC71 cell lines injected into the yolk sac, were likely due to the transplantation of EwS cell lines into an unfavorable environment. In addition, histology performed on larvae injected with EwS cells into the hindbrain ventricle displayed migrated cells to the yolk sac adjacent to the membranous-edges, thereby suggesting their predilection for adhering to a physical structure. However, CD99 staining would be helpful to confirm if these cells are human EwS cells.

The hindbrain ventricle is an additional xenotransplantation site published in previous studies, including melanoma, colorectal cancers, and brain tumours, however, this site has only recently started receiving attention (Nicoli and Presta 2007; Haldi et al. 2006; Wehmas et al. 2016). Given that the hindbrain ventricle is the posterior section of the brain, it provides a cellular environment convenient for xenografting adherent cells. Even though the microenvironment can be especially important for xenografts of cells of neuroectodermal and neural origin, such as glioblastoma and neuroblastoma, we thought it would be useful for performing EwS xenograft into the hindbrain ventricle because of two reasons, 1) the mesenchymal/neural crest origin of EwS, and 2) there is

no osteoclast niche easily accessible to perform microinjection at the larval stage in zebrafish. Therefore, the hindbrain ventricle offers an effective alternative site that is more physiologically relevant to study the migration of EwS cells.

These observations suggest that the yolk sac is a less reliable site for transplanting EwS cancer cells compared to the hindbrain ventricle, especially in the context of migration. The disadvantages of employing the yolk sac as the EwS cell line transplantation site, not observed in the hindbrain ventricle, include its acellular environment, the absorption of the larvae yolk sac during normal development, and sensitivity to cell density.

The yolk sac of zebrafish is an acellular environment predominately composed of different species of lipids, visually shown in **Figure 3.4.2**. While high lipid density can be beneficial for cancer cell proliferation, there are other essential factors missing that are important for cancer functions, such as induced gene expression through tumour to stromal interactions, inflammatory cells and cell adhesion. Although the yolk sac environment may offer a model to investigate the anoikis resistance of cancer cells (Corkery et al. 2011), this may not be the optimal location to inject solid tumour cancer cells, previously stressed from harvesting and labeling, into an additionally stressful foreign environment.

By contrast, the hindbrain ventricle of larvae is a multicellular site, primarily consisting of immature glial cells. While the hindbrain ventricle microenvironment is more similar to that of the brain, and not bone or soft tissue, this microenvironment

may supply more cellular signaling pathways and cell-cell interactions that offer a better representation of EwS metastatic potential. As previously mentioned, the origin of EwS may be of the neural crest, where EwS cells have been identified to express similar cell surface antigens as the neuroectodermal lineage (Lipinski 1986) and genes of neural tissues (Staege et al. 2004).

In addition to the acellular environment of the yolk sac, a previously identified concern was the natural absorption of yolk, as it is the source of nutrition for larvae. Therefore, through the physiological absorption of the yolk sac, nearby xenografted EwS cells within the yolk sac can passively move out into the anterior region. Although it was confirmed that Tetraspeck microspheres were only found to passively spread to the anterior region of zebrafish larvae, and not the tail, it still may compromise the integrity of cancer cell potential to migrate; a variable that does not exist within the hindbrain ventricle (El-Nagger et al. 2015).

Previous studies from our lab have quantified the capacity limit of EwS cells in larvae without resulting in high mortality from tumour burden. It was determined that less than 50 EwS cells injected into the yolk sac resulted in a poor viability of EwS cells. Likewise, injection of greater than 50 EwS cells resulted in a high mortality of larvae. Regarding the hindbrain ventricle, this current study quantified the appropriate number of EwS cells to xenotransplant and determined that approximately 50 cells can be accommodated into the hindbrain ventricle. This maximum capacity can be an advantageous scale to assist in the estimation of injected cell quantity, limiting the

addition of too many cells; whereas the yolk sac is a large cavity that may lead to accidental over burden of EwS cells, and ultimately larvae mortality.

It is important to note, a disadvantage in the hindbrain ventricle is the limited ability of EwS cancer cells to proliferate (refer to **Figure 3.3.1**) in comparison to the reported TC32 cell line, which had a 2-fold increase in cell count by 3dpi in the yolk sac, and a 5-fold increase by 5dpi (El-Nagger et al. 2015). It is unknown why proliferation is limited within the hindbrain ventricle; however, possible explanations could include the lack of time and/or a higher tendency of the EwS cell lines to invade and migrate rather than divide. As shown in the histology of larvae with injected EwS cells within the hindbrain ventricle, mitotic cells were evident, therefore, while proliferation was slow, it was present (**Figure 3.4.2**).

In summary, the hindbrain ventricle is an optimal site to investigate the migration of EwS cell lines within zebrafish larvae, which unlike the yolk sac, is a multicellular environment that maintains the viability of the EwS cancer cells, is not absorbed throughout the research lifespan, and lastly holds an appropriate number of cancer cells within the larvae tolerance, resulting in a low mortality of larvae.

4.1.2 The Zebrafish Xenotransplantation Model Enables Direct Observation of Metastatic Events such as Collective Invasion and Intravasation into the Posterior Cerebral Vein (PCeV) to Escape the Hindbrain ventricle

Metastasis of cancer is a complex process involving numerous steps such as detachment from the primary tumour, intravasation into the circulation/lymphatic system, evasion of immune attacks, extravasation into distant capillary beds, invasion

into surrounding tissues, and ultimately the formation and proliferation of a new secondary tumour (Chambers et al. 2002 and Seyfried et al. 2013). The zebrafish model allows for the visualization of different key steps in metastasis, which various groups have focused on including angiogenesis (He et al. 2012) and migration (El-Nagger et al. 2015). Using the *casper* and *Tg(fli1a: eGFP) casper* larvae lines, xenografted larvae were imaged to visualize the migration of EwS cells out of the hindbrain ventricle. Initially, 3dpi *casper* larvae injected with the TC71 EwS cell line (*STAG2* knockout) were utilized for 12-hour time lapse imaging. Through this approach, images were captured every five minutes in brightfield (white light) and at the wavelength of 541/565nm to image CMTMR labeled cancer cells.

An interesting metastatic event observed was the movement of a single cell traveling out of the hindbrain ventricle, followed by its return for approximately two hours, and finally a repeated escape from the hindbrain ventricle, but with a mass of additional EwS cells following behind (refer to **Figure 3.4.1A**). This specific behaviour may be explained through the reported phenomenon of “leader” and “follower” cancer cells in collective invasion (Wang et al. 2016 and Liu et al. 2017). While the EwS cells were observed migrating together, they could still be visualized as single cells. This observation remains consistent with publications, which reported that while poorly differentiated cells, such as EwS, are less likely to migrate collectively, it has been demonstrated that they still form loosely attached small nests or intertwined cords as they invade stroma, keeping them in close proximity to each other, and thus appear as a collection of cells migrating (Wang et al. 2016). It can therefore be suggested that the

EwS cell that initially left the hindbrain ventricle alone, was a “leader” cell that may then have the potential to communicate with others within the hindbrain ventricle, leading them to another favorable environment. While little is still understood about this process, the time-lapse visual allows for direct observation of this collective invasion and migration process. More replicates are required to further analyze this collective migration behaviour.

It is important to note that the 12-hour time lapse imaging was conducted at room temperature, therefore, enhanced technology that can complete twelve-hour imaging at 35˚C may allow for a greater observation of this collective behaviour, as room temperature may hinder the viability of the cells over an extended period, however it did not appear to be heavily impacted.

While *casper* larvae are an excellent tool to observe the migration of EwS cells, the exact site of migrated cells within larvae, such as the blood vessels or lymphatic system, could not be determined. Therefore, the *Tg(fli1a: eGFP) casper* larvae with fluorescent vasculature were employed. The first important observation was the movement of approximately four cells around the posterior cerebral vein (PCeV) before they all intravasated into the vein and entered circulation (**Figure 3.4.1C**). The majority of intravasated EwS cells traveled anteriorly to the yolk sac prior to separating and traveled through various vessels and routes towards the heart. A labeled illustration of 2 and 5-day old larvae vasculature system are shown in **Figure 4.1.2**.

In addition, EwS cancer cells traveled along the dorsal surface of larvae, specifically in and around the dorsal longitudinal anastomotic vein. As demonstrated, EwS cells have a high tendency to intravasate into veins instead of arteries. In fact, it is recognized that tumours that typically spread through the blood stream, such as sarcomas, commonly metastasize through veins rather than arteries due to their thin walls (Chambers et al. 2002). Although the lymphatic vasculature is not visible within this transgenic line, lymphatic vessels are known to be in close proximity to that of blood vessels, therefore cancer cells seen alongside blood vessels may be within the lymphatic system.

As previously mentioned, histology is a commonly utilized tool for the identification of EwS cells, specifically with H&E and CD99 staining. Using H&E staining, the morphology of small round cells with high nuclear to cytoplasmic ratio can be visualized, two characteristics of EwS. In addition, CD99 is a key biomarker of this disease that can be detected through immunohistochemical staining. Through analysis of the histology slides of 3dpi larvae injected with A673 or TC71 STAG2 knockout cells, a suspicious presence of EwS cell lines along the thin lining of the yolk sac and within the lymphatic vessel was observed, however this was unable to be confirmed by immunohistochemical staining due to technical reasons. These EwS cells likely migrated along the lining post invasion into the yolk sac as it provided a surface of adhesion as well as a high energy source.

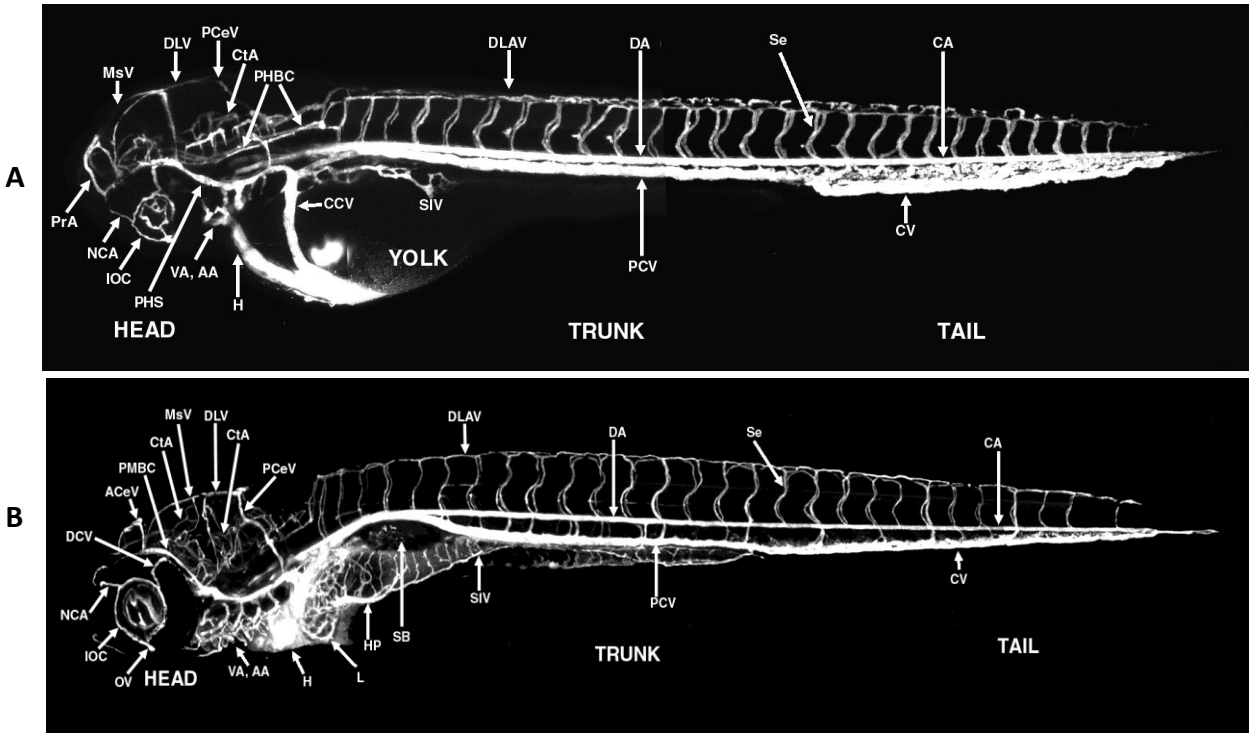

Figure 4.1.2. Labeled illustration of the vasculature system of 2 and 5-day old zebrafish larvae. Two key vessels EwS cells was identified within include the dorsal longitudinal anastomotic vein (DLAV) and posterior cerebral vein (PCeV). (A) is a labeled diagram of a 2dpf and (B) 5dpf zebrafish larvae vasculature. (Figure adopted from Isogai et al. 2001 with permission)

4.1.3 The Zebrafish Xenotransplantation Model can be used to Examine EwS Cell Migration

Given the size and transparency of the zebrafish larvae xenotransplantation model, intravasation, migration and extravasation of TC71 and A673 cell lines were observed at a single cell level with high resolution within almost all of the larvae. Numerous migration assays were conducted to observe multiple sgRNA *STAG2* knockout and control cell lines of TC71 and A673. EwS cell lines were successfully introduced into the hindbrain ventricle of 2dpf zebrafish larvae, which displayed active cell invasion and migration *in vivo* with low mortality of larvae recipients. The low mortality of larvae granted a large sample size of approximately 50-70 larvae per replicate.

Adapted from previous studies, a new larvae xenotransplantation scoring model was developed to study migration of EwS *in vivo*. The body of zebrafish larvae were categorized into three main regions, the dorsal surface, yolk sac and tail, illustrated in **Figure 2.5.2**. The dorsal surface, which extends from the hindbrain ventricle to tail was considered similar to local migration in that it was the closest in proximity to the hindbrain ventricle. The yolk sac was the area of high energy source, therefore migration to this site may be due to chemotaxis. Lastly, the tail was an area of distal migration, distinguished from the dorsal surface as posterior to the cloaca, which as predicted, displayed less migrated EwS cells than the dorsal surface.

To verify the absence of passive spread of EwS cell lines to these regions, fluorescent microspheres were similarly injected into the hindbrain ventricle and monitored for migration over five consecutive days. The presence of microspheres was

absent in all three regions, therefore validating the utility of these three regions for studying EwS cell line migration, initially injected into the hindbrain ventricle. Interestingly, the only passive spread of microspheres was observed to the thymus (refer to **Figure 3.1.4B**). It is unknown why there was passive spread to the thymus, however it is suggested that connections may temporarily exist between the thymus and hindbrain ventricle during the development of zebrafish larvae, as this passive spread to the thymus was only observed at 4 and 5 dpi. It is important to note that the microspheres are smaller than the cells (EwS cell: ~15 microns vs 10 microns microspheres), which may offer microspheres an advantage of moving to adjacent sites more easily due to the biophysical events normally occurring during larval development.

It has been reported in *X. laevis* larvae (tadpole) development that the thymus primordia is first morphologically recognizable as two spherical masses on either side of the hindbrain ventricle, surrounded by neural crest derived mesenchyme that migrate from the posterior hindbrain ventricle to the pharyngeal region (Lee et al. 2013). This could be a developmental force that may force the passive movement of microspheres into the thymus if observed in zebrafish larvae, however no similar studies have been conducted with zebrafish, and further research is necessary to determine the cause.

4.2 *STAG2* Knockout Promotes Increased Migration of EwS Cell Lines

STAG2 is a recently recognized tumour suppressor that upregulates various genes involved with the suppression of metastasis, where it has been found that the overexpression of STAG2 upregulated E-cadherin and caspase-3 &7, and downregulated

MMP2 and MMP9, used in the invasion of cancer cells. Therefore, it is logical that the *STAG2* gene has been determined to be the most mutated gene in the cohesin complex in Ewing sarcoma, present in 15-22% of EwS cases (Thota et al. 2014; Daniloski and Smith 2017). Recently, it was identified that 88% of EwS cases with the loss of STAG2 were metastatic, suggesting that loss of STAG2 is associated with metastasis of EwS (Crompton et al. 2014). To investigate the effects of STAG2 loss in EwS, A673 and TC71 cell lines with either *STAG2* knockout or NT control were injected into the hindbrain ventricle of 2dpf larvae and monitored for migration into the three specified regions over 5 consecutive days. Similar patterns of cell migration were observed for all A673 and TC71 cell lines to each specified region.

As shown in **Figure 3.2.1**, all 5 sgRNA *STAG2* knockouts of A673 and TC71 had the greatest percentage of migration at 3dpi to the dorsal surface, and a gradual decline thereafter. The decline in migrated EwS cells is likely due to the EwS cell relocation to other regions of the larvae. In addition, *STAG2* knockout significantly promoted a greater cell migration at 2 and/or 3dpi in comparison to the controls. Given that the dorsal surface is recognized as local migration, this suggests that *STAG2* knockout promoted an earlier onset of cell migration. Additionally, *STAG2* knockout in TC71 cell lines also promoted significantly increased migration at 4 and/or 5dpi, suggesting overall promotion of cell migration. As previously mentioned, migrated Ewing cell lines to the dorsal surface were predominately found within the DLAV, but additionally were in the lining and anterior of the yolk sac; this represents the ability of EwS cell lines to intravasate and extravasate through numerous routes.

Interestingly, as shown in **Figure 3.2.2 and Figure 3.2.3**, *STAG2* knockout in TC71 cell lines resulted in significantly increased percentage of larvae displaying migrated EwS cell lines within the yolk sac and tail in comparison to controls, but no significance in A673 cell lines. Percentage of larvae with migrated A673 or TC71 cell lines in the yolk sac linearly increased, where the greatest percentage of larvae displaying migrated cells was at 5dpi. One likely explanation is that EwS cell lines capable of migrating are gradually traveling to and finding themselves within the yolk sac by chemotaxis, due to its rich energy composition. In addition to nutritional needs, the yolk sac is rich with numerous lipids, which are essential building blocks for cancer cells to proliferate. This could additionally explain the increasing density of cancer cells observed to the yolk sac in the time-lapse videos.

Similar to the dorsal surface, the percentage of larvae with migrated EwS cell lines in the tail was greatest at 3dpi, and gradually declined thereafter. This decline may also be due to cancer cells ultimately migrating to the yolk sac. Although, *STAG2* knockout in A673 cell lines did not promote cell migration to the yolk sac and tail, *STAG2* knockout significantly promoted migration of TC71 cell lines from 2dpi to 5dpi. In comparison of the three specified regions, the tail can be considered the most distal, and thus require a stronger capability of EwS cell lines to migrate and survive; this suggests that *STAG2* knockout in TC71 cell lines promotes distal migration. It is important to note that no overall difference in migration was observed between the unaltered TC71 and A673 cell lines to all three monitored regions.

In addition to scoring the three regions separately, overall migration was investigated to determine if the decline in migrated EwS cells in the dorsal surface and tail were due to cell mortality or relocation to other regions. Overall migration was gradual, reaching a threshold around 3dpi (**Figure 3.2.4**). This suggests that the decline of migrated EwS cells in the dorsal surface and tail after 3dpi is likely due to the cells traveling towards the yolk sac, demonstrated by the increase in migrated EwS cells in the yolk sac. A clustering of EwS cells to and within the anterior yolk sac was observed through the 12-hour time lapse videos (**Figure 3.4.1B).** In summary, the xenotransplantation of EwS cell lines in larvae, which demonstrated that *STAG2* knockout in EwS cell lines not only promotes the migration of EwS, but also allows for an earlier onset of migration.

The loss of STAG2 and its role in the promotion of metastasis is now recognized to be caused by altered transcription regulation, and thus the downregulation of various genes involved with the suppression of metastasis (Crompton et al. 2014 and Galeev et al 2016). Specifically, the loss of STAG2 has been reported for its role in the altered expression of numerous genes, including *TP53*, *CDKN1A, EWS-FLI1*, all of which play a role in the promotion of metastasis, and to note both A673 and TC71 cell lines have non-functional p53 (May et al. 2013) . Interestingly, it is believed that all three of these genes are interconnected with STAG2, which will be further discussed in section 4.3. Importantly, in context of migration assay results observed in this study, differentiating between A673 and TC71 cell lines may help determine why *STAG2* knockout displayed a greater effect on migration of TC71 cell lines than A673.

4.2.1 Comparison of A673 and TC71 EwS Cell Lines: Differing EWS-FLI1 Expression Levels

EwS cell lines have been developed and described over the past 45 years, and several have undergone genetic analysis. With that said, cell lines have been acquired from tumours of different patients. Therefore, as cancer is a diverse disease, underlying genetic differences are expected between cell lines. The two Ewing sarcoma cell lines investigated in this study were A673 and TC71.

The A673 cell line was derived from a localized tumour in the muscle of a 15-year-old female patient (Martinez-Ramirez et al. 2003), whereas the TC71 cell line was derived from a solid tumour located in the humerus bone of a 22-year-old male that was originally metastatic (Giard et al. 1973). Therefore, another important reason why TC71 showed a higher degree of migration with *STAG2* knockout may be due to the fact that TC71 was derived from a locally recurrent tumour originally metastatic, but A673 was derived from the primary site with no details on metastasis or chemotherapy administration available (Giard et al. 1973). In addition, understanding other factors involved with STAG2 loss and cell migration can help develop a better understanding of the underlying mechanisms of EwS metastasis.

A cell line project conducted by the Institute of Cancer Research (ICR) identified that the TC71 cell line consisted of almost double the number of somatic mutations compared to A673 cells (631 vs. 322 somatic mutations). This increased instability of the TC71 cell line may also be an explanation as to why STAG2 loss has a greater effect on TC71 than A673 (COSMIC 2018). In addition, a study by Franzetti et al determined that

A673 had a greater level of *EWS-FLI1* expression than the TC71 cell line (Franzetti et al. 2017). Therefore, this observation led to the hypothesis that *STAG2* knockout has a greater effect on cell migration in EwS cell lines with lower expression of *EWS-FLI1.*

4.3 *STAG2* Knockout has a Greater Effect on Cell Migration in EwS Cell Lines with Lower Expression of *EWS-FLI1* Translocation

EWS-FLI1 is a key characteristic of EwS recognized for its role in the initiation and progression of this disease. In addition, EwS has recently been identified to grant EwS cells the ability to alternate between EWS-FLI1^{high} (initiation and proliferation) and EWS-FLI1^{low} (promotes metastasis) (Franzetti et al. 2017). How EWS-FLI regulates mechanisms of EwS cell migration and proliferation are still unknown, however, EWS-FLI1 expression is recognized as a modulator of hundreds of genes, some of which are involved with cell-cell or cell-matrix interactions. Therefore, when EwS cell lines have a lower expression of EWS-FLI1, its modulated genes involved with migration are no longer suppressed, and thus promote metastasis. While EWS-FLI1 binds to DNA and acts as an enhancer or promoter of genes, STAG2, also recognized as a modulator of gene transcription, instead alters the structural orientation of chromosomes, bringing together or pulling apart enhancers and promoters (Crompton et al. 2014).

As mentioned, this study demonstrated that loss of STAG2 promotes the migration of TC71 cell lines to the yolk sac and tail of larvae, but not in A673. While this observation was puzzling, a possible explanation was uncovered in a previous study that investigated the impact of EWS-FLI1^{low} and EWS-FLI1^{high} on the metastasis of EwS shown

in **Figure 4.3.1**. The level of EWS-FLI1 expression in A673 and TC71 cell lines was compared at a single cell level and determined that A673 and TC71 cell lines harbour different levels of EWS-FLI1 expression. The majority of A673 cell lines harbour EWS-FLI1^{high} expression, while the majority of TC71 harbour EWS-FLI1^{low} expression. Although TC71 and A673 cell lines share similar loss of STAG2 promotion of migration into the dorsal surface, there was a considerable difference in the effect of *STAG2* knockout on migration to the tail and yolk sac between A673 and TC71 cell lines. Since the tail is the most distant region and the yolk sac a cavity, it can be concluded that *STAG2* knockout in the TC71 cell line promotes cell migration greater than A673. Therefore, it was also concluded that loss of STAG2 has a greater effect on migration of EwS cell lines with lower expression of EWS-FLI1.

No previous studies have been conducted looking at this correlation between EWS-FLI1 and STAG2, however, it is hypothesized that due to EWS-FLI1^{high} expression in A673, the effect of STAG2 loss is either compensated or may be a second hit, promoting metastasis. Clinical studies have reported that *STAG2* mutations commonly arise after diagnosis, indicating its potential involvement with either resistance of sub-clonal EwS cancer cells, or as a secondary mutation after treatment (Tirode et al. 2014; Daniloski and Smith 2017). Therefore, it is hypothesized that a direct connection exists between EWS-FLI1 and STAG2.

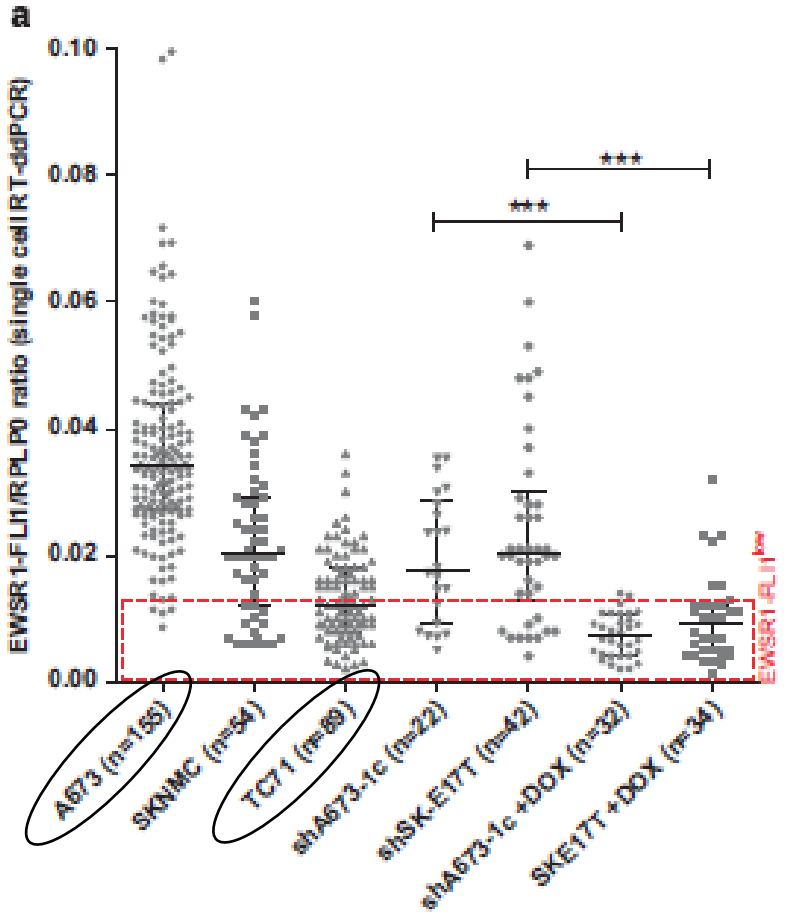

Figure 4.3.1. EWS-FLI1 expression is heterogeneous in EwS cell lines. Gene expression profiling at a single cell level by RT-PCR of EWS-FLI1 and RPLPO mRNA (control). This graph is the representation of EWS-FLI1/RPLPO ratio in A673, TC71 and SK-N-MC EwS cell lines; and the DOX inducible suppression of EWS-FLI1 cell lines. Individual dots represent a single cell. The EWS-FLI1^{low} threshold was defined by the upper limit of the DOX-treated cells range. A673 and TC71 are the two EwS cell lines used in our study. (Figure reproduced from Franzetti et al. 2017 with permission)

4.3.1 A Proposed Connection between Genes: *STAG2* Knockout Reduces the Expression of EWS-FLI1

To further investigate the connection between STAG2 and EWS-FLI1, the impact of STAG2 loss on EWS-FLI1 expression was explored using western blots, which determined that STAG2 loss reduces the expression of EWS-FLI1, as shown in **Figure 3.5.1**. Interestingly, similar to results shown in the migration assays, *STAG2* knockout did not significantly reduce the expression of EWS-FLI1 in A673 cell lines (14% down-regulation) but did in TC71 (42% down-regulation ($p<0.0001$)). This suggests that a mechanism to which STAG2 loss promotes metastasis may be through the downregulation of EWS-FLI1 expression; no previous studies have investigated this phenomenon. While this provides promising evidence towards the potential relationship between EWS-FLI1 and STAG2, these proteins are still poorly understood. Several upregulated and predominately downregulated genes have been identified to be involved with both EWS-FLI1 and STAG2 loss. Through the review of numerous publications, similarities were observed.

Firstly, *CDKN1A* that encodes for p21(WAF1/CIP1), a marker of p53 activity, was reported to be downregulated by STAG2 loss, but paradoxically, STAG2 loss was also associated with a higher *TP53* expression (4-fold increase), suggesting these variants are mutually exclusive. In addition, *TP53* mutations are more commonly co-mutated with STAG2 loss then found alone in Ewing sarcoma (Brohl, A. et al. 2014). Like STAG2 loss, EWS-FLI1 has been identified to alter the expression of G1 regulatory cyclins and cyclin-dependent kinase inhibitors both at the mRNA and protein levels. Suppression of *EWS-FLI1* has also been reported to result in the overexpression of *TP53*, where EWS-FLI1

downregulates both p21 and p53. The ETS domain of EWS-FLI1 directly interacts with p21, as it carries the promoter of the *p21* gene. Specifically, EWS-FLI1 can silence *TP53* through either the Notch signaling pathway or the formation of a protein complex involving EWS-FLI1 and p53 (Van der Ent et al. 2014). While it is unclear if the interaction occurs directly or is mediated by an oncogenic binding partner, STAG2 could potentially partake in this mechanism, however studies are required to investigate this hypothesis.

In addition to the overlapping regulated genes between STAG2 and EWS-FLI1, the reduction of EWS-FLI1 expression due to STAG2 loss, and the implications of EWS-FLI1^{low} expression on cell migration, it has been reported that STAG2 loss may affect the binding of EWS-FLI1 to a subset of chromatin binding locations as shown in **Figure 1.3.2**. In a study conducted by Crompton et al, STAG2 loss resulted in decreased expression of enriched genes otherwise upregulated by EWS-FLI1 (Crompton et al. 2014). This suggests that STAG2 loss may also play a key role in both the alteration of transcription activity of genes and the transcriptional activity of EWS-FLI1. Additional studies are necessary to confirm the role of EWS-FLI1 and STAG2 towards the metastasis of this disease and their potential role in specific hallmarks of cancer that promotes metastasis.

4.4 *STAG2* Knockout does not Play a Significant Role in Anoikis Resistance

Two essential characteristics that cancer cells harbour for successful metastasis include the ability to migrate and mechanisms for cell survival. An important obstacle cancer cells must overcome to metastasize is the ability to avoid apoptosis, specifically

resistance to anoikis. Anoikis is a programmed cell death induced by the loss of adhesion to the ECM or other cells. In the attempt to further investigate mechanisms that STAG2 loss may participate in to promote metastasis, additional experiments were conducted to determine if STAG2 loss promoted anoikis resistance in EwS cell lines.

Initially, it was hypothesized that STAG2 may play a role in anoikis resistance due to an observation; this experiment consisted of the co-injection of lenti-virus fluorescent transduced A673 and TC71, *STAG2* knockout and control cell lines that were permanently labeled with separate colours. When the labeled cell lines were injected into the yolk sac, an anoikis inducing environment due to lack of adhesive surfaces, the control cells displayed reduced fluorescence in comparison to the *STAG2* knockouts from 3-5dpi. It is important to note that for these cells to remain fluorescent, they must be viable, therefore this observation suggested that *STAG2* knockout EwS cells were surviving better than the controls within the anoikis-promoting environment.

In addition, as mentioned, *CDKN1A* is downregulated by STAG2 loss, and encodes for the caspase-3 mediated protein involved with the execution of apoptosis (Gartel and Tyner 2002). Therefore, it was hypothesized that STAG2 loss may promote anoikis resistance. However, no significant difference was observed in A673 and TC71 EwS cell lines between *STAG2* knockout and control for both the flow cytometry and alamarBlue® cell viability assay as shown in **Figure 3.6.1-2.** This suggests that alternative mechanisms, aside from STAG2 may play a more vital role in the anoikis resistance of EwS.

4.5 Clinical Applications

The xenotransplantation zebrafish model provides a powerful drug screening technique to investigate thousands of drugs to evaluate their impact on not only cancer cells, but the treated host. As mentioned, a previous study utilized the zebrafish xenotransplantation model to determine the implications of the co-treatment of YK-4-279 and Nutlin 3, an inhibitor of mdm2 (negative regulator of p53). The co-treatment of these drugs interfered with EWS-FLI1 transcriptional activity and successfully inhibited the proliferation and migration of EwS cell lines within the zebrafish cancer model (Wietske van der et al. 2014). Through the establishment of STAG2 as an important regulator of metastasis, future drug trials can be conducted on *STAG2* knockout cell lines xenotransplanted into zebrafish larvae, and its potential role with EWS-FLI1.

In addition, while there are no current treatments specifically targeting STAG2, due to the loss thereof, developing a better understanding of the relationship to metastasis and downstream factors of STAG2 loss may lead to the development of future targetable treatments to improve the poor survival of this disease.

4.6 Advantages and Limitations to Zebrafish Larvae as the Xenotransplantation Model

The utilization of zebrafish larvae as a xenotransplantation model has provided numerous opportunities to study cancer, including real-time *in vivo* cell behaviour and migration that cannot be observed in other cancer models. Due to the transparent nature of the zebrafish larvae, especially that of *caspers*, injected EwS cell lines can be directly observed within the zebrafish without having to sacrifice the host. However,

zebrafish larvae are limited in the observation of some metastatic processes such as tumour dormancy, a key process in the relapse of cancer. While cancer cells can be injected into adult zebrafish, an adult zebrafish is typically only kept in a research laboratory for two years, whereas dormant cells typically last longer. One solution to this problem is the serial transplantation of these cell lines, where non-migrated cells and migrated cells are separately harvested from larvae and re-xenografted into additional larvae hindbrain ventricle to observe the migration behaviour (Taylor and Zon 2009). One issue that may arise in this experiment, given the small size of zebrafish larvae, is the technical difficulty harvesting migrated EwS cells, which were typically seen individually and thus may prove to be difficult.

Labeling EwS cell lines with CMTMR dye has provided the opportunity to observe the behaviour and migration of EwS cell lines within the transparent zebrafish model. A limitation with this labeling process is the weakening fluorescence around 3dpi. While this was reduced when provided protection from direct bulb light of the incubator, as CMTMR is sensitive to light, fluorescence may be reduced due to cells dividing. In addition, the intense autofluorescence of the yolk sac can lead to difficulties interpreting the presence of migrated cells into the yolk sac, especially if only few are present. While one solution may be utilizing another dye, such as CMFDA (green), with an excitation/emission (492/517 nm maxima) dramatically brighter than red, zebrafish larvae have been observed to express green autofluorescence, increasing the risk of false positives.

The immune system is another important factor in the context of cancer cell metastasis, where host immune cells such as tumour-associated macrophages, myeloid-derived suppressor cells, and regulatory T cells have been shown to promote tumour growth, invasion and metastasis; however, this concept was not investigated in this study (Smith and Kang 2013). The immune system can be divided into the innate and adaptive immune response, however as mentioned, the adaptive immune response is not developed within larvae until 4-6 weeks post fertilization, therefore cell migration of EwS cell lines was investigated in a host lacking these specific immune cells, such as T cells. While the lack of adaptive immune cells was beneficial in that no immunosuppression was necessary prior to xenotransplantation, interactions of the adaptive immune response in the context of EwS migration and progression was lacking. Nonetheless, the innate immune response is present within larvae at the 2-7dpf time period used in this study.

Lastly, zebrafish have been recognized to share approximately 70% protein coding genes with humans, however, zebrafish are not the same species as humans and harbour a lower genetic conservation than that of mammalian cancer models. Although, with the establishment and development of transgenic humanized zebrafish, we can directly observe the impact of gene expression and the lack thereof. Further animal models in closer relation to humans must also be utilized, however, zebrafish can serve as an initial screening strategy to perform as a faster selection process for potential treatments.

4.7 Future Directions

In this thesis, it was demonstrated that zebrafish larvae can serve as a primary mainstream model to study EwS, and that the hindbrain ventricle is the optimal location to inject EwS cells to study cell migration. It is important to note that EwS proliferation was limited within the hindbrain ventricle, therefore, it would be important to investigate proliferation of A673 and TC71 EwS cell lines within the yolk sac. While this was attempted in this thesis, the high larval mortality rate proved difficult to get a large enough sample size. Additionally, all EwS cell lines displayed a linear increase in migration to the yolk sac of xenotransplantation larvae, hypothesized to be the result of chemotaxis, however, CD99 staining is required for further confirmation of EwS cells within the yolk sac. To confirm this hypothesis, FBS, the *in vitro* source of nutrients for cell lines, could be injected into the yolk sac to further enrich the nutritional quantity within the yolk sac prior to the injection of EwS cells into the hindbrain ventricle.

It was demonstrated that STAG2 loss not only resulted in a reduced expression of EWS-FLI1, but *STAG2* knockout had a greater effect on cell migration in EwS cell lines with lower expression of EWS-FLI1 (TC71). Therefore, to further investigate this phenomenon, *EWS-FLI1* can be additionally knocked down in A673 cell lines with *STAG2* knockout. Since the A673 cell line is identified to harbour a high expression of EWS-FLI1, whereas a low expression in the TC71 cell line, it can be therefore hypothesized that if *STAG2* knockout has a greater effect on EwS cells with a lower expression of EWS-FLI1, than by the knockdown of *EWS-FLI1* in A673 cell lines, *STAG2* knockout will result in a significantly increased cell migration, especially to the tail and yolk sac of the recipient

larvae. It is important to note that while EWS-FLI1 expression was not directly compared between the two cell lines in this study, there did not appear to be a qualitative difference observed by western blot. While this could be due to the fact that A673 cell lines display a greater heterogeneity in EWS-FLI1 expression than TC71 cells, this needs to be further investigated (Franzetti et al. 2017). Furthermore, this suggests that other important partners may contribute to the increased effect of STAG2 knockout in TC71 cell lines.

Through review of numerous studies, it was determined that both STAG2 loss and EWS-FLI1^{low} expression resulted in increased *TP53* expression, in addition to promoting metastasis (Albini and Pfeffer 2006; Li et al. 2010; Van der Ent et al. 2014; Brohl et al. 2014; Crompton et al. 2014). While it is unknown how *TP53* overexpression can promote metastasis in other cancers such as intestinal tumours (Albini and Pfeffer 2006), determining the implications of *TP53* overexpression can be utilized to develop a better comprehension of the relationship between EWS-FLI1 and STAG2 through the mechanism and rationale of *TP53* overexpression. Additionally, it is important to reiterate that both A673 and TC71 cell lines harbour a complete loss of p53 (frameshift and non-sense mutation, respectively), therefore to further investigate this phenomenon, the additional EwS cell line, TC32 with functional p53 and the absence of STAG2 and p21 (marker of p53 activity) can be used to investigate the expression level.

As previously mentioned, although implications of the immune system on EwS cell migration was not investigated in this study, other transgenic zebrafish fluorescent reporter lines, such as *Tg(mpx:eGFP)* (neutrophil-specific) and *Tg(meg1:eGFP)*

(macrophage-specific), can be employed to investigate the interaction between EwS and innate immune cells (Di et al. 2017). In addition, the contribution of macrophages and neutrophils towards the invasion and migration of EwS cells could be further investigated by selectively removing these cell populations, for example, through targeted knockdown of neutrophil or macrophage essential genes transiently using morpholino oligonucleotides (MOs) or permanently through gene editing (e.g. CRISPR).

Lastly, as previously mentioned, EwS cell lines (A673 and TC71) with *STAG2* knockout or controls were injected into the hindbrain ventricle of larvae. At 3dpi the larvae were sacrificed, and the heads separated from their body. These samples were sent for targeted transcriptome analysis to investigate over 365 most commonly mutated genes of cancer to determine the differences in gene transcript levels between *STAG2* knockout and wild-type *STAG2*, and in additional analyze the differences between non-migrated (within hindbrain ventricle) and migrated EwS cell lines (body). With these results, we can determine downstream factors involved with STAG2 loss and cell migration that may lead to future druggable targets.

4.8 Conclusions

In conclusion, the zebrafish larvae were employed as a xenotransplantation model to study EwS and the contribution of STAG2 loss on cell migration and invasion. Moreover, the hindbrain ventricle was determined to be the optimal site to inject fluorescently labeled EwS cells, allowing for the observation of migration into three specified locations, the dorsal surface, yolk sac and tail. Through analysis of 12-hour

time lapse imaging, it was determined that EwS cell lines utilize veins of the zebrafish to escape the hindbrain ventricle, such as the PCeV.

STAG2 knockout was demonstrated to promote EwS cell migration within the zebrafish model. Specifically, *STAG2* knockout enhanced cell migration of both A673 and TC71 cell lines locally to the dorsal surface, but only TC71 cells to the tail and yolk sac. This suggests that STAG2 loss promotes cell migration of TC71 cells more than A673 cells. It was found that EWS-FLI1 expression is high in A673, whereas low in TC71 cell lines (Franzetti et al. 2017), leading to the hypothesis that *STAG2* knockout promotes cell migration in EwS cells with lower expression of EWS-FLI1. This is consistent with other studies that have shown that EWS-FLI1^{low} promotes EwS metastasis. In addition, *STAG2* knockout was determined to reduce the expression of EWS-FLI1.

Through results acquired in this study, it is proposed that there exists a direct connection between EWS-FLI1^{low} and STAG2 loss, which together may promote the metastasis of EwS. In the attempt to clarify this relationship, the implications of STAG2 loss, and fluctuating EWS-FLI1 expression levels, a web chart was developed summarizing the cross-over interactions reported in literature and experimental observations (**Figure 4.8**). To explore additional mechanisms that STAG2 loss may contribute to promote metastasis of EwS, it was hypothesized that *STAG2* knockout promoted anoikis resistance, however, this was not found to be the case. Lastly, the ability to anatomically separate metastatic from non-metastatic cells in zebrafish larvae provides a unique opportunity to identify downstream genes that are differentially expressed in migrating cells that may represent driver lesions and therapeutic targets.

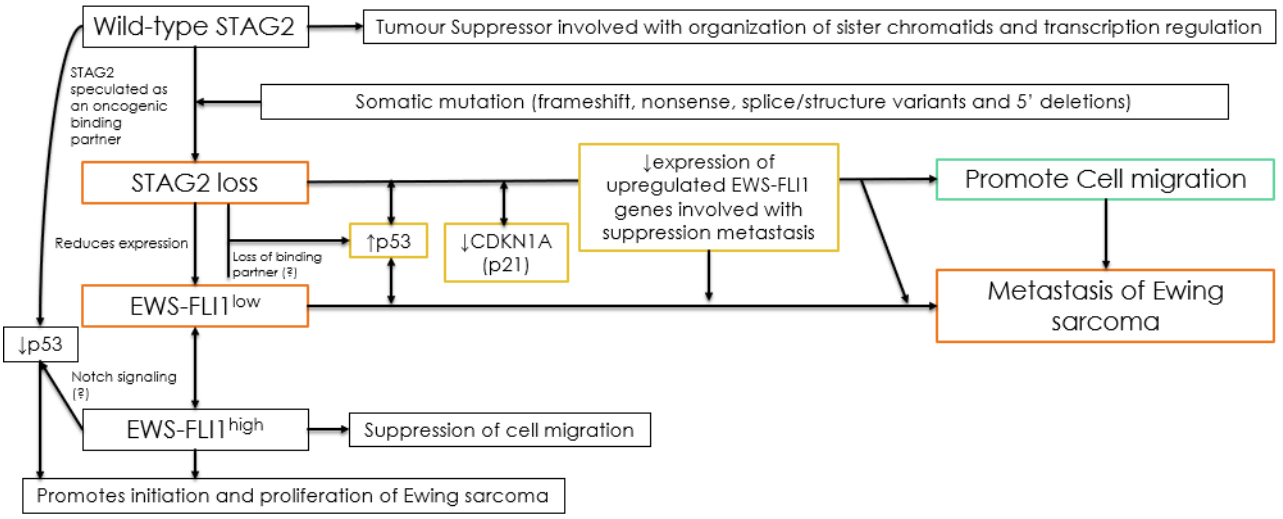

Figure 4.8. Proposed hypothesis of the connection between STAG2 and EWS-FLI1 toward the promotion of EwS metastasis based on results of this study and literature review. Both STAG2 loss and EWS-FLI1^{low} expression has been demonstrated in this study and reported in literature to promote EwS migration and metastasis.

References

Albini, A., & Pfeffer, U. (2006). A new tumor suppressor gene: invasion, metastasis, and angiogenesis as potential key targets.

Alsarraj, J., & Hunter, K. W. (2012). Bromodomain-containing protein 4: a dynamic regulator of breast cancer metastasis through modulation of the extracellular matrix. *International journal of breast cancer*, *2012*.

Ambros, I. M., Ambros, P. F., Strehl, S., Kovar, H., Gadner, H., & Salzer-Kuntschik, M. (1991). MIC2 is a specific marker for Ewing's sarcoma and peripheral primitive neuroectodermal tumors. Evidence for a common histogenesis of Ewing's sarcoma and peripheral primitive neuroectodermal tumors from MIC2 expression and specific chromosome aberration. *Cancer*, *67*(7), 1886-1893.

Baruchel, S., Pappo, A., Krailo, M., Baker, K. S., Wu, B., Villaluna, D., ... & Blaney, S. M. (2012). A phase 2 trial of trabectedin in children with recurrent rhabdomyosarcoma, Ewing sarcoma and non-rhabdomyosarcoma soft tissue sarcomas: a report from the Children's Oncology Group. *European Journal of Cancer*, *48*(4), 579-585.

Brohl, A.S., Solomon, D.A., Chang, W., Wang, J., Song, Y., Sindiri, S., Patidar, R., Hurd, L., Chen, L., Shern, J.F. and Liao, H. (2014). The genomic landscape of the Ewing Sarcoma family of tumors reveals recurrent STAG2 mutation. *PLoS genetics*, *10*(7), e1004475.

Burgert Jr, E. O., Nesbit, M. E., Garnsey, L. A., Gehan, E. A., Herrmann, J., Vietti, T. J., ... & Thomas, P. (1990). Multimodal therapy for the management of nonpelvic, localized Ewing's sarcoma of bone: intergroup study IESS-II. *Journal of Clinical Oncology*, *8*(9), 1514-1524.

Cavazzana, A. O., Navarro, S., Noguera, R., Reynolds, P. C., & Triche, T. J. (1988). Olfactory neuroblastoma is not a neuroblastoma but is related to primitive neuroectodermal tumor (PNET). *Progress in clinical and biological research*, *271*, 463.

Chambers, A. F., Groom, A. C., & MacDonald, I. C. (2002). Metastasis: dissemination and growth of cancer cells in metastatic sites. *Nature Reviews Cancer*, *2*(8), 563.

Chaturvedi, A., Hoffman, L.M., Jensen, C.C., Lin, Y.C., Grossmann, A.H., Randall, R.L., Lessnick, S.L., Welm, A.L. and Beckerle, M.C. (2014). Molecular dissection of the mechanism by which EWS/FLI expression compromises actin cytoskeletal integrity and cell adhesion in Ewing sarcoma. *Molecular biology of the cell*, *25*(18), 2695-2709.

Chiang, S. P., Cabrera, R. M., & Segall, J. E. (2016). Tumor cell intravasation. *American Journal of Physiology-Cell Physiology*, *311*(1), C1-C14.

Cripe, T. P. (2010). Ewing sarcoma: an eponym window to history. *Sarcoma*, *2011*.

Crompton, B. D., Stewart, C., Taylor-Weiner, A., Alexe, G., Kurek, K. C., Calicchio, M. L., ... & Thorner, A. R. (2014). The genomic landscape of pediatric Ewing sarcoma. *Cancer discovery*, *4*(11), 1326-1341.

Daniloski, Z., & Smith, S. (2017). Loss of Tumor Suppressor STAG2 Promotes Telomere Recombination and Extends the Replicative Lifespan of Normal Human Cells. *Cancer research*, *77*(20), 5530-5542.

Delov, V., Muth-Köhne, E., Schäfers, C., & Fenske, M. (2014). Transgenic fluorescent zebrafish Tg (fli1: EGFP) y1 for the identification of vasotoxicity within the zFET. *Aquatic toxicology*, *150*, 189-200.

Di, Q., Lin, Q., Huang, Z., Chi, Y., Chen, X., Zhang, W., & Zhang, Y. (2017). Zebrafish nephrosin helps host defence against Escherichia coli infection. *Open biology*, *7*(8), 170040.

El-Naggar, A. M., Veinotte, C. J., Cheng, H., Grunewald, T. G., Negri, G. L., Somasekharan, S. P., ... & Kyle, A. H. (2015). Translational activation of HIF1α by YB-1 promotes sarcoma metastasis. *Cancer cell*, *27*(5), 682-697.

Faguet, G. B. (2008). The war on cancer: an anatomy of failure, a blueprint for the future. *Dordrecht: Springer*.

Fonnum, F., Myhre, O., Sterri, S. H., & Bogen, I. L. (2003). Free radical formation and signal pathways in cerebellar granule cells. *Journal of Neurochemistry*, *87*, 155.

Fraher, D., Sanigorski, A., Mellett, N. A., Meikle, P. J., Sinclair, A. J., & Gibert, Y. (2016). Zebrafish embryonic lipidomic analysis reveals that the yolk cell is metabolically active in processing lipid. *Cell reports*, *14*(6), 1317-1329.

Franzetti, G. A., Laud-Duval, K., Van Der Ent, W., Brisac, A., Irondelle, M., Aubert, S., ... & Chavrier, P. (2017). Cell-to-cell heterogeneity of EWSR1-FLI1 activity determines proliferation/migration choices in Ewing sarcoma cells. *Oncogene*, *36*(25), 3505.

Gartel, A. L., & Tyner, A. L. (2002). The role of the cyclin-dependent kinase inhibitor p21 in apoptosis 1 supported in part by NIH grant R01 DK56283 (to ALT) for the p21 research and Campus Research Board and Illinois Department of Public Health Penny Severns Breast and Cervical Cancer grants (to ALG). 1. *Molecular cancer therapeutics*, *1*(8), 639-649.

Gierisch, M. E., Pfistner, F., Lopez-Garcia, L. A., Harder, L., Schäfer, B. W., & Niggli, F. K. (2016). Proteasomal degradation of the EWS-FLI1 fusion protein is regulated by a single lysine residue. *Journal of Biological Chemistry*, *291*(52), 26922-26933.

Goessling, W., North, T. E., & Zon, L. I. (2007). New waves of discovery: modeling cancer in zebrafish. *Journal of Clinical Oncology*, *25*(17), 2473-2479.

Grier, H. E., Krailo, M. D., Tarbell, N. J., Link, M. P., Fryer, C. J., Pritchard, D. J., ... & Donaldson, S. S. (2003). Addition of ifosfamide and etoposide to standard chemotherapy for Ewing's sarcoma and primitive neuroectodermal tumor of bone. *New England Journal of Medicine*, *348*(8), 694-701.

Grigore, A. D., Jolly, M. K., Jia, D., Farach-Carson, M. C., & Levine, H. (2016). Tumor Budding: The Name is EMT. Partial EMT. *Journal of clinical medicine*, *5*(5), 51.

Guillon, N., Tirode, F., Boeva, V., Zynovyev, A., Barillot, E., & Delattre, O. (2009). The oncogenic EWS-FLI1 protein binds in vivo GGAA microsatellite sequences with potential transcriptional activation function. *PloS one*, *4*(3), e4932.

He, S., Lamers, G. E., Beenakker, J. W. M., Cui, C., Ghotra, V. P., Danen, E. H., ... & Snaar-Jagalska, B. E. (2012). Neutrophil-mediated experimental metastasis is enhanced by VEGFR inhibition in a zebrafish xenograft model. *The Journal of pathology*, *227*(4), 431-445. Heare, T., Hensley, M. A., & Dell'Orfano, S. (2009). Bone tumors: osteosarcoma and Ewing's sarcoma. *Current opinion in pediatrics*, *21*(3), 365-372.

Horowitz, M. E., Tsokos, M., & DeLaney, T. F. (1992). Ewing's sarcoma. *CA: a cancer journal for clinicians*, *42*(5), 300-320.

Howlader, N. A. M. N. (2010). Surveillance epidemiology and end results (SEER) cancer statistics review, 1975-2008. *National Cancer Institute*.

Huang, K., Chen, L., Zhang, J., Wu, Z., Lan, L., Wang, L., ... & Liu, Y. (2014). Elevated p53 expression levels correlate with tumor progression and poor prognosis in patients exhibiting esophageal squamous cell carcinoma. *Oncology letters*, *8*(4), 1441-1446.

Ilaslan, H., Schils, J., Nageotte, W., Lietman, S. A., & Sundaram, M. (2010). Clinical presentation and imaging of bone and soft-tissue sarcomas. *Cleveland Clinic journal of medicine*, *77*, S2-7.

Isogai, S., Horiguchi, M., & Weinstein, B. M. (2001). The vascular anatomy of the developing zebrafish: an atlas of embryonic and early larval development. *Developmental biology*, *230*(2), 278-301.

Iwamoto, Y. (2007). Diagnosis and treatment of Ewing's sarcoma. *Japanese Journal of Clinical Oncology*, *37*(2), 79-89.

Kadin, M. E., & Bensch, K. G. (1971). On the origin of Ewing's tumor. *Cancer*, *27*(2), 257-273.

Kolb, E. A., Gorlick, R., Reynolds, C. P., Kang, M. H., Carol, H., Lock, R., ... & Kurmasheva, R. T. (2013). Initial testing (stage 1) of eribulin, a novel tubulin binding agent, by the pediatric preclinical testing program. *Pediatric blood & cancer*, *60*(8), 1325-1332.

Krakhmal, N. V., Zavyalova, M. V., Denisov, E. V., Vtorushin, S. V., & Perelmuter, V. M. (2015). Cancer invasion: patterns and mechanisms. *Acta Naturae (англоязычная версия)*, *7*(2 (25)).

Laale, H. W. (1977). The biology and use of zebrafish, Brachydanio rerio in fisheries research. *Journal of Fish Biology*, *10*(2), 121-173.

Lau, L., Supko, J. G., Blaney, S., Hershon, L., Seibel, N., Krailo, M., ... & Baruchel, S. (2005). A phase I and pharmacokinetic study of ecteinascidin-743 (Yondelis) in children with refractory solid tumors. A Children's Oncology Group study. *Clinical Cancer Research*, *11*(2), 672-677.

Lee, G., Kim, H., Elkabetz, Y., Al Shamy, G., Panagiotakos, G., Barberi, T., ... & Studer, L. (2007). Isolation and directed differentiation of neural crest stem cells derived from human embryonic stem cells. *Nature biotechnology*, *25*(12).

Lee, Y. H., Williams, A., Hong, C. S., You, Y., Senoo, M., & Saint-Jeannet, J. P. (2013). Early development of the thymus in Xenopus laevis. *Developmental Dynamics*, *242*(2), 164-178.

Li, Y., Tanaka, K., Fan, X., Nakatani, F., Li, X., Nakamura, T., ... & Iwamoto, Y. (2010). Inhibition of the transcriptional function of p53 by EWS–Fli1 chimeric protein in Ewing Family Tumors. *Cancer letters*, *294*(1), 57-65.

Lipinski, M., Hirsch, M. R., Deagostini-Bazin, H., Yamada, O., Tursz, T., & Goridis, C. (1987). Characterization of neural cell adhesion molecules (NCAM) expressed by Ewing and neuroblastoma cell lines. *International journal of cancer*, *40*(1), 81-86.

Liu, Q., Zhang, H., Jiang, X., Qian, C., Liu, Z., & Luo, D. (2017). Factors involved in cancer metastasis: a better understanding to “seed and soil” hypothesis. *Molecular cancer*, *16*(1), 176.

Martinez-Ramirez, S., Sanchez-Cortes, S., Garcia-Ramos, J. V., Domingo, C., Fortes, C., & Blanco-Varela, M. T. (2003). Micro-Raman spectroscopy applied to depth profiles of carbonates formed in lime mortar. *Cement and Concrete Research*, *33*(12), 2063-2068.

May, W. A., Grigoryan, R. S., Keshelava, N., Cabral, D. J., Christensen, L. L., Jenabi, J., ... & Reynolds, C. P. (2013). Characterization and drug resistance patterns of Ewing's sarcoma family tumor cell lines. *PloS one*, *8*(12), e80060.

Nesbit Jr, M. E., Gehan, E. A., Burgert Jr, E. O., Vietti, T. J., Cangir, A., Tefft, M., ... & Kissane, J. M. (1990). Multimodal therapy for the management of primary, nonmetastatic Ewing's sarcoma of bone: a long-term follow-up of the First Intergroup study. *Journal of Clinical Oncology*, *8*(10), 1664-1674.

Nesbit Jr, M. E., Gehan, E. A., Burgert Jr, E. O., Vietti, T. J., Cangir, A., Tefft, M., ... & Kissane, J. M. (1990). Multimodal therapy for the management of primary, nonmetastatic Ewing's sarcoma of bone: a long-term follow-up of the First Intergroup study. *Journal of Clinical Oncology*, *8*(10), 1664-1674.

Ozaki, T. (2015). Diagnosis and treatment of Ewing sarcoma of the bone: a review article. *Journal of Orthopaedic Science*, *20*(2), 250-263.

Pantel, K., & Brakenhoff, R. H. (2004). Dissecting the metastatic cascade. *Nature Reviews Cancer*, *4*(6), 448.

Peters, J. M., Tedeschi, A., & Schmitz, J. (2008). The cohesin complex and its roles in chromosome biology. *Genes & development*, *22*(22), 3089-3114.

Riggi, N., Cironi, L., Provero, P., Suvà, M.L., Kaloulis, K., Garcia-Echeverria, C., Hoffmann, F., Trumpp, A. and Stamenkovic, I.(2005). Development of Ewing's sarcoma from primary bone marrow–derived mesenchymal progenitor cells. *Cancer research*, *65*(24), 11459-11468.

Saitoh, M. (2018). Involvement of partial EMT in cancer progression. *The Journal of Biochemistry*.

Sankar, S., & Lessnick, S. L. (2011). Promiscuous partnerships in Ewing's sarcoma. *Cancer genetics*, *204*(7), 351-365.

Seyfried, T. N., & Huysentruyt, L. C. (2013). On the origin of cancer metastasis. *Critical reviews in oncogenesis*, *18*(1-2), 43.

Smith, H. A., & Kang, Y. (2013). The metastasis-promoting roles of tumor-associated immune cells. *Journal of molecular medicine*, *91*(4), 411-429.

Solomon, D. A., Kim, T., Diaz-Martinez, L. A., Fair, J., Elkahloun, A. G., Harris, B. T., ... & Samuels, Y. (2011). Mutational inactivation of STAG2 causes aneuploidy in human cancer. *Science*, *333*(6045), 1039-1043.

Staege, M. S., Hutter, C., Neumann, I., Foja, S., Hattenhorst, U. E., Hansen, G., Afar, D., & Burdach, S. E. (2004). DNA microarrays reveal relationship of Ewing family tumors to both endothelial and fetal neural crest-derived cells and define novel targets. *Cancer research*, *64*(22), 8213-8221.

Stoletov, K., & Klemke, R. (2008). Catch of the day: zebrafish as a human cancer model. *Oncogene*, *27*(33), 4509.

Teicher, B. A., Bagley, R. G., Rouleau, C., Kruger, A., Ren, Y., & Kurtzberg, L. (2011). Characteristics of human Ewing/PNET sarcoma models. *Annals of Saudi medicine*, *31*(2), 174.

Thota, S., Viny, A. D., Makishima, H., Spitzer, B., Radivoyevitch, T., Przychodzen, B., ... & Maciejewski, J. P. (2014). Genetic alterations of the cohesin complex genes in myeloid malignancies. *Blood*, *124*(11), 1790-1798.

Toomey, E. C., Schiffman, J. D., & Lessnick, S. L. (2010). Recent advances in the molecular pathogenesis of Ewing's sarcoma. *Oncogene*, *29*(32), 4504.

van der Ent, W., Jochemsen, A. G., Teunisse, A. F., Krens, S. F., Szuhai, K., Spaink, H. P., ... & Snaar-Jagalska, B. E. (2014). Ewing sarcoma inhibition by disruption of EWSR1–FLI1 transcriptional activity and reactivation of p53. *The Journal of pathology*, *233*(4), 415-424.

van der Lelij, P., Lieb, S., Jude, J., Wutz, G., Santos, C. P., Falkenberg, K., ... & Kovar, H. (2017). Synthetic lethality between the cohesin subunits STAG1 and STAG2 in diverse cancer contexts. *Elife*, *6*.

van Zijl, F., Krupitza, G., & Mikulits, W. (2011). Initial steps of metastasis: cell invasion and endothelial transmigration. *Mutation Research/Reviews in Mutation Research*, *728*(1), 23-34.

Veinotte, C. J., Dellaire, G., & Berman, J. N. (2014). Hooking the big one: the potential of zebrafish xenotransplantation to reform cancer drug screening in the genomic era. *Disease models & mechanisms*, *7*(7), 745-754.

Wang, H., Zhong, J., Wu, C., Liu, Y., Zhang, J., Zou, X., ... & Tang, A. (2017). Stromal antigen 2 functions as a tumor suppressor in bladder cancer cells. *Oncology reports*, *38*(2), 917-925.

Wang, X., Enomoto, A., Asai, N., Kato, T., & Takahashi, M. (2016). Collective invasion of cancer: perspectives from pathology and development. *Pathology international*, *66*(4), 183-192.

Wehmas, L. C., Tanguay, R. L., Punnoose, A., & Greenwood, J. A. (2016). Developing a Novel Embryo–Larval Zebrafish Xenograft Assay to Prioritize Human Glioblastoma Therapeutics. *Zebrafish*, *13*(4), 317-329.

Welch, D. R. (2006). Defining a cancer metastasis. *AACR education book 2006*, 111-115.

Whang-Peng, J., Triche, T. J., Knutsen, T., Miser, J., Kao-Shan, S., Tsai, S., & Israel, M. A. (1986). Cytogenetic characterization of selected small round cell tumors of childhood. *Cancer Genetics*, *21*(3), 185-208.

White, R. M., Sessa, A., Burke, C., Bowman, T., LeBlanc, J., Ceol, C., ... & Zon, L. I. (2008). Transparent adult zebrafish as a tool for in vivo transplantation analysis. *Cell stem cell*, *2*(2), 183-189.

Womer, R. B., West, D. C., Krailo, M. D., Dickman, P. S., Pawel, B. R., Grier, H. E., ... & Weiss, A. R. (2012). Randomized controlled trial of interval-compressed chemotherapy for the treatment of localized Ewing sarcoma: a report from the Children's Oncology Group. *Journal of Clinical Oncology*, *30*(33), 4148.

Zhao, M., Li, Z., & Qu, H. (2015). An evidence-based knowledgebase of metastasis suppressors to identify key pathways relevant to cancer metastasis. *Scientific reports*, *5*, 15478.

Appendix A: Catalog Numbers of Materials Used

2-Mercaptoethanol: **M-7522** Sigma

BSA (bovine serum albumin) **9048-46-8** Bioshop

DMEM (1X): **11965092** Gibco

MicroBCA™ protein assay kit: **23235** Thermo Scientific

Microscope slides for dissociation: **12-550-15** Thermo Fisher

Mini-protean TGX precast gels **456-9035** BioRad

PCR tubes: **PCR-0208-cp-c** Axygen

Puromycin: **A11138-03**

RPMI 16400 (1X): **11875-093** Gibco

Sodium Fluoride (NAF): **57920-100G** Sigma

Sodium orthovanadate (Na_3VO_4): **56508-10G** Sigma

StemPro® Accutase: **A11105-01** Gibco

Thermocycler: **22331** Eppendorf

Trisglycine: **1610734** Sigma

TRIzol™ reagent: **15596026** Ambion

Trypsin (0.25%): **25200-056** Gibco

β-glycerolphosphate: **G9422** Gibco

Transfer buffer: **1610734** Sigma

Ultrapure™ LMP agarose (0.7%): **16520-050** Invitrogen

Sodium pyruvate: **11360-070** Gibco

PBS: **10010-023** Gibco

Twelve-well plates: **10062-894** VMR

Culture flasks: **10062-860** VWR

123 CountBeads: **01-1234-42** Invitrogen

Supersignal® West Dura Extended Duration Substrate: **34075** Thermo Scientific

Agarose: **BP160-500** Fisher Scientific

Tris/glycine buffer (10x) : **1610734** Sigma

TBS (10x) : **170-6435** Sigma

SDS (10%) solution : **1610416** Sigma

Immun-Blot® LF PVDF: **162-0260** BioRad

FBS: **080450** Wisent

Precision Plus Protein™ unstained standards: **161-0363** BioRad

Precision Plus Protein™ all blue standards: **161-0373** BioRad

β-actin rabbit mAb: **126205** Cell Signaling

CMTMR: **C2925** Invitrogen

Pharminogen PE Annexin V apoptosis detection kit : **559763** BD

SA-2 antibody : **Sc-81852** Santa Cruz Biotech

FLI1 antibody : **ab15289** abcam

Chloroform : **C-2432** Sigma

Laemmli buffer : **161-0747** BioRad

Phasemaker tubes: **A339937** Introgen Thermo Scientific

Nuclease free water: **AM9937** Sigma

7AAD: **00699350** Invitrogen

AlamarBlue® cell viability reagent: **1100** Dal

EDTA: **15575-038** Introgen Lifetech

Trypan Blue (0.4%): **1520-061** Gibco

Appendix B: Copyright Permission

Figure 1.1.4

License Number	4351500248402
License date	May 17, 2018
Licensed Content Publisher	Elsevier
Licensed Content Publication	Seminars in Diagnostic Pathology
Licensed Content Title	Ewing sarcoma
Licensed Content Author	Eun-Young K. Choi,Jerad M. Gardner,David R. Lucas,Jonathan B. McHugh,Rajiv M. Patel
Licensed Content Date	Jan 1, 2014
Licensed Content Volume	31
Licensed Content Issue	1
Licensed Content Pages	9
Type of Use	reuse in a thesis/dissertation
Portion	figures/tables/illustrations
Number of figures/tables/illustrations	1
Format	both print and electronic
Are you the author of this Elsevier article?	No
Will you be translating?	No
Original figure numbers	Figure 2 A and B
Title of your thesis/dissertation	Fish Tales: Loss of STAG2 Promotes Metastasis of Ewing Sarcoma
Expected completion date	Jun 2018
Estimated size (number of pages)	150
Attachment	
Requestor Location	Dalhousie

Figure 1.3.2

License Number	4351511111875
License date	May 17, 2018
Licensed Content Publisher	American Association for Cancer Research
Licensed Content Publication	Cancer Discovery
Licensed Content Title	The Genomic Landscape of Pediatric Ewing Sarcoma
Licensed Content Author	Brian D. Crompton,Chip Stewart,Amaro Taylor-Weiner,Gabriela Alexe,Kyle C. Kurek,Monica L. Calicchio,Adam Kiezun,Scott L. Carter,Sachet A. Shukla,Swapnil S. Mehta,Aaron R. Thorner,Carmen de Torres,Cinzia Lavarino,Mariona Suñol,Aaron McKenna,Andrey Sivachenko,Kristian Cibulskis,Michael S. Lawrence,Petar Stojanov,Mara Rosenberg,Lauren Ambrogio,Daniel Auclair,Sara Seepo,Brendan Blumenstiel,Matthew DeFelice,Ivan Imaz-Rosshandler,Angela Schwarz-Cruz y Celis,Miguel N. Rivera,Carlos Rodriguez-Galindo,Mark et al.
Licensed Content Date	Nov 1, 2014
Licensed Content Volume	4
Licensed Content Issue	11
Type of Use	Thesis/Dissertation
Requestor type	academic/educational
Format	print and electronic
Portion	figures/tables/illustrations
Number of figures/tables/illustrations	1
Will you be translating?	no
Circulation	10
Territory of distribution	North America
Title of your thesis / dissertation	Fish Tales: Loss of STAG2 Promotes Metastasis of Ewing Sarcoma
Expected completion date	Jun 2018
Estimated size (number of pages)	150
Attachment	
Requestor Location	Dalhousie